



저작자표시-비영리-변경금지 2.0 대한민국

이용자는 아래의 조건을 따르는 경우에 한하여 자유롭게

- 이 저작물을 복제, 배포, 전송, 전시, 공연 및 방송할 수 있습니다.

다음과 같은 조건을 따라야 합니다:



저작자표시. 귀하는 원저작자를 표시하여야 합니다.



비영리. 귀하는 이 저작물을 영리 목적으로 이용할 수 없습니다.



변경금지. 귀하는 이 저작물을 개작, 변형 또는 가공할 수 없습니다.

- 귀하는, 이 저작물의 재이용이나 배포의 경우, 이 저작물에 적용된 이용허락조건을 명확하게 나타내어야 합니다.
- 저작권자로부터 별도의 허가를 받으면 이러한 조건들은 적용되지 않습니다.

저작권법에 따른 이용자의 권리는 위의 내용에 의하여 영향을 받지 않습니다.

이것은 [이용허락규약\(Legal Code\)](#)을 이해하기 쉽게 요약한 것입니다.

[Disclaimer](#)

공학박사학위논문

피스톤 링 마찰력 측정시스템 개발

Development of a New Measurement System
for Piston Ring Friction

2022 년 8 월

서울대학교 대학원

기계항공공학부

오 현 정

피스톤 링 마찰력 측정시스템 개발

Development of a New Measurement System for Piston Ring Friction

지도교수 민 경 덕

이 논문을 공학박사 학위논문으로 제출함

2022 년 4 월

서울대학교 대학원

기계항공공학부

오 현 정

오현정의 공학박사 학위논문을 인준함

2022 년 6 월

위 원 장 : 송 한 호 (인)

부위원장 : 민 경 덕 (인)

위 원 : 황 원 태 (인)

위 원 : 장 시 열 (인)

위 원 : 박 성 욱 (인)

Acknowledgment

I could not have finished my degree without these people, especially their love and support.

First of all, I would like to express my gratitude to my adviser, Prof. Kyoungdoug Min. He gave me an opportunity to experience one of the hardest time in my life, yet to follow my passion. He has always stood by to get me through all the hardships. His great patience has saved me from myself and my past. And I will always remind his advices rooted from his profound affection and insights towards me.

I would like to appreciate professionals in the field who have helped me to finish this work successfully. Dr. Kyoung-pyo Ha first brought up the idea and gave me financial and technical supports until the system had a proper format. During the development process, I had to re-design and re-make each component of the system. Without Mr. Backsik Kim and Mr. Changhee Kim, the system cannot be existed as the way it is today. Since this work was conducted with a low budget, I deeply appreciate for full material support from Kistler Korea Co. and especially Mr. Dongheun Shin and Mr. Jincheol Park. For the further steps of this work, Mr. Jinwoo Cho willingly connected me and my measurement system to the industry. His team from Hyundai Motor Company including Mr. Seokju Oh and the measurement center made more in-depth research possible. Korea Piston Ring Inc. provided me their products and empirical knowledge of piston rings which I highly appreciate.

Thanks to my lab members. Without their patience and sacrifice, I might

not have been able to end this exhausting long journey to accomplish my Ph.D. Special thanks to Dr. Yunjung Kim for full language support. I could not have been able to express my work through this thesis any better without her.

And, of course, I am always overwhelmed by unconditional love and support from my beloved family. I want to express my eternal love with all my heart to Yura, Jinho, Youjin, Hyeonju, and Yushin.

Last, but not least, I would like to thank my dear friends and inspirational pole dancers. They gladly shared a truly powerful feminine energy whilst working in a yet masculine industry. It is always empowering for me to stand up as a confident female engineer.

Abstract

Development of a New Measurement System for Piston Ring Friction

Hyunjung Oh

Department of Mechanical and Aerospace Engineering
The Graduate School
Seoul National University

Due to the piston dynamics and its wide lubricating range, various factors can affect the friction change, including piston and ring designs, and environmental parameters such as engine oil temperature, engine speed, and in-cylinder pressure. It is important to separate the total piston friction into two major friction parts, piston skirt friction and ring friction to observe the effect of each factor on the piston friction.

Though various measurement methods for the piston friction have been developed in the past, the piston ring friction has not been investigated separately from the entire piston friction considering both engine motoring and firing conditions.

A new measurement system was developed to examine the piston ring friction in detail based on floating liner method. In comparison to conventional floating liner experiments, one another piston was adopted above the conventional

crank-piston system to minimize friction from thrust force. The measuring piston is connected with the conventional piston by adding an extended connecting rod in between. The new system has double pistons. Therefore, with the new system, the measuring piston tends to move straight up and down in the liner. The piston secondary motion including the piston thrust and angular motion can be minimized nearly zero with the new system. Because of its structural characteristic, the piston skirt friction, from the interaction between the piston skirt and the liner, can be excluded with the new system. In addition, the irregular piston ring behavior such as piston ring twist and fluttering from the piston tilting motion can also be excepted. The friction changes from the interaction solely between the piston ring and the liner can be measured. This allows the parametric study of the friction force that occurs only in the piston ring.

The new system has been built up as a reliable system through many updates. To implement the stable combustion with the floating liner, a gas seal has to be applied. However, it is difficult to maintain the liner in a floating state and seal the combustion gas at the same time. To compromise these two opposite aspects, several gas sealing methods were reviewed and tested. The gas seal showed the same sealing performance with the conventional fixed liner. Moreover, in order to minimize the disturbing extra force factors on floating liner and to measure only the friction force, the extra force factors are eliminated in two approaches. The system is modified to minimize these factors. On the other hand, the extra force factors are measured to exclude the effective amount from the measured friction data.

Furthermore, the geometrical change of the entire system was made for more reliable friction measurement. With the modified system, only piston can be taken out from the engine, and the boundary conditions can be maintained

throughout the several repetitive experiments. The data repeatability was confirmed with the experimental results.

Various factors affecting lubrication conditions of piston rings were tested. The piston friction force is measured under the main engine operating conditions, which include engine oil temperature, engine speed, and in-cylinder pressure. Friction data shows a good agreement with the Stribeck curve as the engine operating parameter changes. Additionally, the tension effect of Oil Control Ring (OCR) was examined. The friction force change follows the amount of OCR tension changes. Through the experimental results drawn with the new system, it is possible to provide a quantitative analysis on friction. The newly developed device can highly contribute to fundamental piston ring researches.

**Keywords: Piston ring friction; Double pistons; Floating liner;
Piston thrust force; Piston secondary motion; Piston tilting;
Extended connecting rod**

Student Number: 2014-21875

Contents

Abstract	i
List of Figures	vii
List of Tables.....	xiv
Nomenclature.....	xv
Chapter 1. Introduction	1
1.1 Research background and motivations	1
1.2 Literature review	7
1.2.1 Piston rings.....	7
1.2.2 Piston ring dynamics	10
1.2.3 Calculation of piston ring friction	13
1.2.4 Piston friction measurement.....	25
1.3 Research objectives	29
1.4 Structure of the thesis	30
Chapter 2. Development Process of a New Piston Ring Friction Measurement System – Engine V1	31
2.1 Design concept	31
2.2 Engine structure.....	43
2.3 In-cylinder gas sealing method.....	48

2.4 Experimental setup & conditions	59
2.5 Experimental results from Engine V1	68
2.6 Remaining issues from Engine V1	77
Chapter 3. Development Process of a New Piston Ring Friction	
Measurement System – Engine V2	78
3.1 Design improvements from Engine V1	78
3.2 Extra force elimination	87
Chapter 4. System Verification	101
4.1 Base piston ring friction study.....	101
4.1.1 Oil temperature effect.....	106
4.1.2 Engine speed effect	112
4.1.3 Data repeatability	118
4.1.4 Each ring friction.....	120
4.1.5 Engine load effect.....	123
4.1.6 Piston thrust force effect.....	128
4.2 Piston ring design parameter study.....	133
4.2.1 Ring tension effect.....	133
Chapter 5. Conclusion and Future Works	138
5.1 Conclusion.....	138
5.2 Future works.....	141

References..... 146

국 문 초 록..... 153

List of Figures

Figure 1-1. Key technologies for reducing CO₂ emissions under the BLUE
 Map scenario [7] 4

Figure 1-2. CO₂ emission regulations of passenger cars [10, 11] 5

Figure 1-3. Energy loss distribution in a light-duty vehicle [9] 6

Figure 1-4. Piston rings (Three-ring pack) [37, 45] 9

Figure 1-5. Forces acting on piston ring [40]12

Figure 1-6. Stribeck curve [13]21

Figure 1-7. Piston ring hydrodynamic lubrication [29]22

Figure 1-8. Force acting on radial direction of the piston ring [32]23

Figure 1-9. Gas flow model in ring pack [35]24

Figure 2-1. (a) “A comparison of side force ($F_{y/0}$ and $F_{y/10}$) measured in a
 FRISC engine configuration with 0 and 10 mm liner offset.
 Effect on friction force (F_z) depends on speed and load.” [23]
37

(b) “Friction power loss versus deg CA in motored and fired operation. Data derived from Fz traces of Fig. 2-1. (a) and piston velocity. Pf/0, Pf/10: 0 and 10 mm offset.” [23]	37
Figure 2-2. Schematic diagram of a new measurement system and previous research	38
Figure 2-3. Piston force distribution according to a distance between piston and crankshaft	39
Figure 2-4. Dynamics simulation of double pistons engine using RecurDyn	40
Figure 2-5. Dynamics simulation results – contact force between piston and liner at firing condition (700 rpm, IMEP 4bar)	41
Figure 2-6. Dynamics simulation results – piston tilt angle at firing condition (800 rpm, IMEP 5bar)	42
Figure 2-7. Engine V1 structure – cross sectional view	45
Figure 2-8. Detailed view of floating liner (V1) – Liner temperature sensors and load cells	46
Figure 2-9. Floating liner assy. – 4 sectioned coolant jacket	47

Figure 2-10. Various gas seal and gas pressure compensation methods [25, 26, 27]	53
Figure 2-11. Incylinder gas sealing process – cross sectional view	54
Figure 2-12. Additional gas seal friction – 3 different prototype seals	55
Figure 2-13. Gas seal placement of Engine V1	56
Figure 2-14. Gas seal joint shape	57
Figure 2-15. Gas seal placement in cylinder head groove	57
Figure 2-16. Incylinder pressure comparison	58
Figure 2-17. Incylinder pressure loss with final gas seal	58
Figure 2-18. Measurement system set-up	61
Figure 2-19. Schematic diagram of test cell set-up	62
Figure 2-20. Each load cell position	63
Figure 2-21. Load cell installation	64
Figure 2-22. Friction force at motoring/firing conditions	72
Figure 2-23. Friction force at various firing conditions	73
Figure 2-24. Friction force drop according to spark timing	74

Figure 2-25. Friction force at various engine speeds	75
Figure 2-26. Friction force at various oil temperature	76
Figure 3-1. Cylinder head block modification	81
Figure 3-2. Extended con-rod modification	82
Figure 3-3. Design changes from Engine V1 – cross sectional view (Intake- side cut)	83
Figure 3-4. Engine V2 (L – Engine rear view, R – Engine front view)	84
Figure 3-5. Detailed structure of Engine V2 – 90 ° engine front-intake cutting view	85
Figure 3-6. Piston disassembly process – 3 pieces extended con-rod	86
Figure 3-7. Force balance of the floating liner [12]	91
Figure 3-8. Film type strain gauges in 4 engine directions	92
Figure 3-9. Gas force measurement	93
Figure 3-10. Minimization of crankcase pressure oscillation	94
Figure 3-11. Signal distortion from inertia effect	96
Figure 3-12. Friction force data before inertia force consideration	97
Figure 3-13. Friction force data after inertia force consideration	98

Figure 3-14. Friction force data before inertia force consideration at engine firing condition	99
Figure 3-15. Friction force data before and after inertia force consideration at engine firing condition	100
Figure 4-1. Floating liner roundness profile	103
Figure 4-2. Oil temperature effect on piston friction	108
Figure 4-3. Liner roughness measurements (R_z, R_a)	109
Figure 4-4. Honing condition – microscopy	110
Figure 4-5. Piston friction power at various oil temperature	111
Figure 4-6. Engine/piston speed effect on piston friction at 30°C	114
Figure 4-7. Engine/piston speed effect on piston friction at 60°C	115
Figure 4-8. Engine/piston speed effect on piston friction at 90°C	116
Figure 4-9. FMEP at various engine speed and oil temperature	117
Figure 4-10. Averaged friction power and standard error at various engine operating conditions	119
Figure 4-11. Averaged friction power of each piston ring and skirt at 30°C	

.....	122
Figure 4-12. Averaged friction power of each piston ring and skirt at 60°C	122
Figure 4-13. Piston friction force at motoring and firing conditions	125
Figure 4-14. Piston friction force at various firing conditions	126
Figure 4-15. Piston friction power at various firing conditions	127
Figure 4-16. Thrust and inertia force comparison at motoring condition (800 rpm)	130
Figure 4-17. Thrust force comparison of upper and lower pistons	131
Figure 4-18. Wear comparison of piston skirts for upper and lower pistons	132
Figure 4-19. Piston friction force as OCR tension change at 30°C	135
Figure 4-20. Piston friction force as OCR tension change at 60°C	135
Figure 4-21. Piston friction force as OCR tension change at 90°C	136
Figure 4-22. Averaged frictional power change according to OCR tension with corresponding error bars	136

Figure 4-23. FMEP for each OCR tension at various engine speed and oil temperature (30°C and 90°C)	137
Figure 5-1. Friction force at various engine speeds	143
Figure 5-2. Floating liner inertia force at various engine speeds	144
Figure 5-3. Modified friction force at various engine speeds	145

List of Tables

Table 2-1. Base engine specifications	36
Table 2-2. Ring specifications	65
Table 2-3. Experimental conditions	66
Table 4-1. Ring specifications	104
Table 4-2. Floating liner roughness	105
Table 4-3. Liner-piston clearance (design target values)	105

Nomenclature

A_{Ci}	Asperity contact area
A_H	Effective area for hydrodynamic film
B	Piston ring width
B_h	Half width of piston ring
$F_{c,asp}$	Radial force due to asperity contact
$F_{c,oil}$	Radial force due to hydrodynamic pressure
F_f	Total friction force
$F_{f,asp}$	Friction force due to asperity contact
$F_{f,oil}$	Friction force due to oil film
h	Oil film thickness
h_0	Minimum oil film thickness
h_{fp}	Ring position with no radial tension
\overline{h}_T	Average ring-liner gap
K_r	Ring stiffness constant
N_a	Number of contact asperity
P_{AC}	Asperity contact force per unit area
r_B	Bore radius
U	Piston speed
ECU	Engine control unit
EVO	Exhaust valve open timing
EVC	Exhaust valve close timing
IVO	Intake valve open timing
IVC	Intake valve open timing
TDC	Top dead center
BDC	Bottom dead center
TCR	Top compression ring

<i>SCR</i>	Second compression ring
<i>SI</i>	Spark ignition
<i>OCR</i>	Oil control ring
<i>DPI</i>	Dual-port injection
<i>N/A</i>	Naturally aspired

Greek letters

δ	Combined roughness
μ	Oil dynamic viscosity
λ	Oil film thickness and surface roughness ratio
\emptyset	Viscous dissipation in the oil film
\emptyset_x, \emptyset_y	Pressure flow factors
\emptyset_C	Contact factor
\emptyset_S	Shear stress factor
σ	Average RMS roughness
τ_H	Viscous shear stress
τ_{Ci}	Asperity contact shear stress

Chapter 1. Introduction

1.1 Research background and motivations

Green House Gas (GHG) emission becomes a threat for our life beyond an issue. As the humanity of this era experiences the consequences of the climate change more frequently at a distance, an amount of the global GHG emission is now reconsidered belatedly. The main cause of the GHG emission is due to an excessive usage of fossil fuels in the past decades.

Since the beginning of the industrial revolution, global energy consumption has increased tremendously, and it is estimated annually at approximately 400 exajoules (EJ). To this day, the majority of the energy produced based on fossil fuels has had significant adverse impact on our environment [1]. As shown in Fig. 1-1, 38% of CO₂ emissions, the largest portion, is expected to come from end-use energy efficiency [7]. Moreover, Hølemberg and Erdemir [6] reported that up to 23% (119 EJ) of the world's total energy consumption originates from tribological contacts in total. The 20% (103 EJ) is used to overcome friction and 3% (16 EJ) is used to remanufacture worn parts and spare equipment due to wear and wear-related failures. In other words, the accumulative energy loss from tribology is considerable and needs to be reduced.

Nearly 30% of all energy produced is consumed by transportation vehicles alone [1]. Especially CO₂, a GHG, is emitted from the combustion process of fossil fuel. Because most of transportation vehicles use the Internal Combustion Engines (ICEs) as a main power source, a huge amount of the extra CO₂ accumulates in the atmosphere. Recently, the ICEs, one of the most used fuel

driven power systems, are pointed out as a main cause of the CO₂ emission which have faced the question of maintenance or abolition.

Many nations have attempted to convert ICEs into zero-emission vehicle systems. Certainly, CO₂ neutral mobility is the long-term target of the entire automotive industry [8]. However, the majority of the vehicles on actual roads still have ICEs. COP26 in Glasgow agreed on converting existing cars to zero-emission cars by 2035 [2]. Similarly, after the Paris Agreement in 2015, experts have determined the total phase-out period of combustion cars as being prolonged by the capability gaps in the energy infrastructures between nations. Therefore, a contribution to the reduction in CO₂ emissions is still required for existing combustion cars.

To reach net-zero emissions by 2050, CO₂ emission regulation of passenger cars has to be more and more stringent every year. Figure 1-2 [10] Shows the CO₂ emission targets of two main parties as well as South Korea. European Union (EU) has the strongest emission regulations which have been announced to reduce CO₂ emission from 130 g/km of 2015 limits to 59 g/km until 2030. The United States (US) targets 102.5 g/km until 2026, and South Korea's goal is set to 70 g/km by 2030 [11].

Engine friction loss has constantly been an issue to improve fuel efficiency. Mechanical friction loss is inevitably linked to fuel consumption owing to the nature of engines with moving parts. The pie charts in the Fig. 1-3 depicts the (a) powertrain losses and (b) the average cycle friction losses due to the piston skirt, piston rings and bearings at 4000 rpm, full load [9]. As seen in Fig. 1-2, mechanical friction accounts for approximately 4–15% of the total fuel energy for a typical estimate of friction for ICEs [3]. The friction of the piston and piston ring system accounts for approximately 50–60% of the total engine friction loss [4].

The majority of the piston assembly friction comes from the (i) piston-skirt/ liner interaction, or (ii) ring-pack/liner interaction [3]. Piston ring friction losses account for approximately 20% of the total mechanical losses in modern ICEs [5]. Piston ring friction accounts for a significant amount of the total mechanical friction. As piston rings are consumables, piston friction loss can be improved by simply replacing the piston rings. Therefore, it is significant to study piston ring friction for existing ICEs.

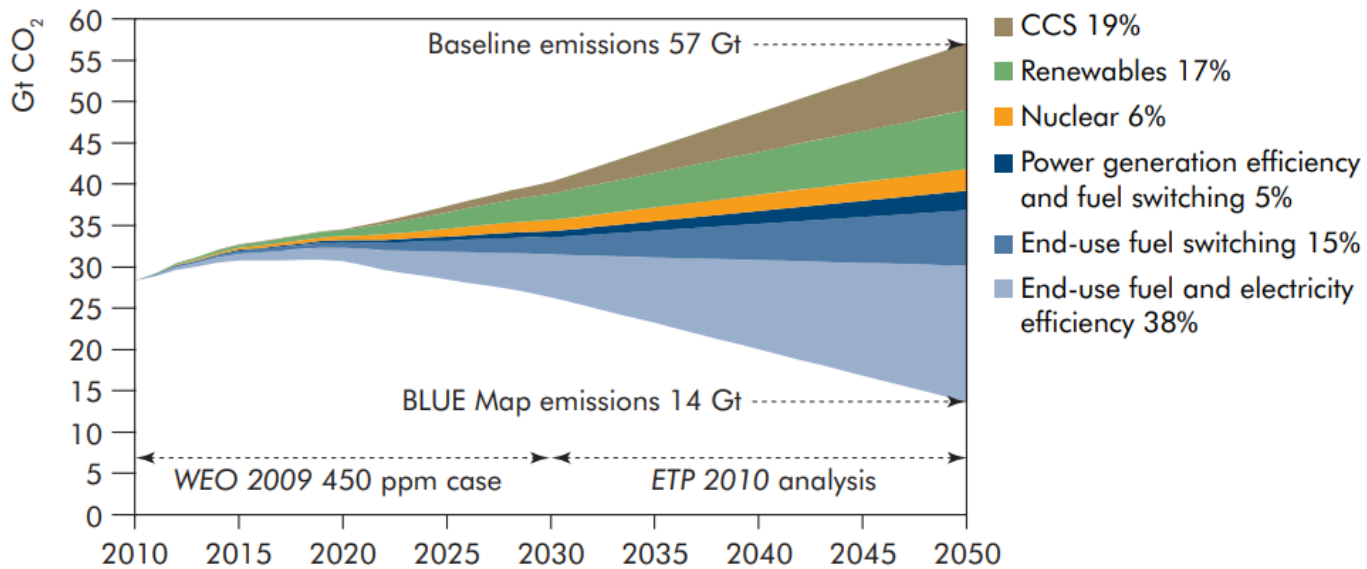


Figure 1-1. Key technologies for reducing CO₂ emissions under the BLUE Map scenario [7]

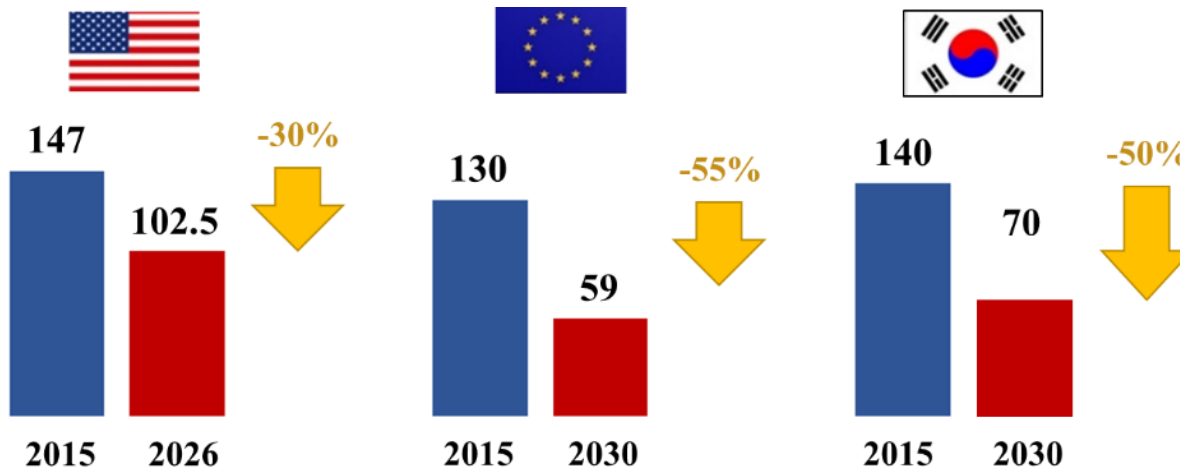
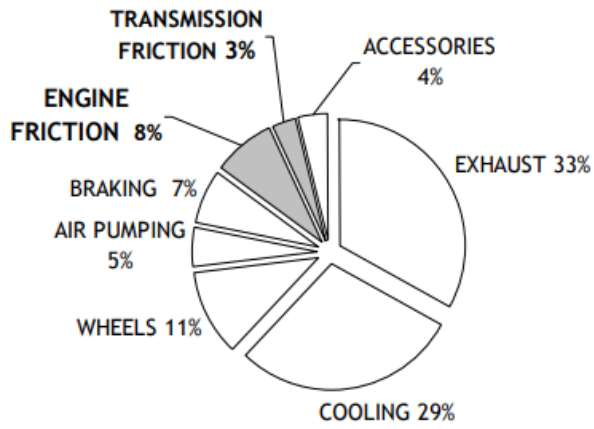
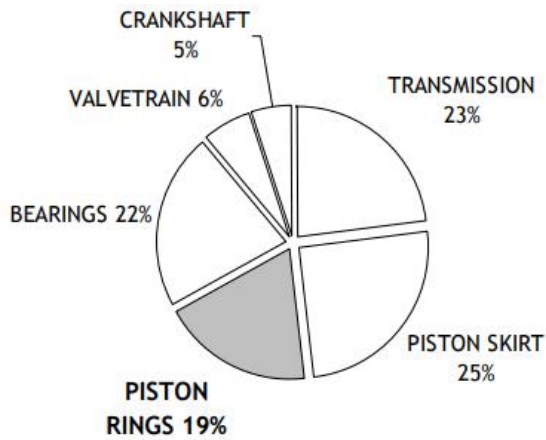


Figure 1-2. CO₂ emission regulations of passenger cars [10, 11]



(a) Powertrain losses



(b) Engine and transmission friction losses

Figure 1-3. Energy loss distribution in a light-duty vehicle [9]

1.2 Literature review

1.2.1 Piston rings

Piston ring pack in this study consists of three rings. Figure 1-4 shows a typical three-piece ring pack for a piston and the cross-sectional view of each ring. Two compression rings are installed in the grooves close to the combustion chamber. These two compression rings form a gas-tight barrier between the piston and cylinder wall in order to seal the combustion chamber [38]. The cross-sectional view of Top Compression Ring (TCR) is similar to a rectangle. Its outer surface contacting the cylinder wall has a barrel profile in micron scale to create the oil film between contacting ring and liner surfaces. It allows the ring form a hydrodynamic pressure to improve lubrication [39]. The shapes of outer surface and inter surface can be varied for better gas sealing with considering in-cylinder gas pressure. The outer surface of Second Compression Ring (SCR) is microscale tapered in the upper part, and it has a balance under cut in the lower part. When these two figures combine, it allows the ring scrape excessive oil down and seals the gas at the same time. Additionally, the taper-faced rings lead the ring-liner surface in a break-in phase faster.

Lastly, Oil Control Ring (OCR) is placed close to the oil supply. OCR commonly consists of two or three pieces. The type in two pieces has one scraping body that contacts on liner surface and a cylindrical coil spring. The coil spring is located inner groove of the scraping body, and it creates tension between liner wall and the outer surface of the scraping body. Similarly, the type in three pieces has two thin scraping plates and one spacer. The two thin plates don't have tension

itself, but the spacer creates tension by the assembled two plates. Since the coil spring or the spacer creates the tension flexibly, contacting the surface maintains regardless of cylinder deformation. With these two representative figures, OCR scrapes out an excessive oil through oil drain holes made in the groove. As all three rings are contacting on the liner wall with their pre-tensions, the rings become a path of the heat transfer from the piston to the coolant of the liner wall. Therefore, piston and piston rings can maintain acceptable temperature and lubricating conditions throughout entire engine operating conditions.

All three rings have essential roles on not only engine combustion, but also piston lubrication. To achieve the low piston ring friction, ring design parameters such as geometry, tension, material, and coating can be varied. Because piston rings have a high design versatility, it is important to study piston ring friction in further detail to acquire advantages of both combustion performance and friction.

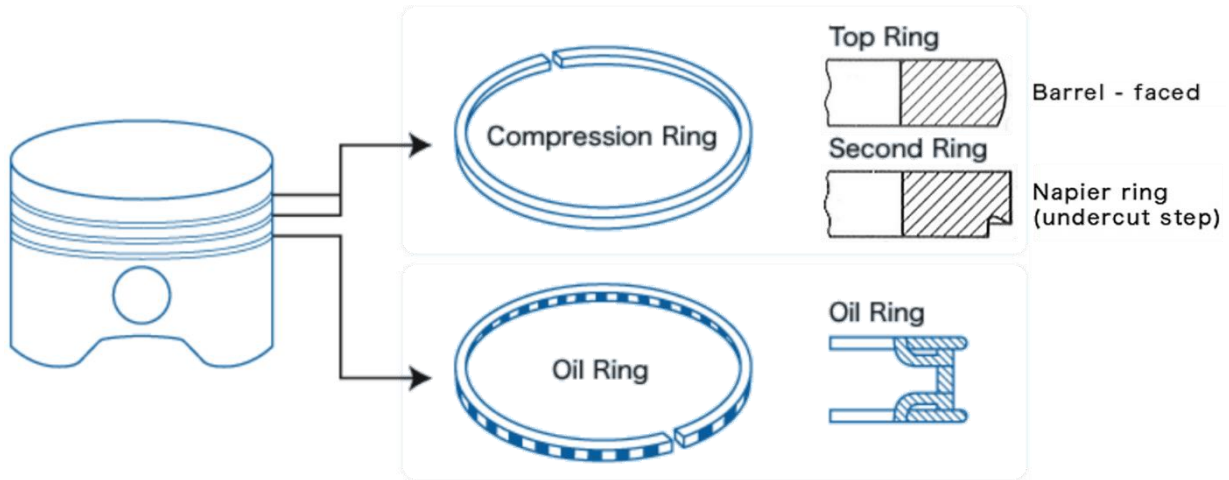


Figure 1-4. Piston rings (Three-ring pack) [37, 45]

1.2.2 Piston ring dynamics

Piston ring dynamics can be categorized in three groups; radial, axial ring motions and ring twist. The radial and axial ring motions are defined by radial force balance and piston axial motion. The forces acting on piston ring can be represented as shown in Fig. 1-5. Pressure around the ring differs as the pressure zones are divided by piston rings. Piston inertia differs as piston speed changes. And piston friction and contact force are varied by the amount of oil film created between the ring and the liner wall.

For the angular motion of the rings, the angle can be created between rings and ring land grooves, and the movement is also called ring twist. The ring twist can affect the ring and groove contact characteristics, ring stability, and blow-by [43]. When the ring outer surface is lower than inner surface, it is called negative static ring twist. On the other hand, when the ring outer surface moves towards TDC, it is called positive static ring twist. Positive static ring twist occurs when groove gas pressure in the piston ring land works on piston inner bevel. An inner bevel shape of the ring inner surface intends to make static ring twist so that the direction of the ring twist is set in one direction throughout engine cycles. Usually, the top compression rings adopt an inner bevel shape for the positive static twist. Due to the fact that the large piston tilt angle near compression TDC influences the top ring tilt significantly against liner, which can result in poor lubrication [42]. It could help the engine keep the lower oil consumption.

Moreover, there is ring flutter when the gas pressure for the top and bottom of the ring oscillates until it balances out. The ring inertia force, the gas force on the negative static ring twist position, and the relative positions of ring

and ring land groove influence on the ring flutter. The ring flutter occurs when the land groove tilt angle is bigger than the static twist angle [44]. The second compression ring generally creates the ring flutter when it is on a negative static twist. In addition, the top compression ring is on a negative static twist especially at high speed and low load operating conditions [43].

Ring dynamics is complex when the piston secondary motion occurs. Piston tilting motion influences ring dynamics by changing land gas pressures and ring position. The ring tilting motion creates a different solid contact according to the amount of the ring twist along the ring outer surface profile. Ring running surface profiles on the liner changes under ring dynamic twist and piston tilt motion [47]. The piston secondary motion can be affected by several variables such as piston material, weight, and shape and clearance characteristics of the skirt. If the friction effect from the variables caused by piston thrust dynamics can be excluded, piston ring friction can be studied from the initial state before piston tilting interaction.

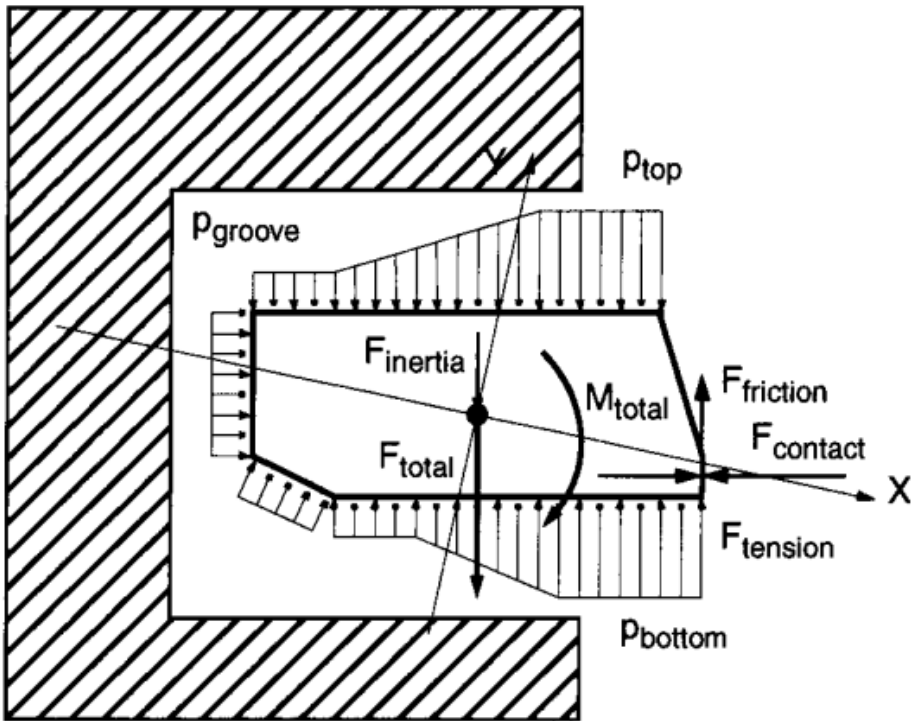


Figure 1-5. Forces acting on piston ring [40]

1.2.3 Calculation of piston ring friction

Piston friction has been mainly studied due to its significant contribution to mechanical friction losses. It is complicated to analyze piston friction as it has a wide lubrication regime, from boundary friction to hydraulic friction. Unlike the friction on journal bearings, the oil supply is not consistent for the pistons. Generally, the oil residue on a crankshaft is sprinkled to the cylinder line, as the crankshaft rotates. Meanwhile, scattered oil droplets from the piston oil jet that is targeted on piston cooling path act as lubricant. However, in either way, the actual amount of oil inlet for piston lubrication changes as engine operating condition changes. Also the piston oil supply varies according to the piston and piston ring pack dynamics. Therefore, the entire lubrication conditions from boundary lubrication to hydrodynamic lubrication need to be reviewed for piston friction analysis.

Figure 1-6 [13] shows Stribeck curve, which indicates a coefficient of friction (ratio of tangential force to normal force) change according to engine operating conditions. The main affecting factors to friction force can be represented as a dimensionless number, Hersey number.

The Hersey number is defined as:

$$H_s = \frac{\mu \cdot N}{\sigma} \tag{1.1}$$

where μ is the dynamic viscosity of the lubricant ($N \cdot s/m^2$), N is the rotational speed of the engine (m/s), and σ is the normal load per length of the tribological

contact (N/m) [13]. Hersey number can be substituted in λ ; that is fluid film thickness to roughness ratio of two affecting surfaces.

The coefficient of friction can be expressed as:

$$f = \alpha f_s + (1 - \alpha) f_L \quad (1.2)$$

where f_s is the metal-to-metal coefficient of dry friction, f_L is the hydrodynamic coefficient of friction, and α is metal-to-metal contact constant, varying between 0 and 1. As $\alpha \rightarrow 1$, $f \rightarrow f_s$, and the friction is called ‘Boundary Lubrication’; that is, close to solid friction. The lubricating film between two surfaces is too thin so that it cannot prevent solid contact. In this lubrication regime, the λ is below 1. On the other hand, as $\alpha \rightarrow 0$, $f \rightarrow f_L$, and the friction is called ‘Hydrodynamic Lubrication’. The lubricant film is sufficiently thick that it separates completely the surfaces in relative motion. Therefore, the λ for the hydrodynamic lubrication regime exceeds 3. And, in between these regimes, there is a ‘Mixed Lubrication’ where the transition from boundary to hydrodynamic lubrication occurs [13].

The oil film thickness between piston ring and liner can be calculated simply with the one-dimensional Reynolds equation under the following assumptions [23]:

- Oil is a Newtonian fluid. That is, the shear stress of the flow is proportional to the shear rate.
- Inertia force can be ignored.
- Gravity can be ignored. The gravity acting in the oil film is much smaller than the pressure and shearing force.

- The oil film thickness is very small compared to the dimensions of the sliding surface. Therefore, the viscosity and pressure can be regarded as constant.
- Oil has the same velocity with the sliding surface.
- The viscosity of the fluid is constant.

The Reynolds equation can be written as follows:

$$\frac{d}{dx} \left(h^3 \frac{dp}{dx} \right) = 6\mu U \frac{dh}{dx} + 12\mu \frac{dh}{dt} \quad (1.3)$$

As illustrated in Fig. 1-7, if the profile of the ring face is assumed to be a parabolic law (barrel-shape profile), then the oil film thickness can be expressed as:

$$h = h_0 + ax^2 \quad (1.4)$$

Ting et al. (1974) used the following equation based on the viscosities according to the temperatures at two locations to determine the viscosity distribution along the liner [30].

$$\mu = \mu_1 + \frac{1}{2}(\mu_0 - \mu_1) \left(1 - \cos \theta + \frac{1}{2\lambda} \sin^2 \theta \right) \quad (1.5)$$

The oil film pressure at the oil inlet is same as the ambient pressure, and the oil film breaks down on the downstream side, as seen in Fig. 1-7.

$$x = x_0 \rightarrow p = p_1 \text{ and } \frac{dp}{dx} = 0$$

$$x = -x_i \rightarrow p = p_2$$

(1.6)

The radial equilibrium condition is given by:

$$\frac{1}{B} \int_{x=-B_h}^{x=B_h} p(x) dx = p_g + p_t$$

(1.7)

where p_g is the gas pressure acting on the ring groove, p_t is the pressure due to the ring radial tension force:

$$p_t = \frac{F_{R,t}}{2\pi r_B B}$$

(1.8)

The viscous friction force is calculated by integrating the shear stress:

$$\tau_H(x) = -\mu \frac{U}{h(x)} - \frac{h(x)}{2} \frac{dp}{dx}$$

(1.9)

for effective ring domain on hydrodynamic lubrication.

Patir and Cheng introduced the average flow model [31] considering the surface roughness. With the model, the original Reynolds equation is

reconstructed with the flow factors ϕ_x , ϕ_y , ϕ_s and contact factor ϕ_c . The average Reynolds equation is as follows:

$$\frac{\partial}{\partial x} \left(\phi_x \frac{h^3}{12\mu} \frac{\partial p}{\partial x} \right) + \frac{\partial}{\partial y} \left(\phi_y \frac{h^3}{12\mu} \frac{\partial p}{\partial y} \right) = \phi_c \left(\frac{U_1 + U_2}{2} \frac{\partial h}{\partial x} + \frac{\partial h}{\partial t} \right) + \frac{U_1 - U_2}{2} \sigma \frac{\partial \phi_s}{\partial x} \quad (1.10)$$

where the average gap $\overline{h_T}$ that considers the asperity contact between lubricated surfaces is defined as:

$$\overline{h_T} = \int_{-h}^{\infty} (h + \delta) f(\delta) d\delta \quad (1.11)$$

and

$$\phi_c = \frac{\partial \overline{h_T}}{\partial h} = \int_{-h}^{\infty} \phi(s) ds \quad (1.12)$$

As shown in Fig. 1-8, the radial force equilibrium of the piston ring is considered:

$$F_{tot} = F_{c,oil} + F_{c,asp} - F_{R,t} - F_{R,g} = 0 \quad (1.13)$$

where $F_{c,oil}$ is the oil thrust load and $F_{c,asp}$ is the normal load on asperities. The $F_{c,asp}$ can be calculated with the Greenwood and Williamson model [33]. With the equation, solid-to-solid contact force per unit contact area. The force of two rough surfaces is assumed to have Gaussian distributions:

$$F_{c,asp} = 2\pi R \int_0^B P_{AC}(h) dx \quad (1.14)$$

When the gas force is only acting on the ring groove side ($F_{R,g}$):

$$F_{R,g} = 2\pi B r_B p_g \quad (1.15)$$

The $F_{R,t}$ can be calculated with the elastic ring tension:

$$F_{R,t} = K_r (D_{fp} - 2r_B - 2h_0) \quad (1.16)$$

where D_{fp} is the free ring diameter.

With the force equilibrium, h_0 , the minimum ring distance from the cylinder wall, can be determined. Gelinck and Schipper [34] introduced friction force and coefficient calculation.

$$F_f = F_{f,asp} + F_{f,oil} = \sum_{i=1}^{N_a} \iint_{ACi} \tau_{Ci} dA_{Ci} + \iint_{AH} \tau_H dA_H \quad (1.17)$$

The friction coefficient can be obtained as:

$$f = \frac{F_f}{F_R} = \frac{F_{f,asp} + F_{f,oil}}{F_{c,asp} + F_{c,oil}} = \frac{\sum_{i=1}^{N_a} \iint_{ACi} \tau_{Ci} dA_{Ci} + \iint_{AH} \tau_H dA_H}{F_{c,asp} + F_{c,oil}} \quad (1.18)$$

When the gas pressure works on the piston, in the case for the three ring pack piston, the ring radial force of Top Compression Ring (TCR) and Second Compression Ring (SCR) is affected by gas force. The pressure in the TCR groove (1st land, P_1) is assumed as cylinder gas pressure, and the pressure in the OCR groove (3rd land, P_3) is assumed as an ambient pressure.

As three rings inserted in the piston, gas flows through the end gaps of three rings. And the gas flow zone can be divided in three as shown in Fig. 1-9. If the flow paths between these three zones are assumed as a tapered nozzle, the mass flow rate from the top land to second land can be defined as:

$$\Delta G_1 = \frac{F_1 \psi \phi_1 P_2}{\sqrt{RT_2}} \Delta t \quad (1.19)$$

The flow rate constant from the top to second land can be obtained, and it can be defined in two conditions of the pressure ratio between two lands. According to the pressure ratio, the flow rate constant is defined as:

$$\phi_1 = \sqrt{\frac{2\kappa}{\kappa - 1} \left[\left(\frac{P_2}{P_1} \right)^{2/\kappa} - \left(\frac{P_2}{P_1} \right)^{\kappa+1/\kappa} \right]}, \quad \frac{P_2}{P_1} > 0.528$$

$$\phi_1 = 2.145, \quad \frac{P_2}{P_1} \leq 0.528 \quad (1.20)$$

The mass flow rate and the flow rate constant between second and third lands can also be obtained as above.:

$$\Delta G_2 = \frac{F_2 \psi \phi_2 P_3}{\sqrt{RT_3}} \Delta t$$

$$\phi_2 = \sqrt{\frac{2\kappa}{\kappa-1} \left[\left(\frac{P_3}{P_2}\right)^{2/\kappa} - \left(\frac{P_3}{P_2}\right)^{\kappa+1/\kappa} \right]}, \quad \frac{P_3}{P_2} > 0.528$$

$$\phi_2 = 2.145, \quad \frac{P_3}{P_2} \leq 0.528$$

(1.21)

And the pressure change of second land can be obtained as:

$$\Delta P_2 = \frac{(\Delta G_1 - \Delta G_2)RT_2}{V_2}$$

(1.22)

The pressure value of the second land can be obtained as:

$$P_2 = P_2 + \Delta P_2$$

(1.23)

The flow coefficient (ψ) is determined as 0.86. [36]

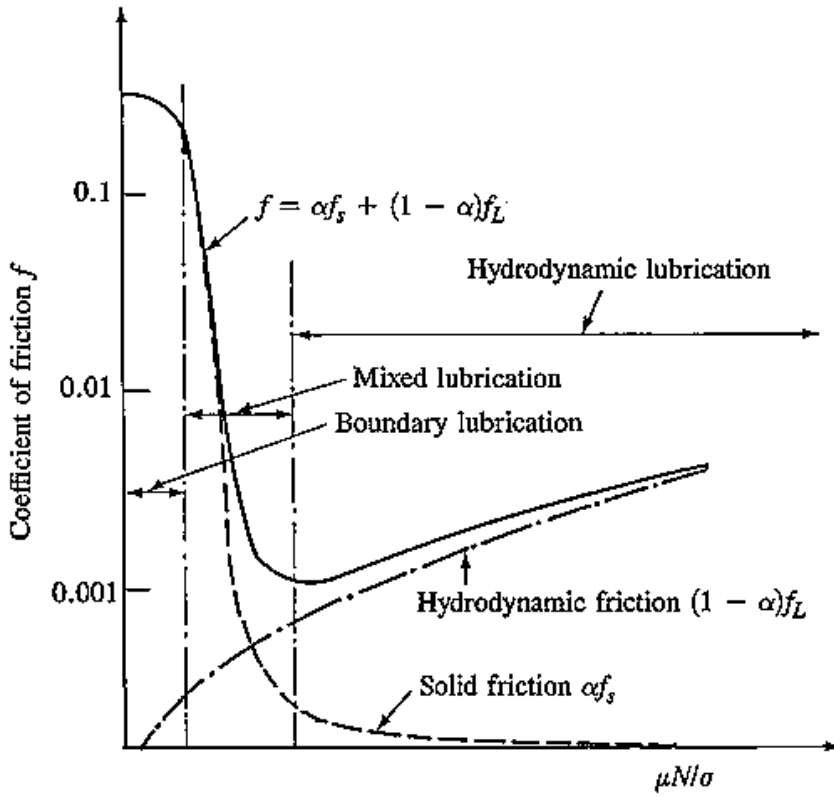


Figure 1-6. Stribeck curve [13]

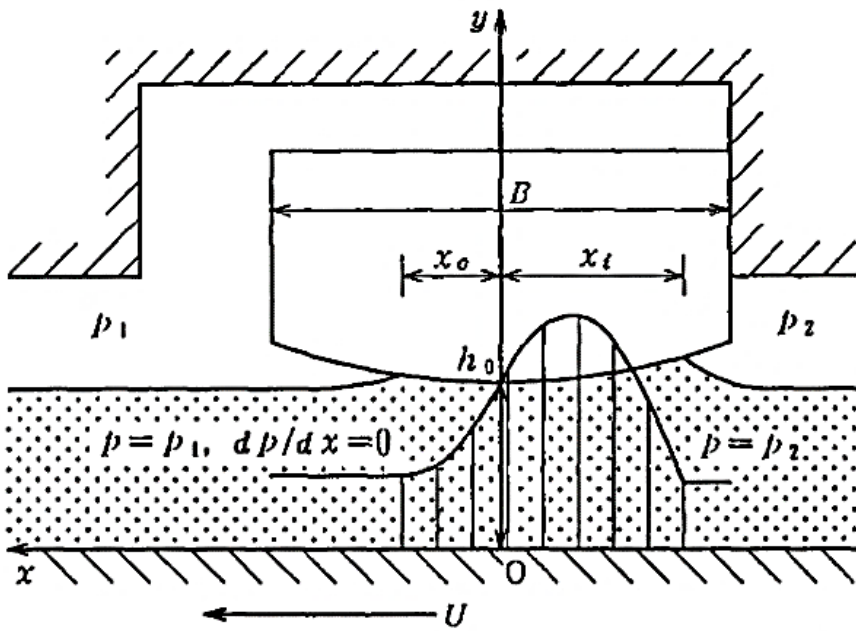


Figure 1-7. Piston ring hydrodynamic lubrication [29]

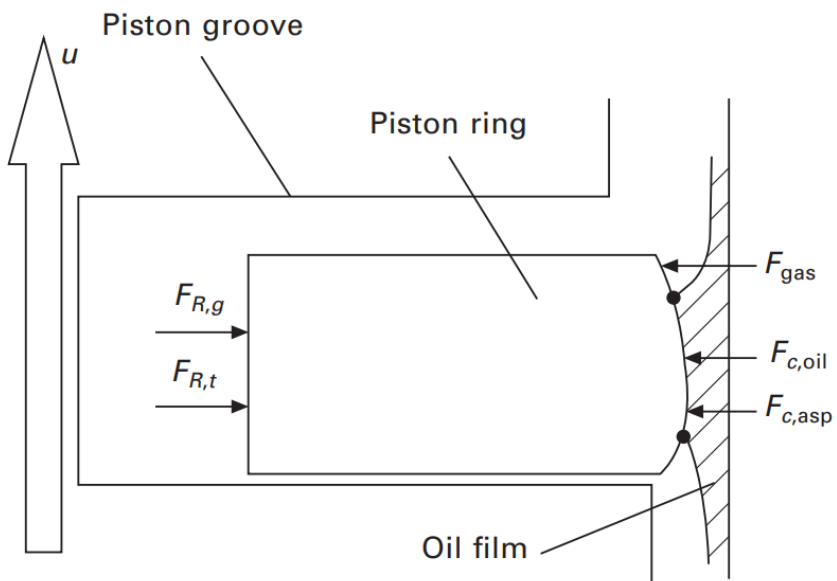


Figure 1-8. Force acting on radial direction of the piston ring [32]

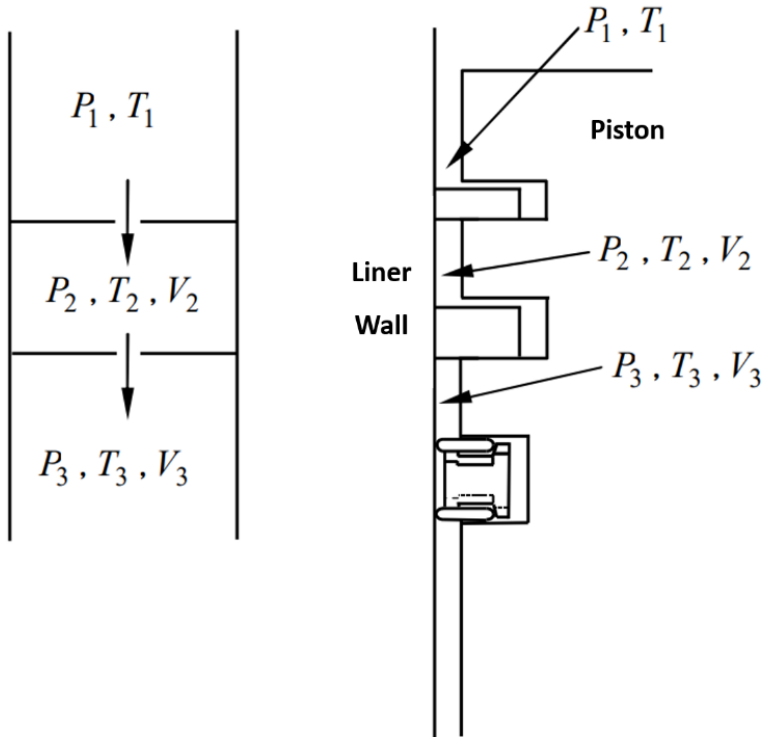


Figure 1-9. Gas flow model in ring pack [35]

1.2.4 Piston friction measurement

It is difficult to obtain piston friction, because it is smaller than the gas force and engine inertia forces. However, measuring piston friction among the entire engine friction is an initial step for piston friction research. Especially, if piston friction forces at various engine crank angles can be measured, it would be valuable not only to know the piston friction loss but also to understand the lubricating behavior between the cylinder wall and the piston assembly. This knowledge is significant for engine designers to reduce fuel consumption and to improve engine endurance [14].

Several methodologies have been developed to measure the piston friction in last decades. The most widely used method is engine strip-down. The strip-down method involves the literal removal of engine components, and the comparison of the engine torque values before and after the disassembly of each part. Consequently, the friction torque of each engine component can be calculated. However, the strip-down method has a risk of increasing measurement errors from engine weight and in-cylinder pressure change while taking out engine components in order. Most importantly, this method obviously cannot be implemented at engine firing conditions.

In addition, indirect measurement methods can be used to observe piston lubricating conditions. The oil film thickness created between the ring surface and liner was measured as an indirect method to estimate the piston friction. Inductive distance sensors are inserted in the piston to measure the radial and axial movement of the piston rings. Piezo-resistive miniature pressure sensors are also inserted in the piston to measure pressure of each piston ring zone. With this experimental approach, the piston ring dynamics and pressure in ring grooves can

be provided to the simulation model for oil film calculation [15]. For the direct oil film measurement, visualization methods using optical devices such as laser-induced fluorescence (LIF) can be adopted. Both partial and full optical window can be replaced from conventional metal liner. Fluorescent agent is added into the lubricating oil, and oil film thickness at each measuring point is known by turning fluorescent output from oil film into voltage change by a Photoelectric Multiplier Tube (PMT) [16]. However, with these introduced methods, it is challenging to achieve reliable experimental data at engine firing conditions. To implement these methods, liner, piston, and ring pack have to be modified from conventional product. Therefore, there is a measurement error compared to the friction data of the conventional liner and piston.

Furthermore, the IMEP method is one of the indirect measurements for piston friction. By measuring the axial force of the connecting rod (con-rod), the piston friction force can be calculated using known values, comprising the gas force acting on the piston and inertia force. The past system required a linkage to route signal cables for the instantaneous con-rod force away from the con-rod [22]. But nowadays, a strain gauge was attached to the con-rod using wireless telemetry technology to measure the force of the con-rod. Therefore, by simply attaching the wireless strain gauge module to a conventional con-rod, engine modifications can be greatly minimized [17]. This is the most compact and easy application for the piston friction estimation. However, the principal drawback is that it involves subtracting two large forces to obtain a small difference which is the friction force. Small errors in the measured or calculated con-rod forces can lead to significant errors in the friction estimate in addition to device stability, which is a challenging method to utilize at engine firing conditions [22].

The floating liner method was introduced to conduct an in-depth study of the piston friction under both motoring and firing engine conditions. Furuhamma was the first to introduce this concept [18, 50]. The principle of a floating-liner device is several piezoelectric load cells intervene at any point of contact between the floating liner and any rigid engine parts, so the liner to be measured and the rest of the engine mounting components move separately [19]. A conventional fixed liner is changed into a liner in a floating state, where the liner can be moved on a microscale. Therefore, the shear force created around the piston drags the liner up and down as the piston moves. Load cells capture the compression and extension force underneath the liner according to the linear movements. Stable piston friction data can be obtained using the floating-liner method under both motoring and firing engine conditions. However, because the floating liner engine from previous research uses a conventional piston-crank system, it captures not only the piston skirt and liner interaction, but also the piston ring-pack and liner interaction.

Several researches have attempted to separate the piston ring-pack friction from the piston friction. Furuhamma and Takiguchi [18] introduced a different setup with a floating liner to measure only the piston ring friction. The cylinder head was then replaced with a guide. Another guide with a slightly smaller diameter was attached to the piston top. Relative to the guide mechanism, the length of the guide was stretched out to minimize the lateral motion of the piston. With this approach, only the piston ring friction can be measured. Other studies, including Cho et al. [20], Takiguchi et al. [41], and Shin et al. [48], have also conducted a similar setup using this method. Söderfjäll et al. [21] added another rod to one of the pistons of a six-cylinder engine. Therefore, the rod was connected to a piston ring holder. The rod is guided by a linear bearing to avoid

contact between the test cylinder liner and ring holder. This means that piston ring friction can be isolated from other friction sources. The piston ring holder was inserted into a test cylinder, which was supported only via load cells, similar to the floating liner method. However, these methods were set up for a rig test of piston rings, and isolation of the piston ring friction under firing conditions has not been attempted.

To overcome limitations from previous studies, a new measurement system for piston ring friction was developed. By adding one more piston to the conventional piston-crank system, the new system can capture only the piston ring friction under both motoring and firing conditions. With the new measurement system, piston ring friction can be measured under various engine operating conditions. The experimental results show that the new system captures friction changes as the engine speed, oil temperature, and in-cylinder pressure change.

1.3 Research objectives

To make existing internal combustion engines sustainable, mechanical energy loss needs to be reduced. Piston ring friction occupies a quarter of total engine friction. Reducing piston ring friction can be a simple approach because of its accessibility and cost. Thus it is important to research piston ring friction. For the initial step of the research, piston ring friction needs to be measured.

Therefore, in this study, a new friction measurement system is developed based on the floating liner method. In comparison to previous researches, only piston ring friction change can be observed with the newly developed system. By minimizing piston thrust force, the piston skirt-liner interaction can be excepted. And the random ring movement from ring groove gas interaction caused by piston secondary motion can also be excepted. Furthermore, two main aspects are considered for more reliable friction measurement.

- 1) Improved a combustion stability for research on firing conditions
- 2) Developed a way to change piston and piston rings only for experiment repeatability
- 3) Eliminated extra force interruption on the measurement

To verify the performance of the new measurement system, piston ring pack friction has measured at various engine operating conditions. Engine speed, oil temperature, and in-cylinder pressure were varied to see lubrication regime change. Additionally, a tension factor of the Oil Control Ring (OCR) has tested to see the newly developed system capturing the friction characteristics of different geometries.

1.4 Structure of the thesis

The thesis consists of five chapters.

Chapter 1 examines the importance of the research and the literature review of previous researched. From Chapter 2 to 3, the development process of the new measurement system is explained. In the Chapter 2, the base design concept of the system is introduced. The experimental results from the first prototype, Engine V1, are shown at various engine operating conditions as well as further improvements are made on Engine V2 to solve the remaining issues from Engine V1. The key improvements are described in Chapter 3. In Chapter 4, the measurement performance of the developed system, Engine V2, is verified with experimental results. Experiments include the parameter changes of the main engine operating conditions. Moreover, the OCR tension effects on friction were tested. The thesis is concluded through Chapter 5 in addition to contributions and future suggestions are discussed.

Chapter 2. Development Process of a New Piston

Ring Friction Measurement System – Engine V1

2.1 Design concept

The measurement system of piston ring friction is designed based on floating liner method. Floating liner method is the most powerful way of existing measurement methods to measure reliable piston friction force at both engine motoring and firing conditions. For conventional floating liner method, force sensors are placed under the floating liner, and measure force changes as piston drags the liner up and down for each stroke. However, the floating liner method in previous studies captures both piston ring-liner and piston skirt-liner interactions as the method uses the conventional piston-crank system. Excluding the effect of the piston secondary motion on the friction has never been conducted under engine firing conditions.

With conventional engine crankshaft-piston structure, measured friction data can be highly distorted by the piston thrust force. Since piston has 6 degrees of freedom, piston can move towards liner wall as rotational motion from crankshaft changes into transitional form on the piston. When the pressure works on the top of the piston, the con-rod and the piston center creates an angle. Depending on the amount of angle and cylinder pressure, the piston would not only have the force along the stroke direction, but also force towards the liner wall. Once the piston contact with the liner occurs, the load cell that supports the floating liner captures the piston thrust motion. This can disturb the load cells

measuring piston friction, which acts in the stroke direction. If the load cells capture the piston thrust force, the piston friction data would be like Fig. 2-1 (a) [23]. Winklhofer et al. investigated the influence of the liner offset from the crankshaft center on the friction force with their floating liner system, FRISC. FRISC engine also has conventional piston-crankshaft system, thus the piston thrust force can be measured with the system if the system does not adapt to the device for excepting the thrust force such as lateral stoppers [24, 50]. As seen in Fig. 2-1 (a), friction force (F_z) fluctuates regardless of piston moving direction at both 0 and 10 mm liner offset cases. And the calculated friction power loss can be anticipated as Fig. 2-1 (b). Because of the thrust force effect on friction force, the negative friction power loss is measured with the FRISC system.

A new structure is developed to exclude piston secondary motion effect on the friction measurement. As this differs from the floating liner concept of previous researches another piston is connected on the top of the conventional piston-crank system. To connect these two pistons, an extended con-rod is assembled on the top of the conventional piston. As shown in Fig. 2-2, a liner for a lower piston is fixed as conventional engines. A floating liner is placed for an upper piston, and load cells are inserted underneath the floating liner. So load cells measure piston friction that solely occurs at the upper piston.

By applying a new design concept—double pistons with the extended con-rod—piston thrust force can be highly reduced compared with the conventional system. As shown in Fig. 2-3, when the length of the con-rod increases, the angle that con-rod creates from the center of the crankshaft decreases. The upper piston has a much smaller angle (θ') than one (θ) of the lower piston. Therefore, the thrust force operating on the upper piston can be reduced to nearly zero. Therefore, with the double pistons structure, friction force

mainly from piston rings can be investigated. And the distortion of the friction force signal can be highly reduced.

To confirm the amount of thrust force that the ‘double pistons’ structure has, a contact force between both pistons and liners which have been calculated with a simulation program. RecurDyn a 3D multi-body dynamics simulation program was utilized. Structural characteristics can be simply interpreted as Fig. 2-4 with the program. The CAD models of the engine parts were used for more accurate inertia effect. As shown in Table 2-1, main engine geometrical values are summarized. For the main effective parameters on piston thrust force, the distance between con-rod big end connected to crankshaft pin journal and con-rod small end connected to lower piston pin is 146 mm. The distance of piston pin centers for upper and lower pistons is 230 mm, thus, the upper piston has the effect of 2.6 times longer con-rod than the lower piston. The clearance between liner and piston for both upper and lower is set as 15 μm in diameter. The clearance variation according to piston skirt profiles for both pistons were not considered. Also the clearances between every rotational joints were not considered. The piston rings were omitted in the model for the piston dynamics analysis mainly focused on piston thrust force as the con-rod length changes. Both upper and lower piston have 0.8 mm piston offsets, but the radial center of upper and lower pistons is same. For the input force, measured in-cylinder gas pressure at engine firing conditions was used in force value for the simulation. The gas force was applied on the top surface of the piston. Shear stress was ignored for revolute joints for piston pins and journal pin. The standard contact force model was used for both upper and lower piston’s contact surfaces. The triangular surface mesh was used for piston skirt, ring lands and corresponding liner surface.

Simulation is implemented to both engine motoring and firing pressure condition. One of the simulation results is plotted in Fig. 2-5. As shown in Fig. 2-5, contact forces for upper and lower pistons can be calculated according to a gas force working on the upper piston. The input gas force is set based on the measured data at 700 rpm, IMEP 4 bar condition. The red dotted line on the figure indicates gas force change on the piston top, which has a different force direction with the calculated contact force directions. The calculated contact force has plus and minus signs, and this sign represents a force direction. A positive force indicates the force working towards piston thrust side same as engine exhaust side, and a negative force indicates piston anti-thrust side same as engine intake side. As shown in Fig. 2-5, the thrust force working on the upper piston is remarkably smaller than the lower piston. The contact force of the lower piston represents the piston thrust force in the conventional piston-crank system. And the contact force of the upper piston represents the piston thrust force of the measuring piston in the ‘double pistons’ system. As seen in the figure, the contact force shows maximum value near in-cylinder pressure peak point. When the peak contact forces for both pistons are compared, the contact force drops from a few thousands Newton at lower piston to nearly zero Newton at upper piston.

Furthermore, the angular motion of the piston can be also minimized with the new system. As shown in Fig. 2-6, the piston tilt angle can be calculated by using the simulation model. The figure shows the piston tilt angle changes at the conventional piston-crank system and also at the upper piston of the new system. As the simulation result shows, the tilt angle of the conventional piston changes drastically at the initial stage of the expansion stroke. The conventional piston slaps to the thrust-side [51]. However, with the ‘double pistons’ structure, the tilt angle of the upper piston barely occurs. The piston tilt angle can be reduced

down to 17 times with the new system when the angles are compared at the peak gas pressure. Thus, the piston angular motion can be ignorable. The irregular piston ring dynamics such as ring twist and fluttering occurred by the gas pressure interactions from piston tilt motion can be excepted with the new system.

This simulation result proves that the new system can minimize the effect of the piston secondary motion. The measuring piston tends to move more straight up and down within stroke direction. Piston skirt and liner interaction and piston ring dynamics from piston tilting can be excluded. Therefore, with the new structure, base study of the piston rings can be implemented first before considering random piston dynamics.

Table 2-1. Simulation set-up

Bore × Stroke	88 mm × 86 mm (Upper piston)
	86 mm × 86 mm (Lower piston)
Piston-liner clearance	15 μm (in diameter)
Center distance	230 mm (Upper piston – Lower piston)
	146 mm (Lower piston – Crankshaft journal pin)
Piston offset	0.8 mm (Upper & Lower pistons)
Material	Steel (Upper & Lower liners, Lower con-rod, Crankshaft)
	Aluminum (Upper & Lower pistons, Extended con-rod)

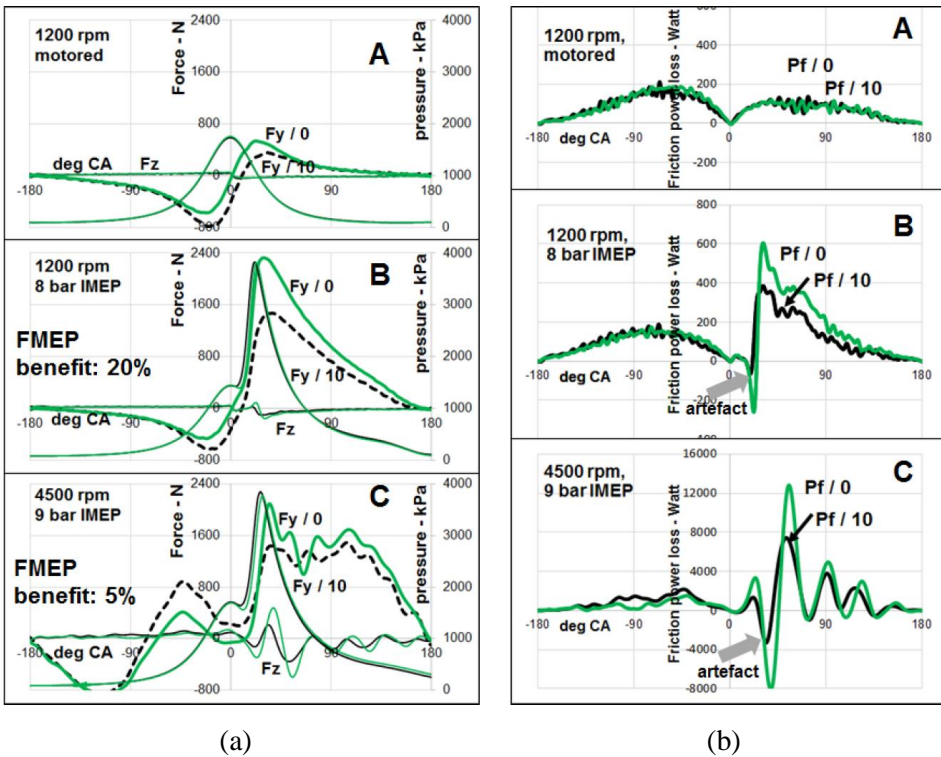


Figure 2-1. (a) “A comparison of side force ($F_y/0$ and $F_y/10$) measured in a FRISC engine configuration with 0 and 10 mm liner offset. Effect on friction force (F_z) depends on speed and load.” [23]

(b) “Friction power loss versus deg CA in motored and fired operation. Data derived from F_z traces of Fig. 2-1. (a) and piston velocity. $P_f/0$, $P_f/10$: 0 and 10 mm offset.” [23]

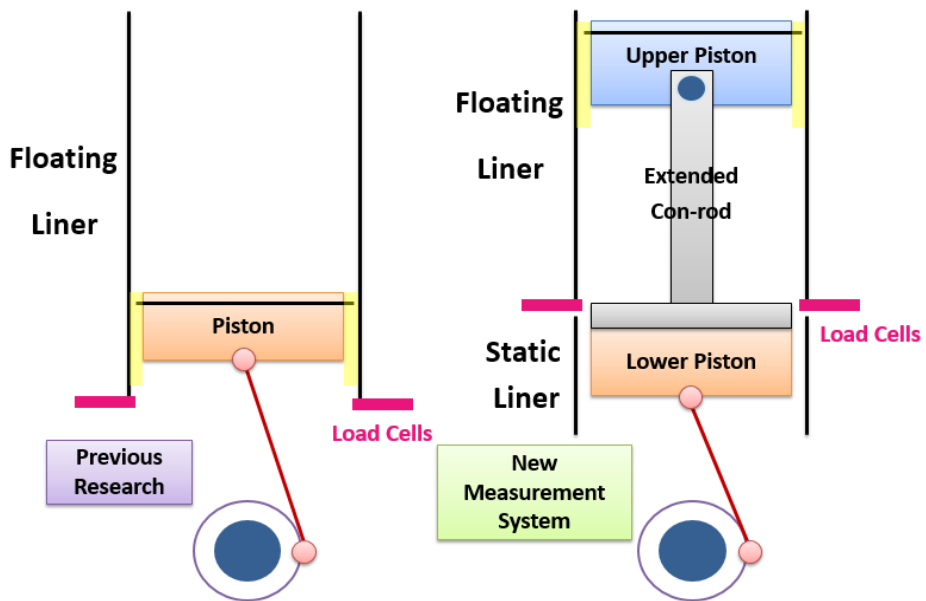


Figure 2-2. Schematic diagram of a new measurement system and previous research

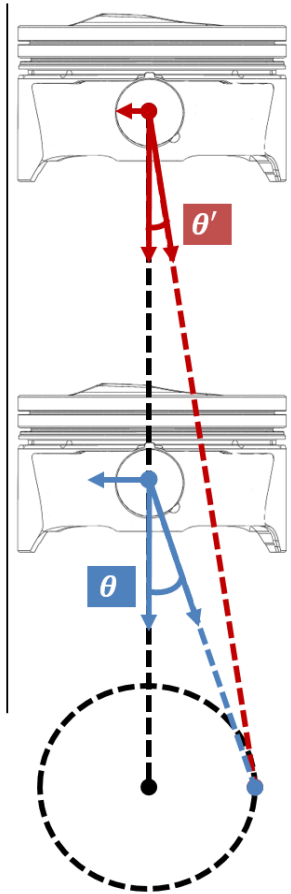


Figure 2-3. Piston force distribution according to a distance between piston and crankshaft

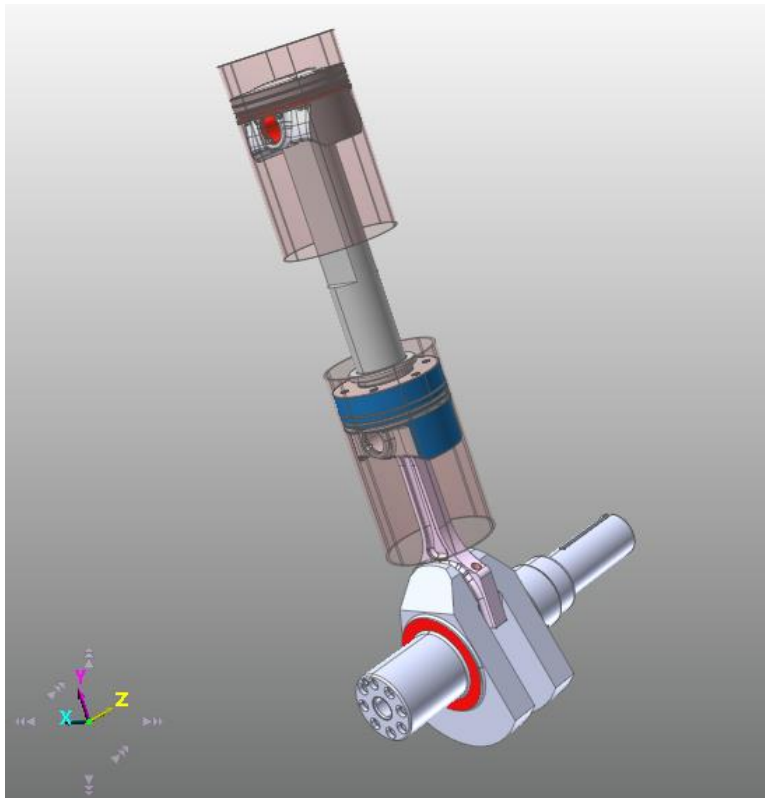


Figure 2-4. Dynamics simulation of double pistons engine using RecurDyn

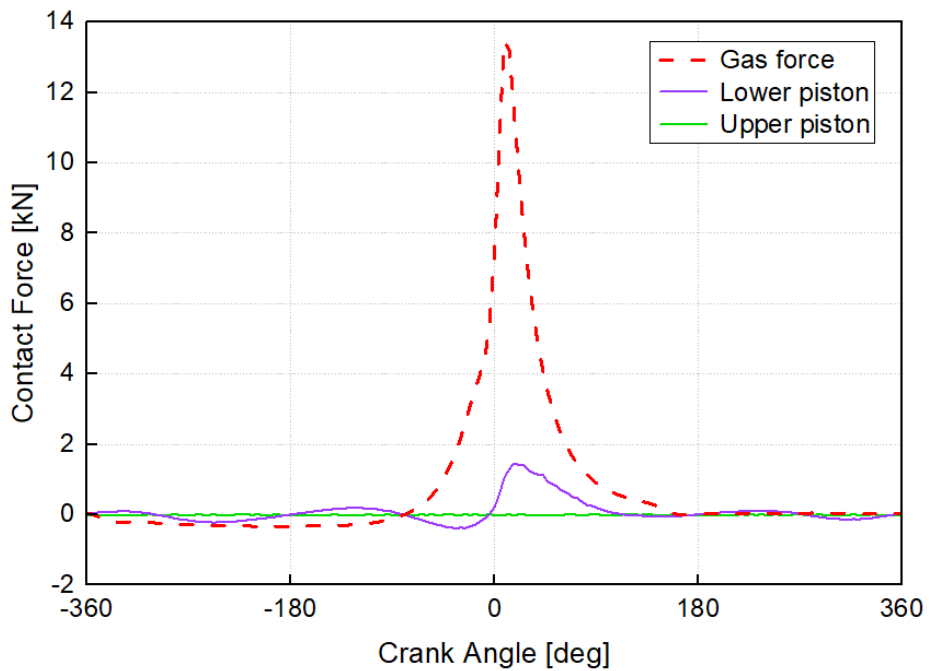


Figure 2-5. Dynamics simulation results – contact force between piston and liner at firing condition (700 rpm, IMEP 4bar)

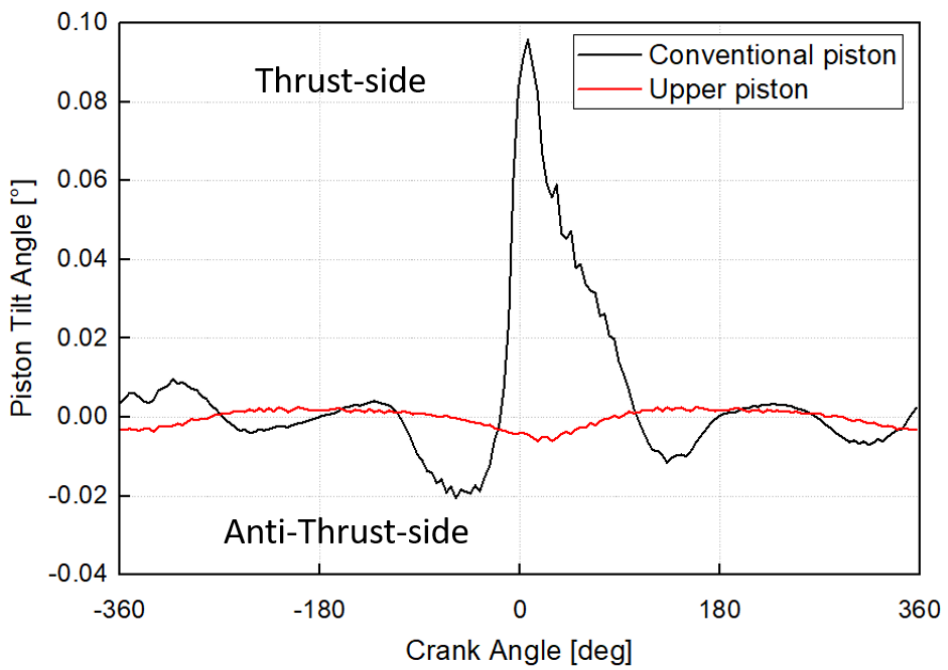


Figure 2-6. Dynamics simulation results – piston tilt angle at firing condition (800 rpm, IMEP 5bar)

2.2 Engine structure

As adopting ‘double pistons’ design on the conventional floating liner engine, the engine consists of two different pistons, liners, and con-rods. As shown in Fig. 2-7, an upper piston with an extended con-rod is placed top of a lower piston. The extended con-rod and the upper piston are connected with a piston pin. Therefore, the upper piston can move solely regardless of the lower piston movement. The radial piston movement from the lower piston can be reduced on the upper piston. And the liners are separated for the upper and lower pistons. Lower piston moves in the lower liner, which is in fixed state like liners in conventional engines. The upper liner is in floating state. Load cells are placed underneath the floating liner, for it to primarily capture friction force of the upper piston. Washer-type load cells are used. The load cells are inserted in between floating liner and floating liner bed as a plain washer. As seen in Fig. 2-8, for more detailed view, a M4 size bolt is fastened through the load cell to give a pre-load.

Since another piston is adopted on the conventional piston-crank system, lubricating oil from the rotating crankshaft cannot be reached to the upper piston. Therefore, as described in Fig. 2-7, an oil jet is placed on the top of the floating liner block. The oil flow path is carved inside the block, so the oil can be provided through the oil jet. The oil jet is targeting under the exhaust-side of the piston skirt. However, by maintaining the oil pressure low, oil pressure does not work on the piston. As oil flows between the upper and lower pistons, the oil spreads by piston movement. There are flow paths on the center of the lower piston and the extended con-rod to send the oil residue to the oil drain.

Total 10 temperature sensors can be placed on the floating liner to measure the actual liner temperature, so lubricating boundary conditions can be easily observed especially at engine firing conditions. Also temperature boundary condition can be maintained same for experimental repeatability. 5 temperature sensors are placed at engine intake-side, and another 5 sensors are placed at engine exhaust-side in Fig. 2-7. As shown in Fig. 2-8, temperature sensors are placed right behind the liner wall along the piston stroke. The temperature sensors are inserted 1 mm behind the liner wall, and 5 sensors can be inserted within the distance of the piston stroke. The distance between sensors is set in 15 mm. Coolant flow paths of the floating liner are placed at the engine front and rear sides as inlets and outlets. The coolant flow paths are separated in 4 sections along the piston stroke direction with the liner grooves as shown in Fig. 2-9. Coolant temperatures can be controlled differently for each section. Each section is divided by the 1.8 mm thickness of the partitions. The placement of temperature sensors and coolant flow paths can be changed easily by rotating the floating liner and coolant jacket case.

Cylinder head sits on the cylinder head block, and the floating liner is inserted in the groove of the cylinder head without touching the groove surface. The clearance between the groove of the cylinder head and the floating liner is set in micro-scale, so the cylinder head and the floating liner do not have solid contact. However, in-cylinder gas needs to be sealed properly to implement the experiments at engine firing conditions. The cylinder head has a sealing ring seat, and the seal contacts with the floating liner inner surface. The gas sealing method of the new system is explained in the following section 2.3.

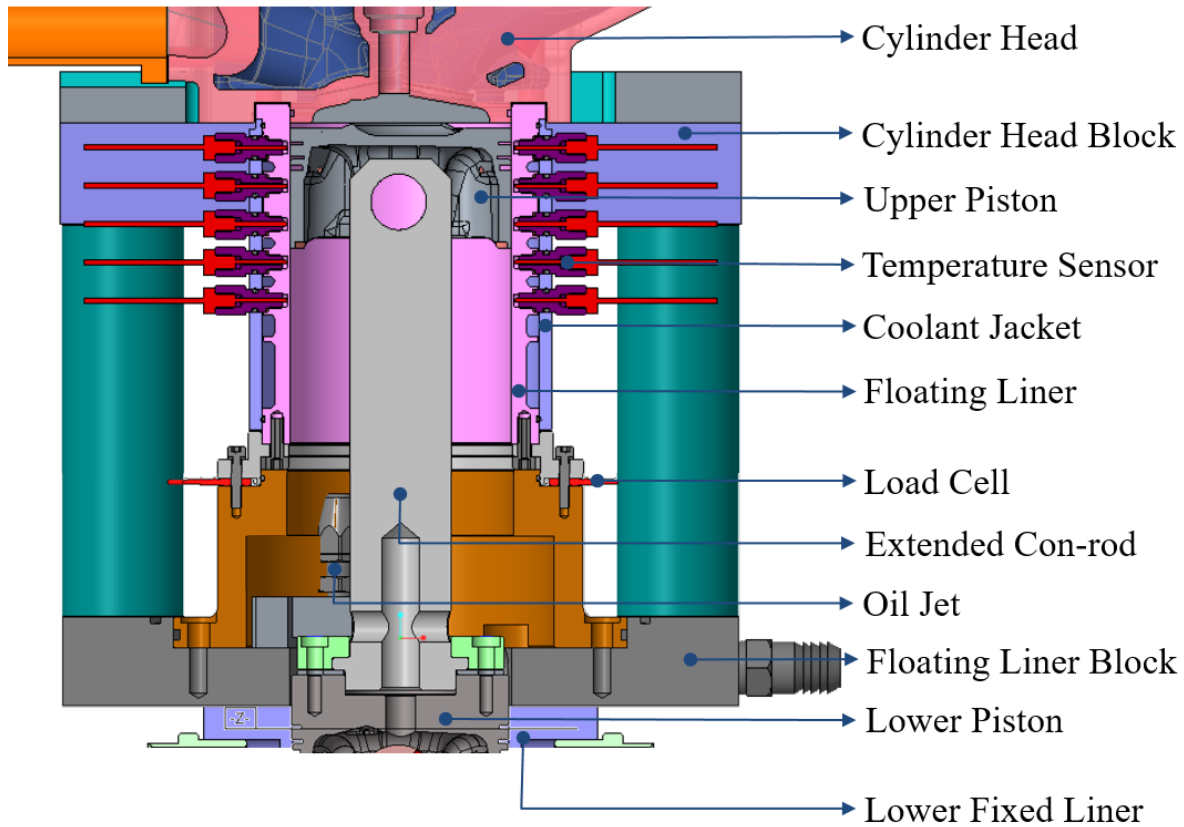


Figure 2-7. Engine V1 structure – cross sectional view

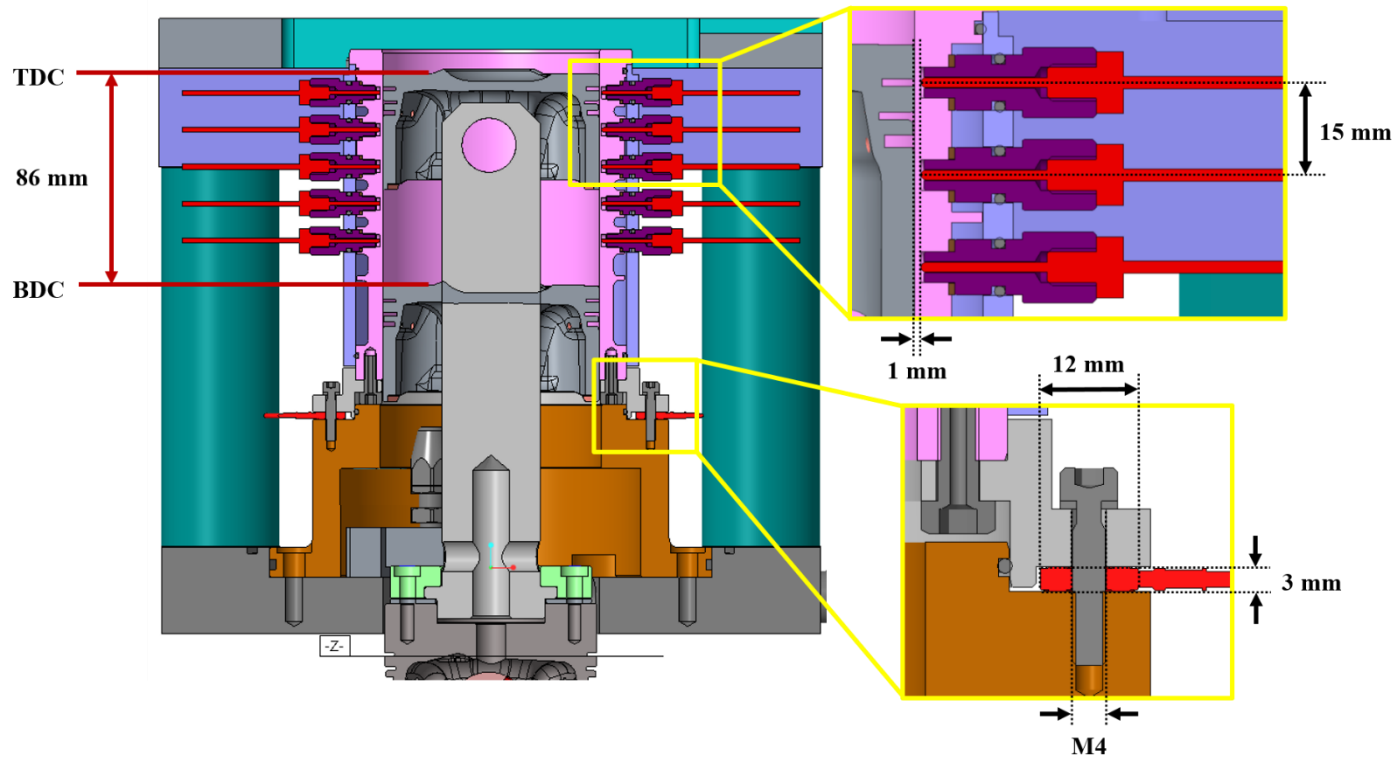


Figure 2-8. Detailed view of floating liner (V1) – Liner temperature sensors and load cells

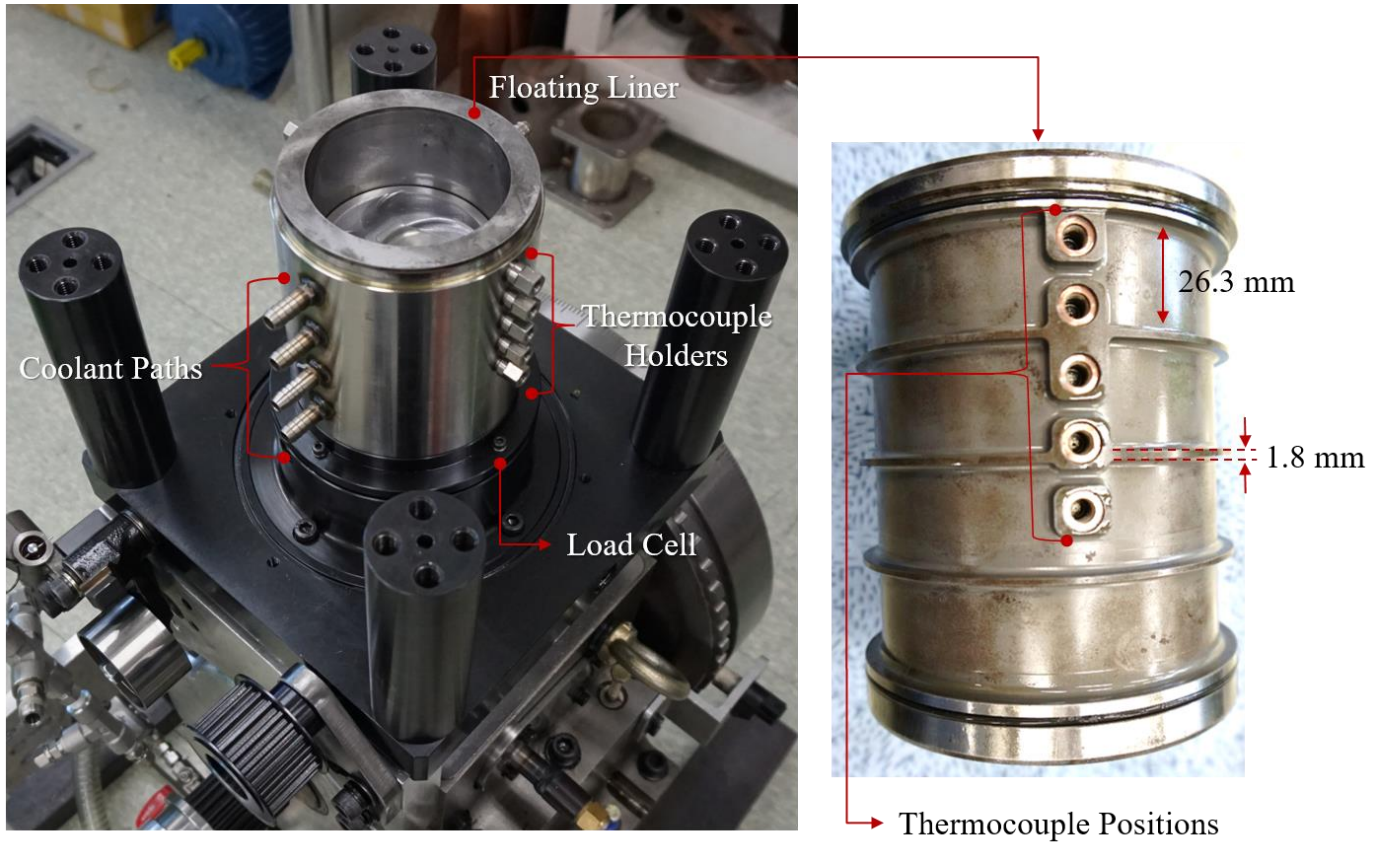


Figure 2-9. Floating liner assy. – 4 sectioned coolant jacket

2.3 In-cylinder gas sealing method

In order to implement the experiment at engine firing conditions, it is most important that the liner should be kept in a floating state as well as it needs to be thoroughly sealed for a stable combustion. To compromise these two opposite aspects, which keep the liner floating state and sealing the in-cylinder gas at the same time, many gas sealing method are introduced in the previous researches.

As shown in Fig. 2-10, floating liner gas can be sealed in 4 representative ways. Fig. 2-10 (a) method is a current gas sealing method for the floating liner engine developed by Furuhamma [28]. And (d) is their earlier design [14]. (b) and (c) have same sealing method but in different seal material. (e) is invented by Ha [25]. Except (c) method, majority of the well-known sealing methods uses O-ring seal. Usually O-ring seal is inserted in a groove of the mechanical part, and O-ring is pressed by the surface of the other part. Since the O-ring is elastic and deformable, O-ring creates a solid contact on the surface. However, when varying pressure such as gas pressure is added to O-ring there are changes of the contact pressure of the O-ring on the surface. Due to its material characteristics, O-ring creates an extra friction proportionally with the gas pressure as it deforms. Therefore, O-ring is a challenging approach for floating liner application, which has to be unbothered by other force factors except piston friction force.

Furthermore, the sealing methods, which cause an extra force on the floating liner from the gas pressure, have to modify the floating liner and the piston to compensate the gas pressure. As adopted on (a), (d), and (e), the gas compensation structure prevents from measuring the gas pressure effect on the

floating liner with sealing the gas properly. However, it increases the system complexity. Therefore, for the base concept of the in-cylinder gas sealing method, (c) is adopted and modified for the new system.

Each gas seal is inserted between a cylinder head and the floating liner as illustrated in Fig. 2-11. When the gas chamber is pressurized, gas pressure is working on the gas seal. The gas pressure makes the seal contact on an inner surface of the floating liner, and the gas seal prevents in-cylinder gas from leaking. During this process, gas seal could make an extra friction on the floating liner. As shown in Fig. 2-11, the gas seal can drag up the floating liner because of the large friction force between the liner and the gas seal. In this situation, the amount of gas seal friction (①) exceeds piston friction (②). This affects piston friction measurement, thus it is important to design the proper gas seal.

Various seal types were tested to reach the final product. During this trial process, observations were made to understand extra friction force from the seal affect measuring piston ring friction force. As shown in Fig. 2-12, three different gas sealing rings were tested at 700 rpm, motoring condition. Except seal type 1, types 2 and 3 show a slightly lower pressure peak near firing TDC. The in-cylinder pressure deviation of all three rings is below 3%, therefore, the sealing ability of all three rings is acceptable to continue the experiments. However, plotted all three rings are showing additional gas seal friction was measured with the piston friction. Since friction force data increases as cylinder pressure increases. The gas seal friction interrupted the physical directions of piston friction. Piston friction force over a thousand Newton was observed near firing TDC at engine motoring condition. The force direction at expansion stroke is supposed to be a negative value, but the measured data shows positive value. Therefore, it is obvious that

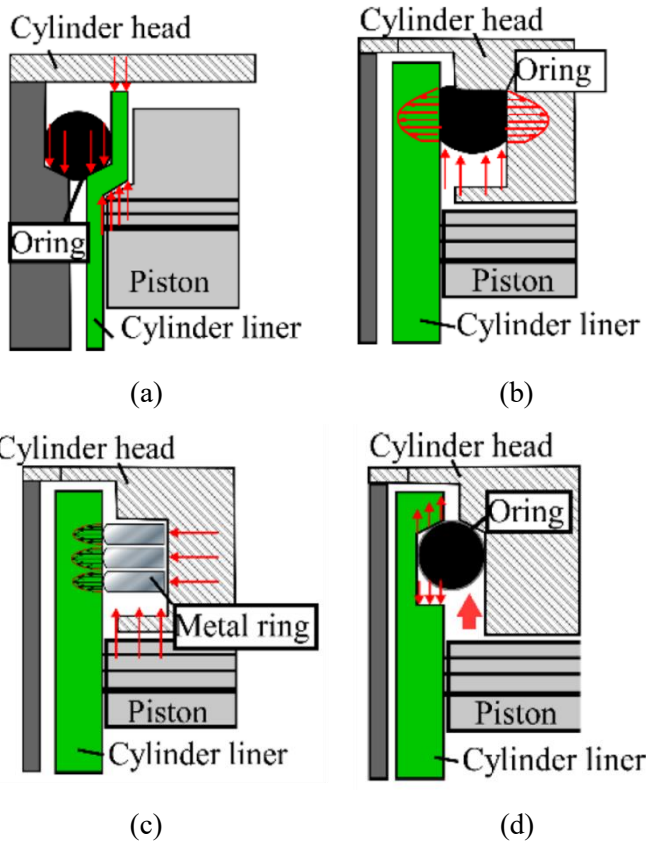
gas seal is affected by in-cylinder gas pressure, and it drags the floating liner upwards which is in the opposite direction of the piston at the expansion stroke.

Type 1 is O-ring type, which showed the same effect of Fig. 2-10 (b). The deformable characteristic of rubber ring caused the strong bond on the liner surface as in-cylinder pressure increases. Likewise, the size of the O-ring is difficult to be controlled to seal the gas properly. As the closed joint shape does not allow the ring to expand in radial direction with pressure change. If the thickness of the O-ring is not big enough, the gas pressure tends to leak through the clearance. In comparison, if the O-ring is thick enough to touch the surface of the floating liner and create the seal area, it's easy to add an extra friction on the floating liner according to deformation. For the type 2 and 3, Rulon material is used, which typically uses as piston rings on engine combustion visualization substituted from commercial steel rings. The Rulon material is known as low friction and high thermal resistance. However, it tends to be worn by the steel liner. The worn pieces from the Rulon gas seal were combined with oil residue at high temperature. It sticks on the floating liner inner surface and cylinder head groove. This material adhesion changes the radial clearance between the floating liner and the cylinder head. The clearance is in micro-scale. As the worn materials block the clearance partially, it causes an extra friction force on the floating liner as shown in Fig. 2-12.

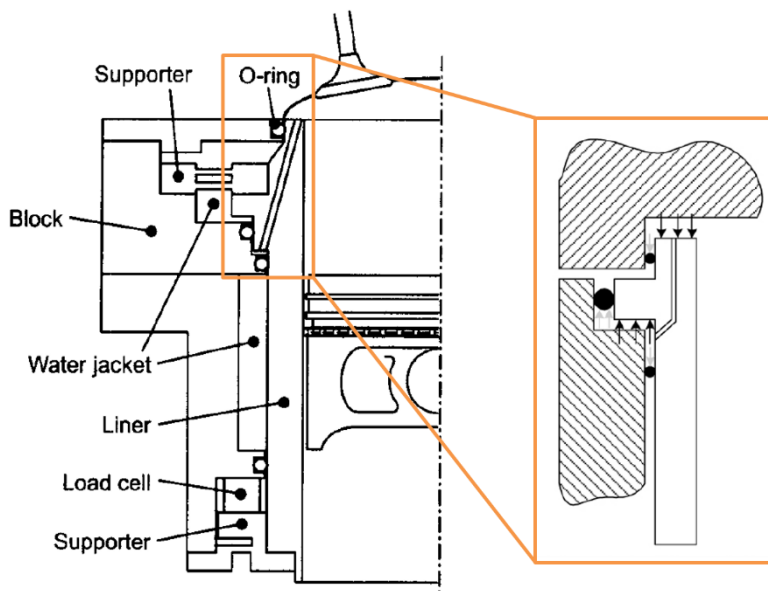
Through the several trial tests including fore-explained gas seal types, thermo-resistive, low friction, and low wear material is used for the final gas seal. For the final gas seal, as shown in Fig. 2-13, inner bevel is placed where the gas pressure works. The gas seal can maintain the sealing surface efficiently. In addition, its effective contact area on the inner radial surface of the floating liner is as small as possible. The gas seal expands in radial direction as gas pressure

increases. To minimize the gas leakage through the gas seal joint, ‘ $\perp \sqsupset$ ’ (step) joint shape is adopted as seen in Fig. 2-14.

Figure 2-15 shows the actual installation of the final product. It shows combustion chamber roof including intake and exhaust valve faces and a spark plug. Around the roof, there is a groove where the top of the floating liner is inserted. In the axial direction of the groove, there is a gas seal seat. The ‘ $\perp \sqsupset$ ’ joint gas seal is inserted in the seat as shown in the Fig. 2-15. With the final sealing ring design, in-cylinder gas can be sealed like conventional engines with the fixed liners. As shown in Fig. 2-16, the in-cylinder gas pressure of both conventional seal type and sealing ring for floating liner is compared at 800 rpm, motoring case. Two cylinder pressure curves match nearly the same as seen in Fig. 2-16. As plotted in Fig. 2-17, the pressure difference between the gas seal used case and the conventional engine case is below 0.1 bar. This indicates the sealing performance of the gas seal is reliable to proceed the friction measurement.



the figure (e) continued on the next page.



(e)

Figure 2-10. Various gas seal and gas pressure compensation methods [25, 26, 27]

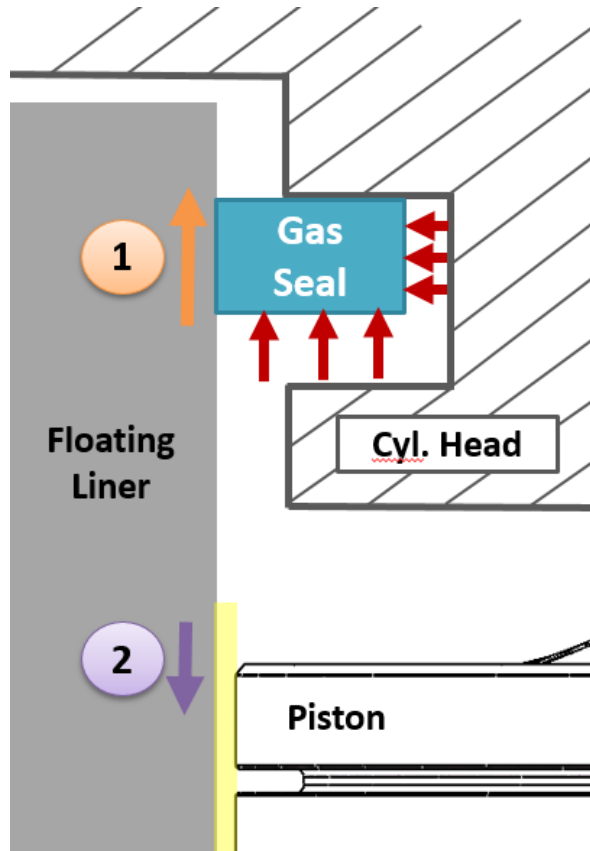


Figure 2-11. Incylinder gas sealing process – cross sectional view

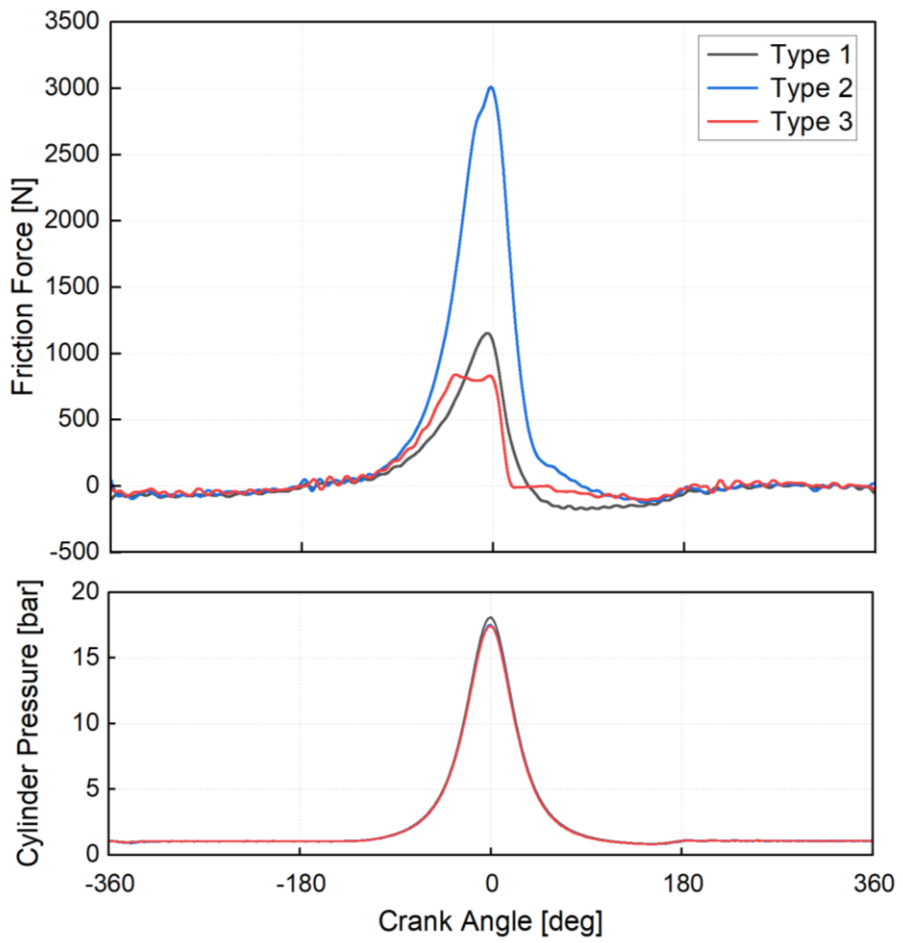


Figure 2-12. Additional gas seal friction – 3 different prototype seals

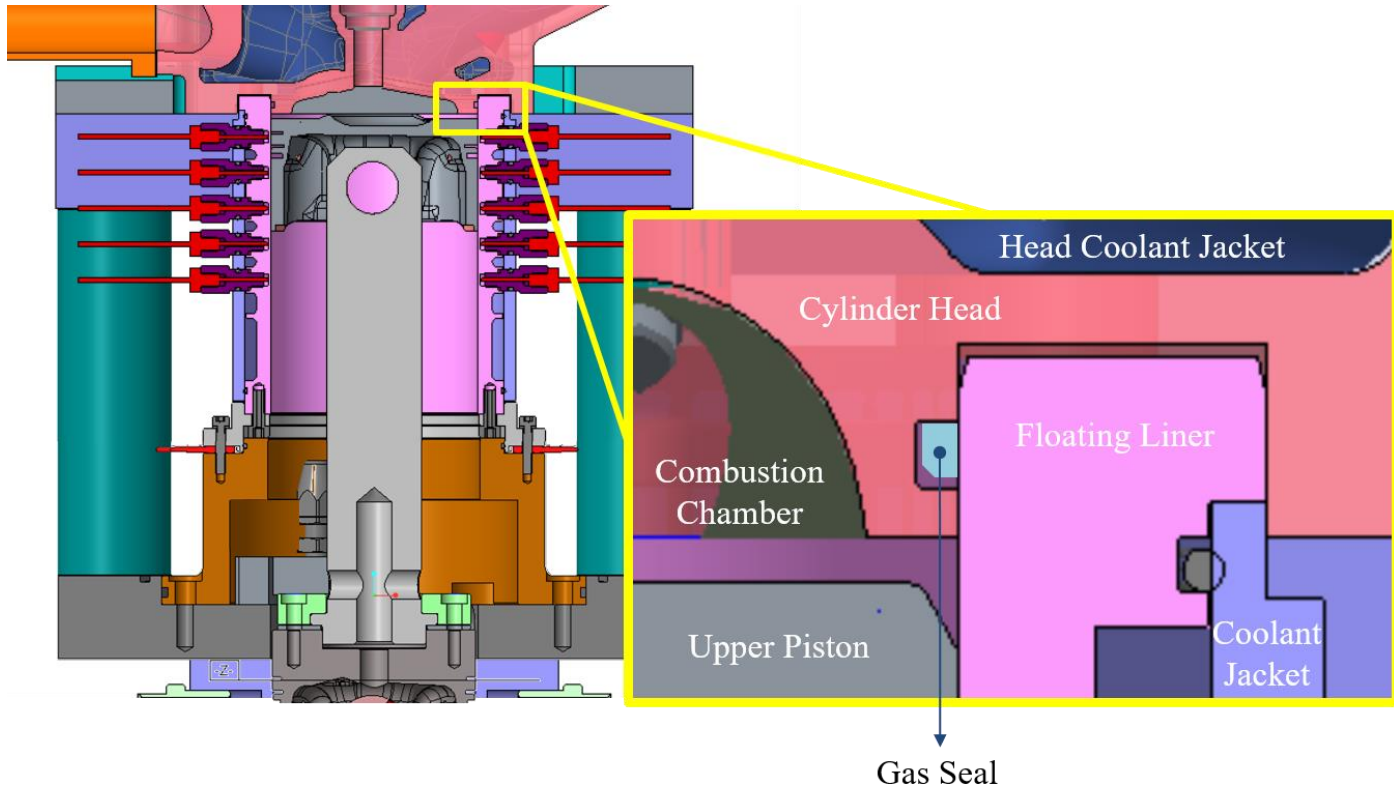


Figure 2-13. Gas seal placement of Engine V1

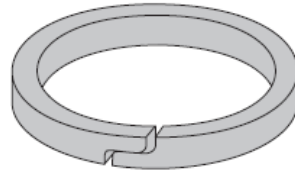


Figure 2-14. Gas seal joint shape



Figure 2-15. Gas seal placement in cylinder head groove

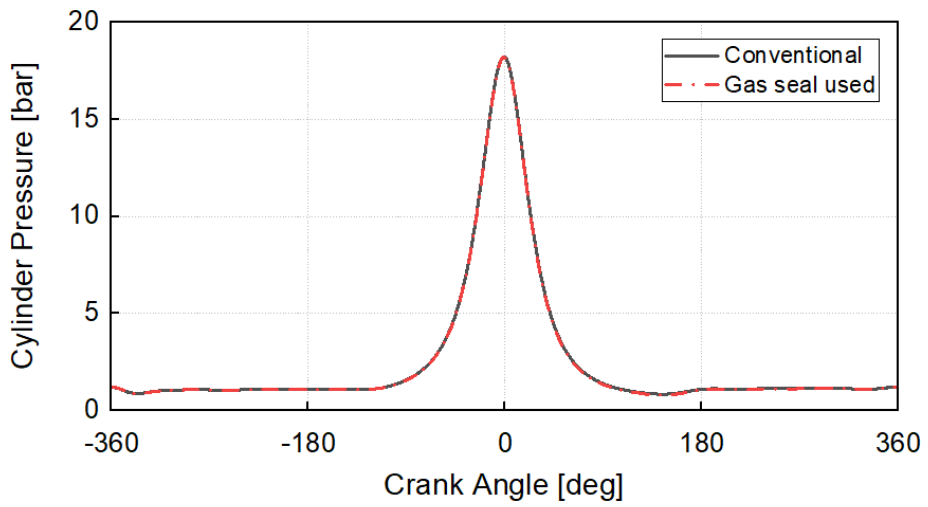


Figure 2-16. Incylinder pressure comparison

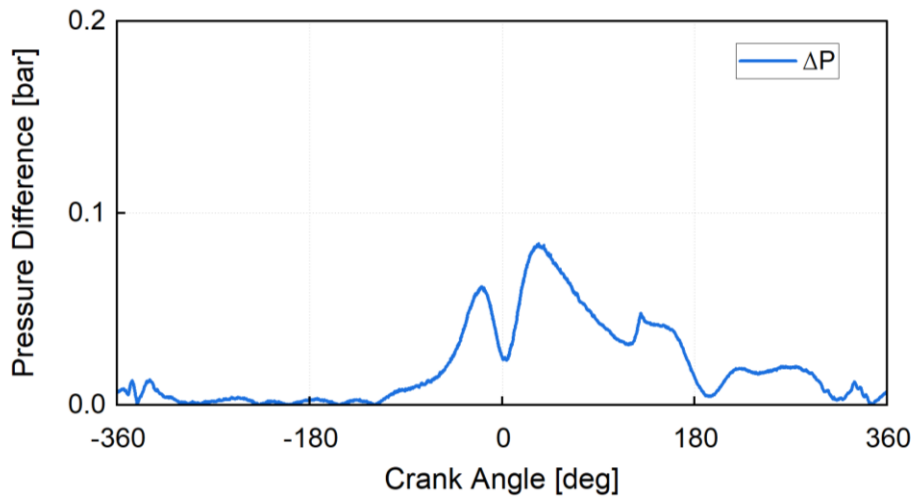


Figure 2-17. Incylinder pressure loss with final gas seal

2.4 Experimental setup & conditions

A 523cc single cylinder SI engine is used as a base engine. The detailed engine specifications are listed in Table 2-2 which focuses on the upper piston and the floating liner because the engine has two pistons and liners. However, for the bore and stroke, both pistons and liners are indicated. For the piston offset, both upper and lower pistons have the same piston offset. The alignment of the both pistons is set regarding the offset value. Main geometrical parameters such as center distance between piston pins are same as fore-mentioned in Table 2-1. As seen on Fig. 2-18, the piston ring friction measurement system is installed on the engine test bed. Visible devices and products in Fig. 2-18 are described.

A schematic setup with the equipment is shown in Fig. 2-19. The in-cylinder pressure of the engine was measured by a Kistler 6056A piezoelectric sensor, and the sensor signal passes through the charge amplifier installed in Kistler Kibox To Go. The vibration data of the floating liner and the engine block was measured by Kistler 8202A accelerometer. Friction data in 4 engine directions were measured by using washer type load cells. As shown in Fig. 2-20, 4 load cells are placed at engine front, rear, intake-side, and exhaust-side in radial direction, 90 ° apart. HBM CLP 7kN load cells and HBM CMA amplifiers are used. The actual load cells can be placed with the blue signal lines like Fig. 2-21. By tightening the M4 bolts for each load cell, nearly 2500 N is applied for each load cell as a pre-load. These signals are logged in Kistler Kibox To Go in every 0.1° crank angle.

The engine combustion was controlled by MOTEC M800 ECU. Mainly, fuel quantities and spark timing were varied by using ECU. Intake throttle valve

was controlled by LabVIEW. Moreover, the coolant temperatures of two liners, oil temperature, and lambda of the exhaust were measured and transmitted to ETAS. These parameters can be observed directly on the host PC.

Three piston rings were inserted in the piston for the experiment. The cross-sectional shape of the top compression ring (TCR) is rectangular and has a symmetric barrel face. The second compression ring (SCR) has a taper and balance under cutting. The oil control ring (OCR) is consisted of two pieces: A M-shaped steel rail and a cylindrical coil spring. The tension values and detailed dimensions of all three rings are listed in Table 2-2. All measured values and drawings in Table 2-3 are provided by the manufacturing company, KPR (Korea Piston Ring INC.).

Three main parameters affecting piston ring friction were tested. The engine speed, load, and oil temperature were varied to observe the changes in the friction force by using the newly invented measurement system. The experimental conditions are listed in Table 2-4. Engine speed was varied up to 2000 rpm except natural frequency range of the entire engine and also floating liner assembly. It was 500 rpm and 1200 rpm each. Engine load was tested up to IMEP 5 bar, and oil inlet and coolant temperatures were set the equivalent. To observe the temperature effect on the friction force, two different temperatures, 30 °C and 60 °C, were tested at engine motoring conditions. The temperatures of both floating liner and oil inlet were maintained the same for each case. As the liner wall temperature affects friction change more dominant than oil inlet temperature, the liner coolant temperature was kept within $\pm 3^{\circ}\text{C}$ of the target temperature for each case.

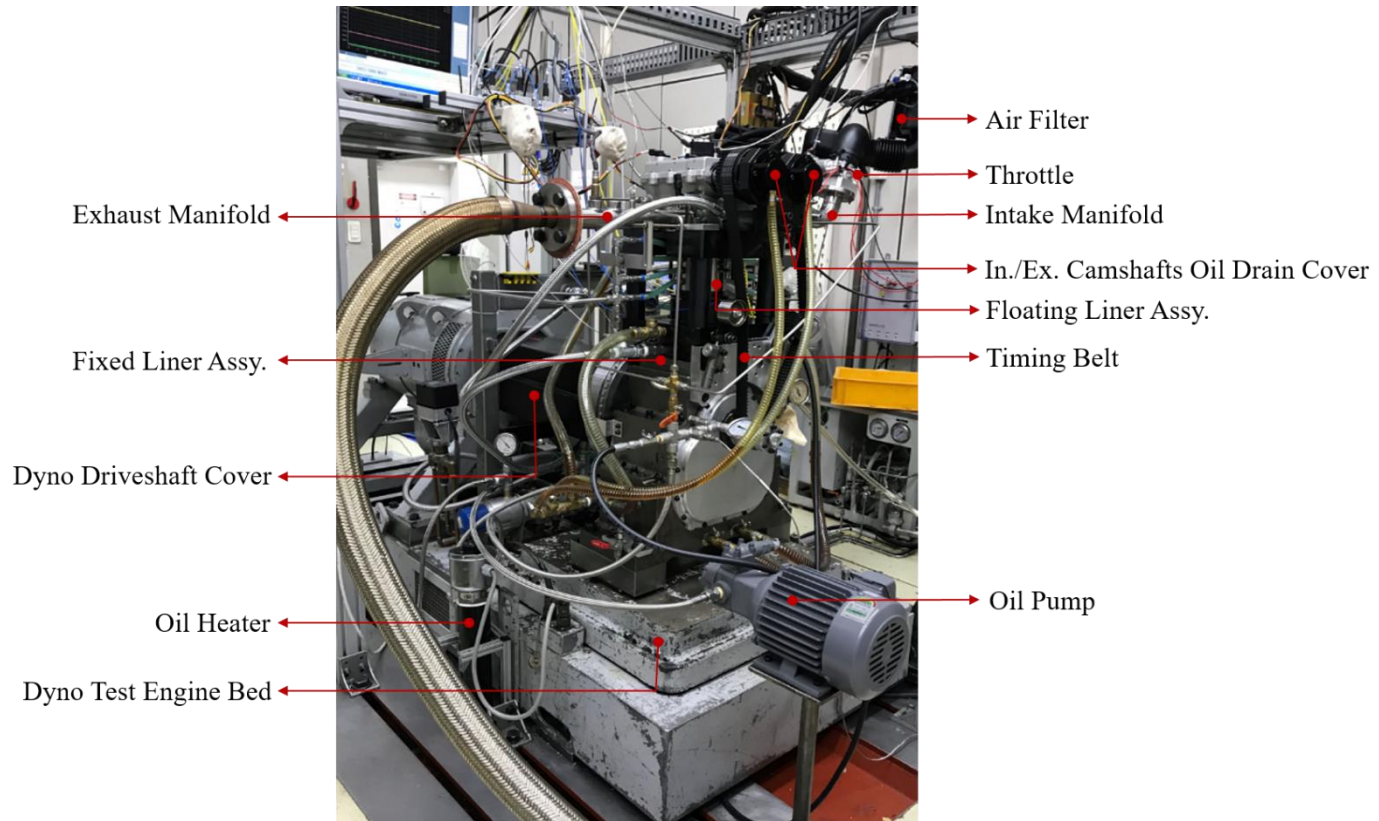


Figure 2-18. Measurement system set-up

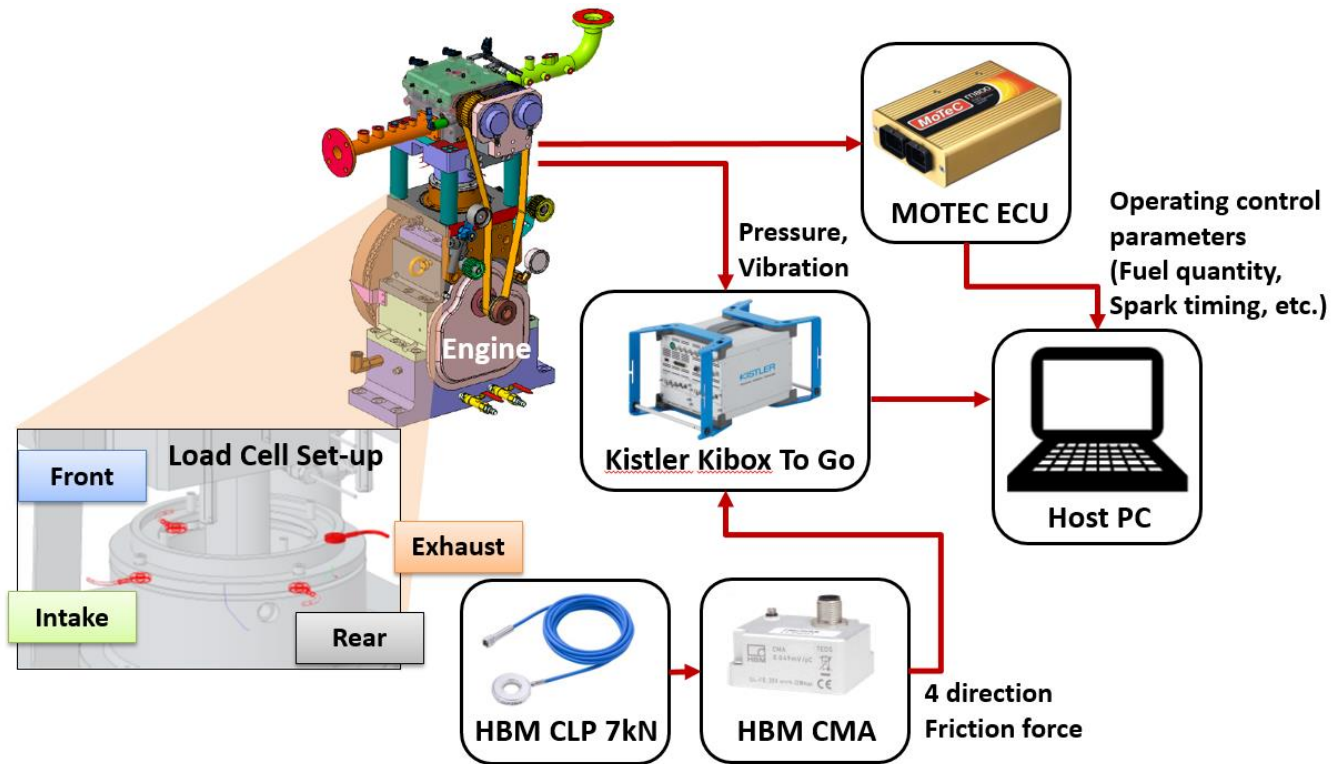


Figure 2-19. Schematic diagram of test cell set-up

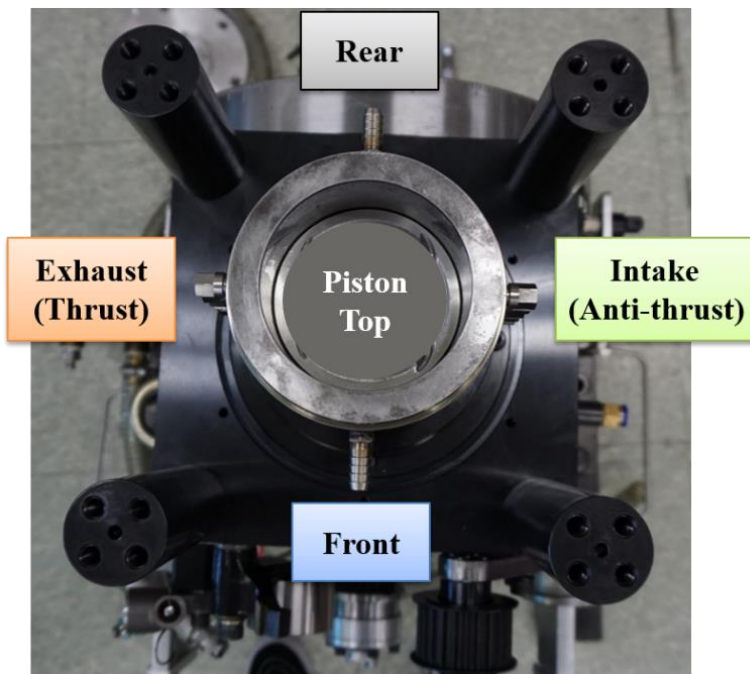


Figure 2-20. Each load cell position

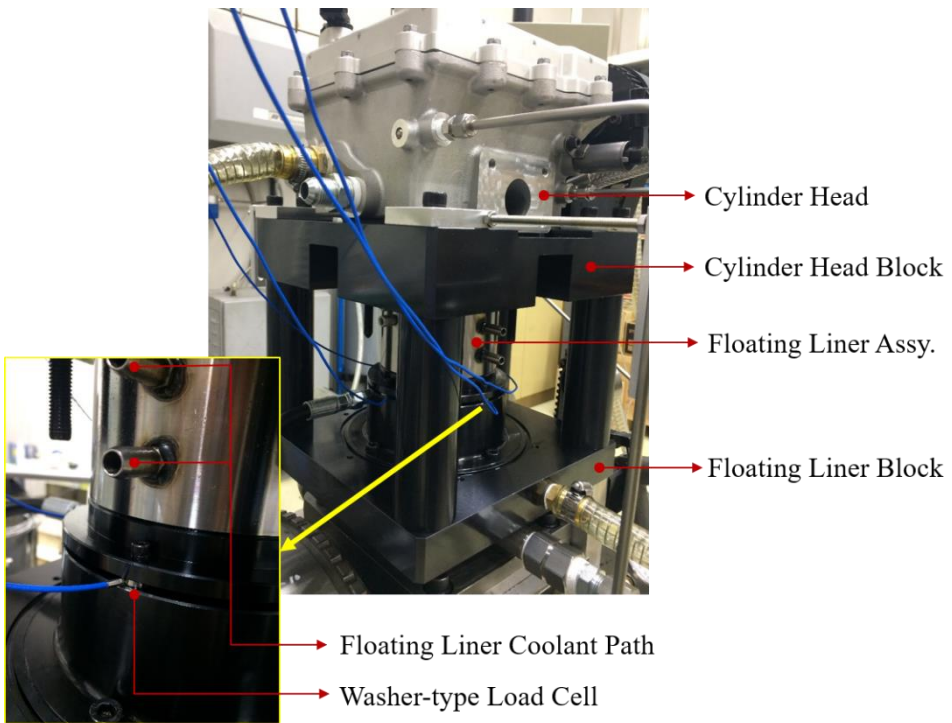


Figure 2-21. Load cell installation

Table 2-2. Base engine specifications

Engine type	Single cylinder, N/A, DPI, SI engine
Displaced volume	523 cc
Bore × Stroke	88 mm × 86 mm (Upper piston)
	86 mm × 86 mm (Lower piston)
Piston offset	0.8 mm
Compression ratio	10.5
EVO	bBDC 68°
EVC	aTDC 1°
IVO	aTDC 10°
IVC	aBDC 67°
Max. valve lift	10 mm

Table 2-3. Test ring specifications

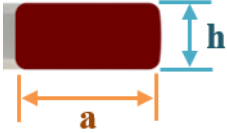
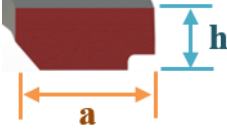
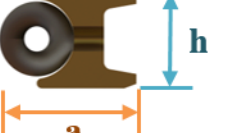
	TCR	SCR	OCR
Tension [N]	8.9	8.0	24.7
End gap [mm]	0.26	0.48	0.33
Description	Symmetric Barrel Faced	Taper / Balance Under Cut	D.V.M / Coil Expander
Cross-sectional view			
Width ; h [mm]	1.17	1.18	1.98
Thickness ; a [mm]	3.13	3.55	2.72

Table 2-4. Experimental conditions

Engine speed [rpm]	600 ~ 2000
Engine load [bar]	IMEP 2 ~ 5
Oil inlet / Coolant temperature [°C]	30, 60 * For the lubricant, SAE 5w-30 is used.

2.5 Experimental results from Engine VI

The motoring and firing conditions were tested at various engine speeds, oil temperatures, and coolant temperatures. The engine speed and load were varied up to 2000 rpm and IMEP 5 bar, respectively, excluding the natural frequency points of the engine. The friction force data for each case was captured 300 cycles. And the plotted data is 300 cycles averaged data with the signal filtering. Low pass filter was used to eliminate the extra noise from engine vibration. The cut-off frequency was set by frequency analysis with observing Fast Fourier Transform (FFT) of the averaged raw data for each case.

The motoring and firing conditions are plotted in Fig. 2-22. Both experiments were performed at 700 rpm. As shown in the graph, the friction force has both positive and negative values. The value changes for every stroke and indicates the force direction. -360° , 0° , and 360° , were considered top dead centers (TDCs). 0° indicates the firing TDC for the firing cases. Similarly, -180° and 180° were considered bottom dead centers (BDCs). A compression stroke occurs from -180 to 0° ; thus, the positive force value represents the compression force of the load cells.

As the in-cylinder pressure increased, the lubrication regime shifted according to the Stribeck curve. The boundary lubrication near the firing TDC, where the crank angle is 0° , shows the highest friction force compared to the other locations. The friction force at IMEP 4 bar shows a higher value around firing TDC than that at motoring condition, for the in-cylinder pressure at IMEP 4 bar condition is higher than that at the motoring condition. In addition, the friction force, especially at the compression and expansion strokes, shows that the force

direction changes as the piston moving direction. As shown in Fig. 2-1, the piston thrust force creates a signal distortion by working on the floating liner. However, the experimental result from the new measurement system doesn't show the force signal distortion such as force direction change within one stroke. Thus, this implies that the piston thrust force can be minimized with the new system. Piston lateral motion did not affect the friction measurement. As a result, changes in piston ring friction were specifically observed in this research.

Similarly, various engine load conditions were tested at 700 rpm, and the results are shown in Fig. 2-23. Figure 2-23 also shows the effect of the in-cylinder gas pressure on the piston ring friction force. As the gas pressure increased, the lubrication condition shifted towards the boundary lubrication regime. Thus, the friction force near the cylinder pressure peak differs considerably between IMEP 4.7 and IMEP 2.4 bar cases.

It has proved that the new system can capture the friction force change as the in-cylinder pressure change with minimized thrust force effect. However, the instant friction drop was measured after firing TDC right before peak pressure. The friction force drop increases as the cylinder pressure increases. If the friction drop is caused by the change of the lubrication regime, the friction force has to be increased which would decrease the friction drop. The further test was implemented to see the tendency of the friction force drop. As shown in Fig. 2-24, friction force was measured at various spark timings. The test was implemented at 1000 rpm. The spark timing was retarded from the reference case, IMEP 4 bar. And the spark timing retarded 5° , 10° , and 15° from the reference, bTDC 8° . In the graph, the friction force at compression and expansion strokes is plotted to see friction force drop in detail with the corresponding cylinder pressure. The crank angles of the cylinder pressure peaks for each case were pointed with the same

colored dots. The cylinder pressure decreases as spark timing is retarded, and the friction force drop occurs near the pressure peak point. It is confirmed that the friction force drop is related with the cylinder pressure change. The friction force drop does not affect the overall friction tendency, because it occurs at near the firing TDC where piston speed is relatively low. Nevertheless, the cause of the friction drop was investigated further and fixed for more reliable friction measurement. It will be explained in the following chapter.

The friction force exhibited different characteristics at various engine speeds under motoring conditions. The change in engine speed is directly related to that in piston speed. When the piston speed increased, the piston ring friction lubrication regime tended to move towards the hydrodynamic lubrication regime. As seen in Fig. 2-25, the friction force at the boundary lubrication decreases with an increase in the engine speed near the dead centers, where the piston speed becomes zero. For the hydrodynamic lubrication zone, the 2000 rpm case shows a higher friction force than the 700 rpm case.

With the new measurement system, the gas pressure effect working on the top of the piston can be eliminated and can be tested. At engine motoring condition without engine load, oil temperature effect and engine speed effect can be observed.

Two different oil temperatures were tested to determine the effect of the oil viscosity on the piston friction. Oil temperatures of 30°C and 60°C were recorded at 700 rpm. As the oil temperature increased, the oil viscosity exponentially decreased. In addition, the lubrication regime changed. As plotted in Fig. 2-26, the boundary friction force near the TDCs and BDCs increased as the oil viscosity decreased. On the other hand, the hydraulic friction force between the TDC and BDC decreased as the oil viscosity decreased. When the oil

temperature increases, the oil tends to flow rather than attach to the liner wall because of its low viscosity. Therefore, the oil pressure is not sufficiently high to prevent metal-to-metal contact when the piston speed is low, such as at TDCs and BDCs. Because the oil film is thinner, the hydraulic shear stress is lower at the position between the TDC and the BDC.

However, as seen in Figs. 2-25 and 2-26, the friction force signal was measured with the noise that has the same frequency with the engine speed. The friction force decreases constantly from initial of stroke to the end of the stroke regardless of the lubrication regime change within a stroke. When there is no pressure on the piston top, the friction force at TDCs would be similar with the friction force at BDCs. In Fig. 2-26, the friction force at crank angle, -180° , diminishes drastically to zero compared with the friction force at 0° , and the tendency repeats.

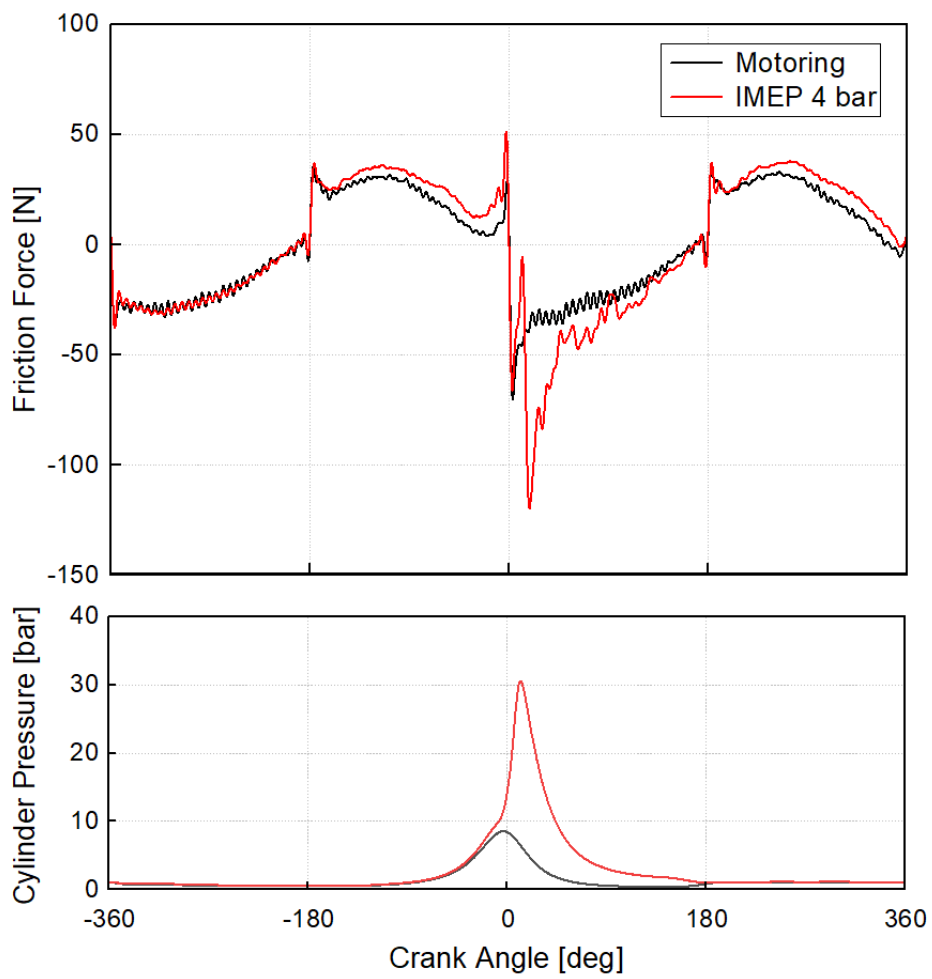


Figure 2-22. Friction force at motoring/firing conditions

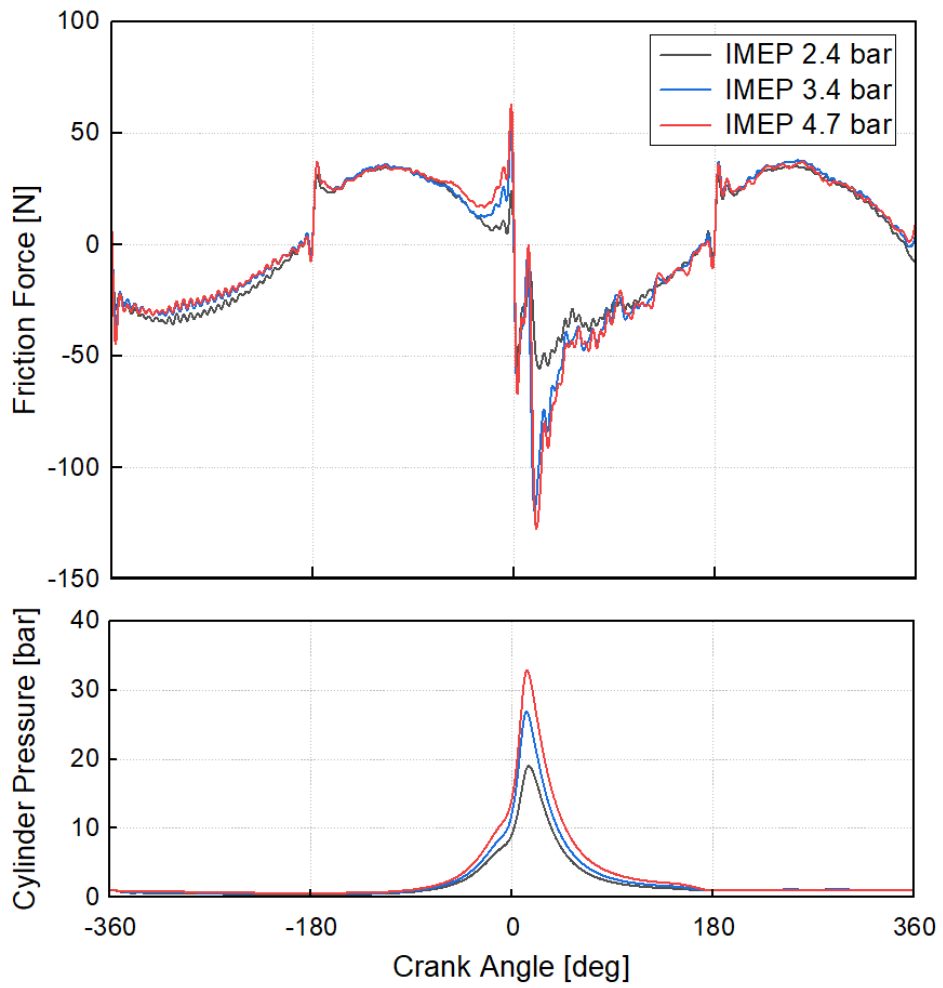


Figure 2-23. Friction force at various firing conditions

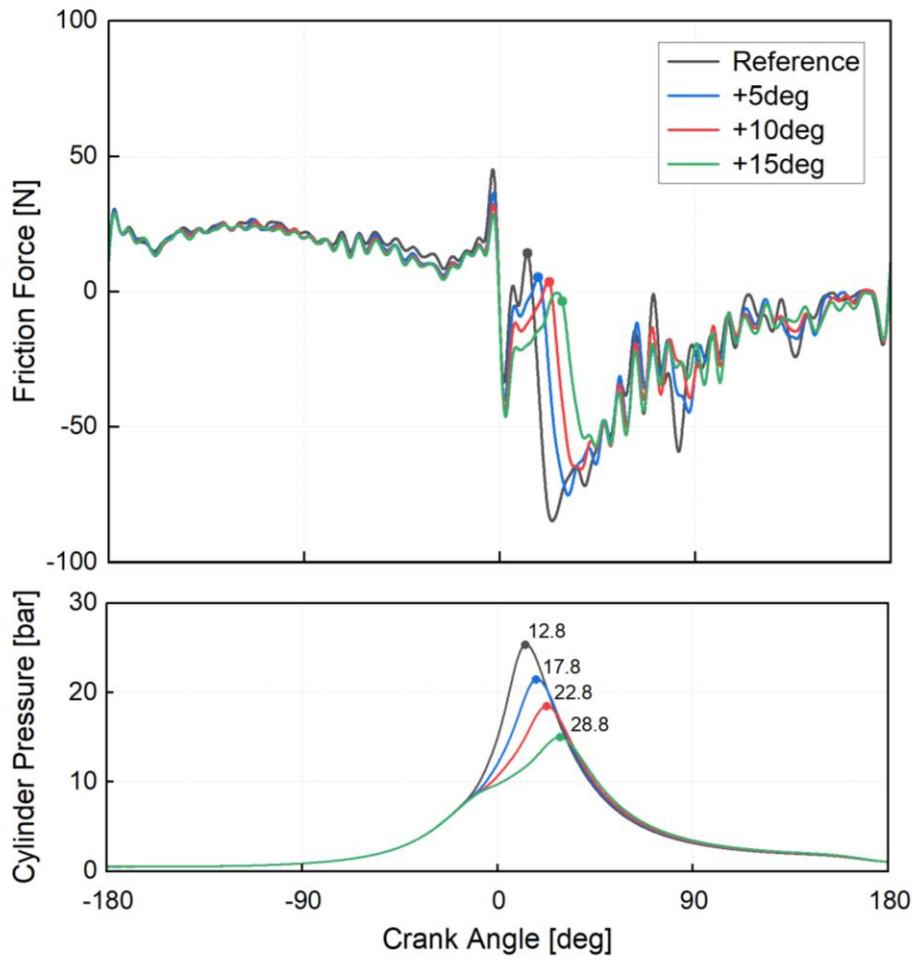


Figure 2-24. Friction force drop according to spark timing

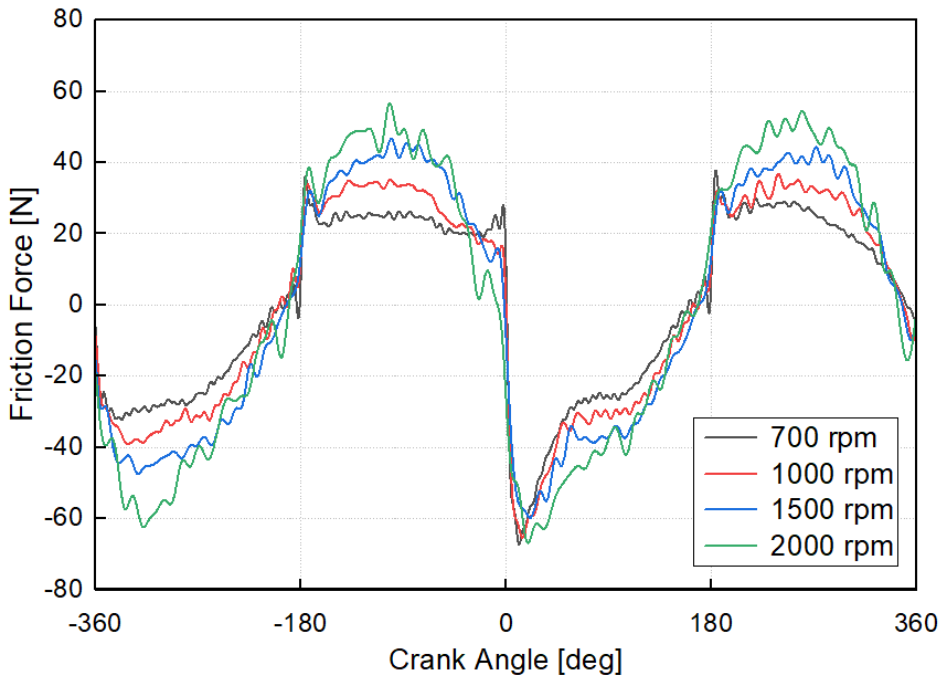


Figure 2-25. Friction force at various engine speeds

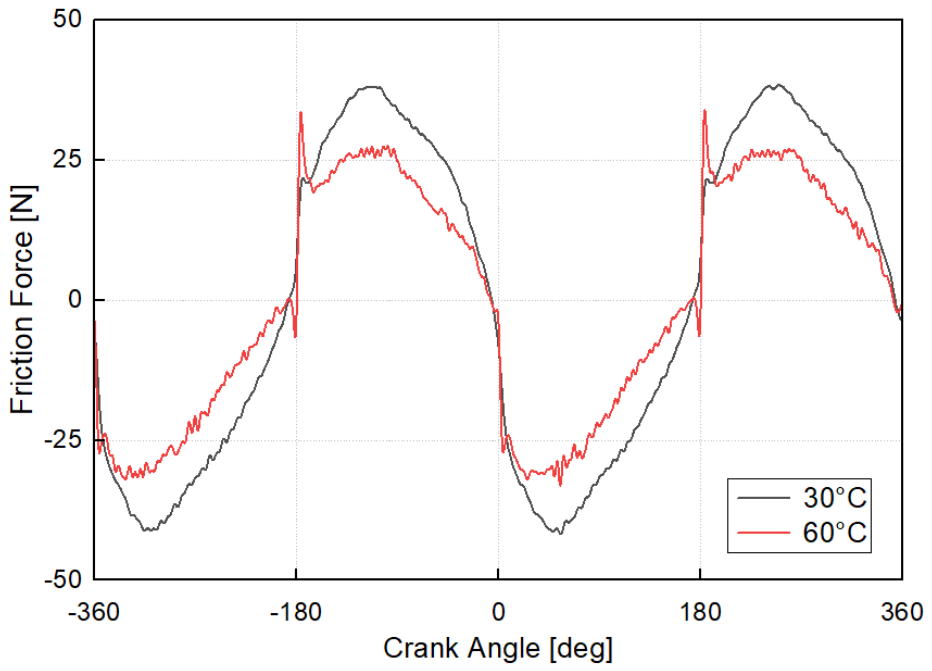


Figure 2-26. Friction force at various oil temperature

2.6 Remaining issues from Engine V1

The floating liner method is useful for investigating piston friction. However, it remains challenging to exclude other force factors from the measured data. The piston secondary motion from the angle created between the con-rod and piston center is highly reduced to investigate the friction force of the piston rings. Therefore, ‘double pistons’ structure was adopted, which is different from the conventional engine structure for the floating liner method. The experimental results show a good agreement with the base theory at various cylinder pressures and oil temperatures, and influence of the piston thrust force is highly reduced on friction measurement.

Although the newly developed measurement system for piston ring friction has proven its ability to track frictional changes, there is a need for further improvement to obtain reliable data. Two main improvements were done for Engine V2. First, a system that can change only the piston and piston ring from the engine was considered to achieve improved repeatability of each experiment. Second, the extra force factors that affect the measurement of only the piston ring friction were checked and removed as much as possible.

Chapter 3. Development Process of a New Piston Ring Friction Measurement System – Engine V2

3.1 Design improvements from Engine V1

While developing engine V1, the engine has undergone several trials to build a more reliable system. Each engine part went through geometry modifications, and especially the clearance between the floating liner and the cylinder head where the gas seal sits had been changed several times. In micro-scale, the clearance cannot be even along the circumference. There was a partial solid contact on relatively smaller clearance area between inner radial surface of the floating liner and the cylinder head groove. The floating liner and the cylinder head are placed in two different engine blocks. It is hard to synchronize the cylinder head center and the floating liner center. The center position could be changed by assembly clearance, so the radial clearance of the inserting area is different between the floating liner and the cylinder head. Therefore, to avoid clearance effect on friction measurement and to synchronize the cylinder head center and floating liner center, inserting areas of cylinder head and head block were modified in cylindrical shape. As shown in Fig. 3-1, the cylinder head seat on the head block has been changed from square shape to circular shape. The inserting area of the cylinder head has been reworked in circular shape accordingly.

Although the experimental results showed a good repeatability for each case at the same experimental condition, there has been an uncertainty on the engine set-up process. Since the clearance between the piston and the liner is in a few tens of micrometers, the relative position between the piston and the floating

liner can affect the friction measurement. There is a high possibility on clearance change between each engine part during assembly process. The uncertainty on clearance management can aggravate the error on experimental results.

In order to investigate piston ring friction with maintaining the same experimental conditions, piston assembly process was reconsidered. For the previous assembly process, engine cylinder head needs to be taken out first to disassemble the piston, similar with the assembly process of the conventional engines. The floating liner has to be disassembled with the piston because of the double pistons structure on engine V1. During the stacking up process from the floating liner to cylinder head, a few micrometer clearances from the bolting process can make a different relative position between the piston and the floating liner. Furthermore, the clearance for the full assembly can be varied by each assembly process. The assembly process of engine V1 was not only time consuming, but also unfavorable for the piston ring experiment.

The engine design has been modified to minimize experimental errors, and a new design is adopted on engine V2. With the new design, the upper piston can be disassembled with keeping the floating liner and the cylinder head installed. As shown in Fig. 3-2, the extended con-rod of engine V2 is divided in three pieces. By taking out the middle piece of the extended con-rod, the upper piston can be disassembled easily without any position changes of the floating liner. In Fig. 3-6, the middle piece of the extended con-rod, which is also referred as a coupling, can be disassembled as moving the piston from TDC to BDC. After taking out the coupling, the piston with the top piece of the extended con-rod can be easily taken out through the window at the floating liner bed. This is a quick and easy process for piston and piston ring exchange without changing other experimental conditions. Therefore, with the improved design, geometrical parameters of piston

rings can be solely evaluated and can be compared each other. As the new piston assembly method is added on Engine V2, the center distance between upper and lower piston pins has been increased as described in Fig. 3-3. The distance has been changed from 230 mm to 288 mm.

Moreover, as shown in Fig. 3-3 on the zoomed in cross-sectional view, the outer edge of the floating liner assembly has been modified into a chamfer. This modification could give an effect of the effective area reduction of the liner top for the leaked gas pressure. The effective area has been reduced approximately 52% from Engine V1. Also the clearance of the flow path has been set for the possible gas leakage to avoid the pressurization on the top of the floating liner.

For the final product, as shown in Figs. 3-4 and 3-5, the Engine V2 follows the similar engine structure with the Engine V1. However, the temperature sensors along the liner in piston stroke direction have been removed for more accurate friction measurement. The thermocouples were set with the ignorable amount of an extra force on the friction measurement with Engine V1, but there is a high possibility on a liner deformation during the manufacture and assembly process of the thermocouples. For the coolant jacket, 4 sectioned flow paths remain the same with the previous version. As seen in Fig. 3-5, the oil jet is placed on the floating liner bed not on the floating liner block like Engine V1. However, similar with the Engine V1, the oil jet pressure is kept low to not to affect piston friction measurement. Besides, four load cells are set at the same side with the Engine V1. For the Engine V2, a shim plate is used between the floating liner bed and the load cells to retain the same flatness throughout the experiments.

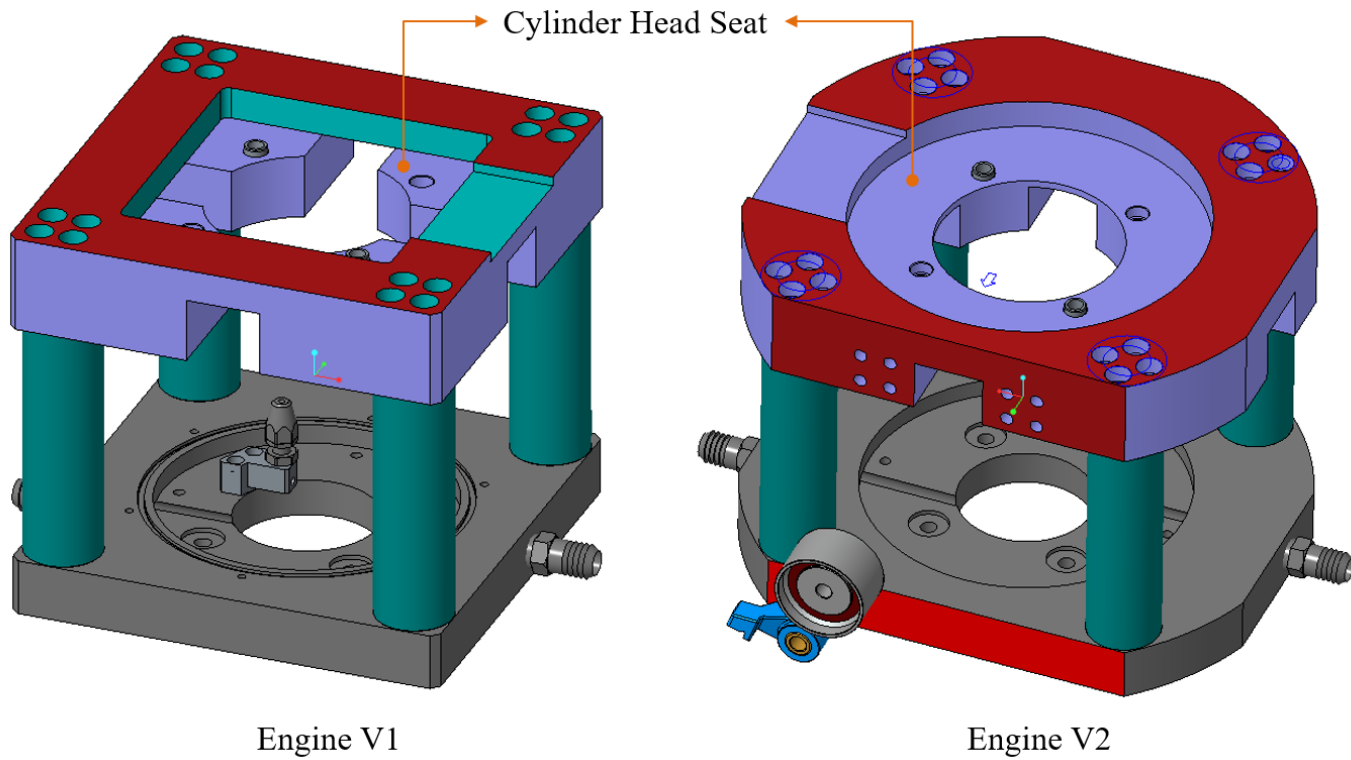


Figure 3-1. Cylinder head block modification

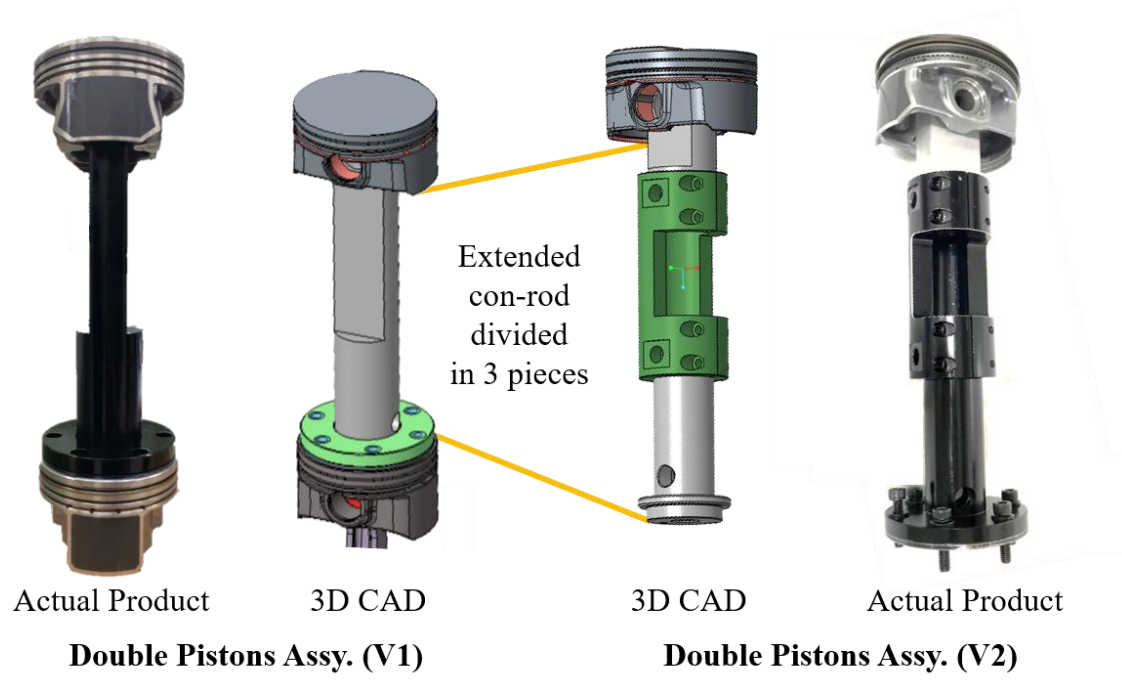


Figure 3-2. Extended con-rod modification

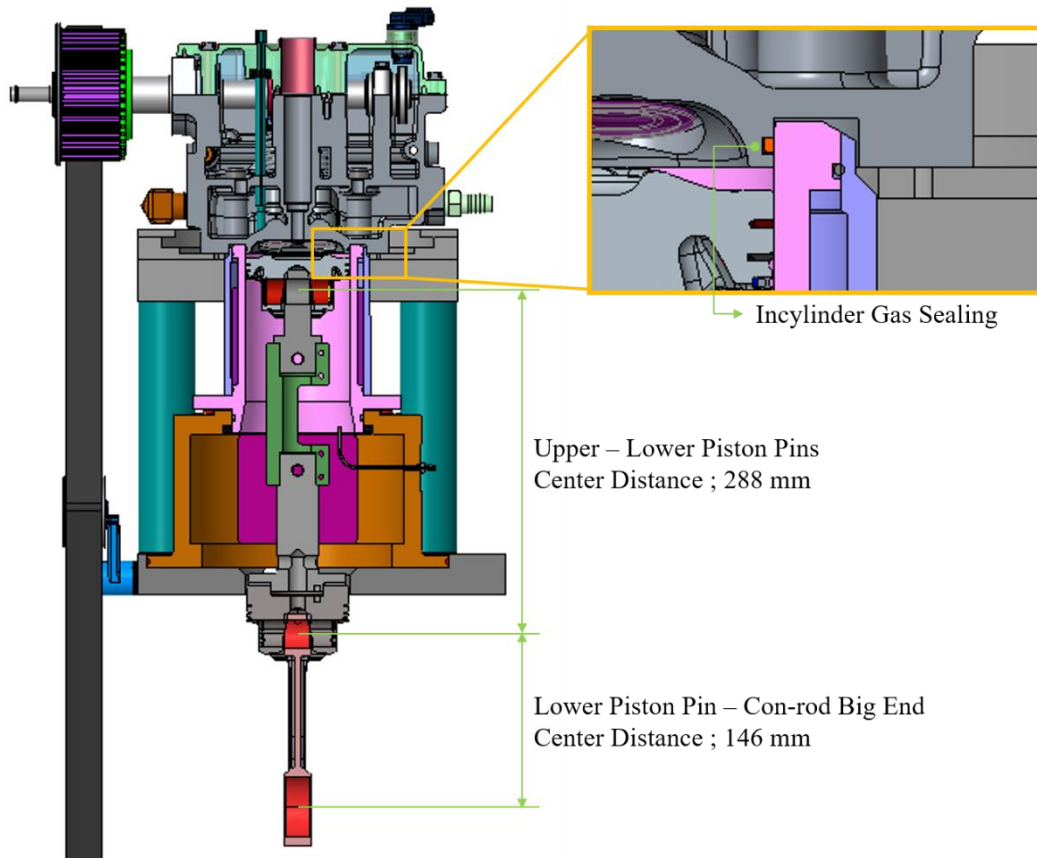


Figure 3-3. Design changes from Engine V1 – cross sectional view (Intake-side cut)

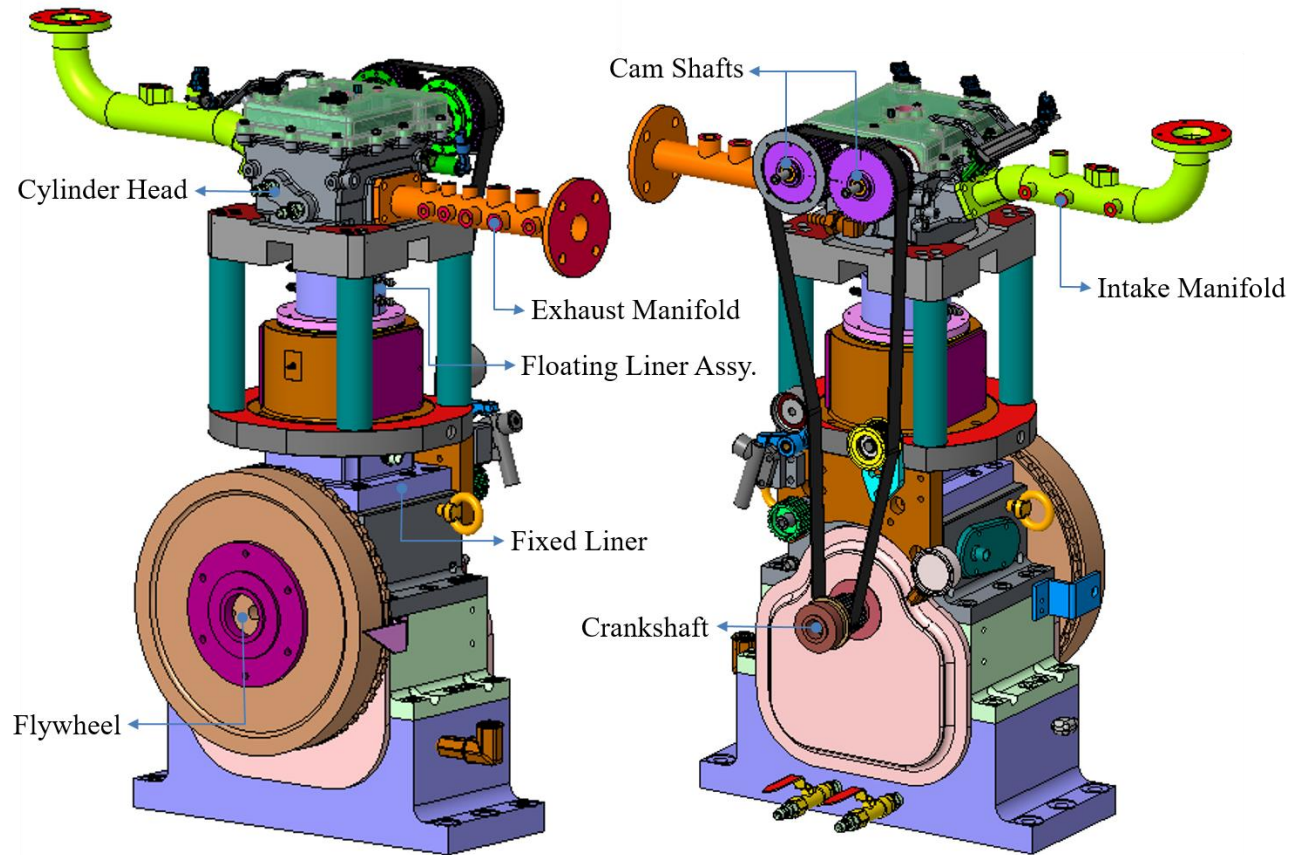


Figure 3-4. Engine V2 (L – Engine rear view, R – Engine front view)

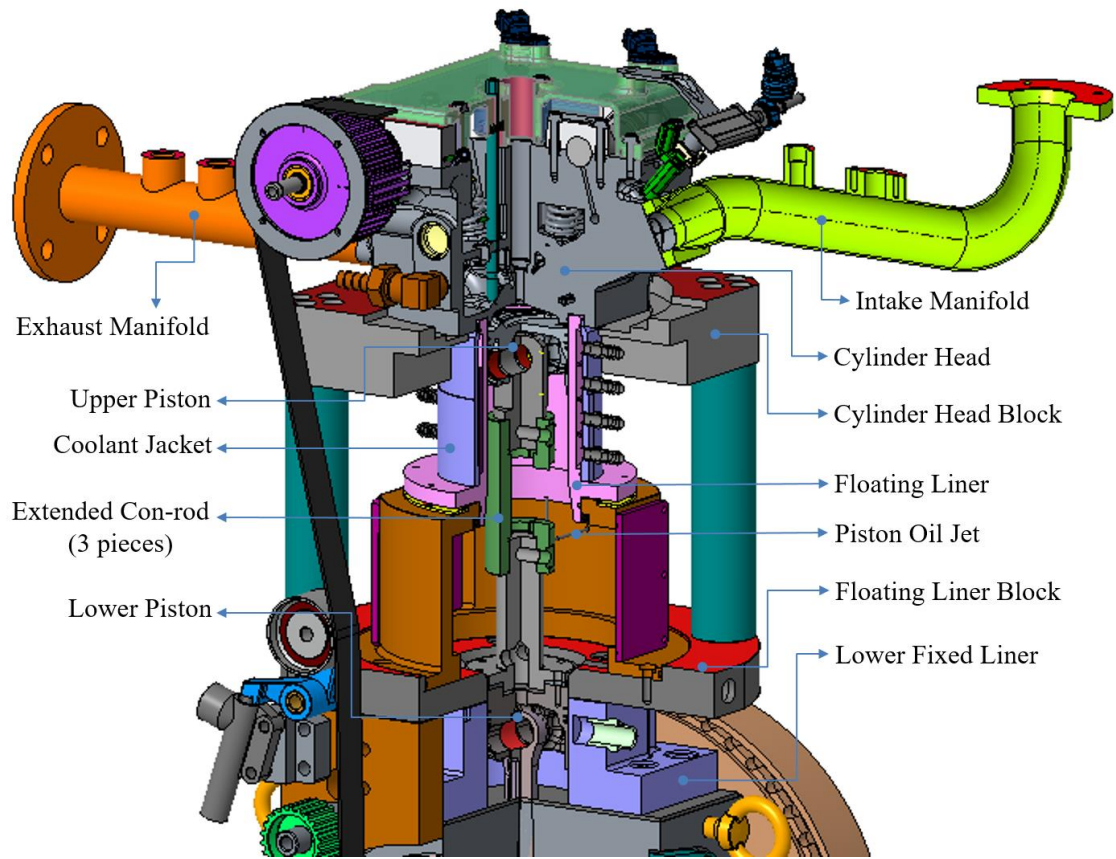


Figure 3-5. Detailed structure of Engine V2 – 90 ° engine front-intake cutting view

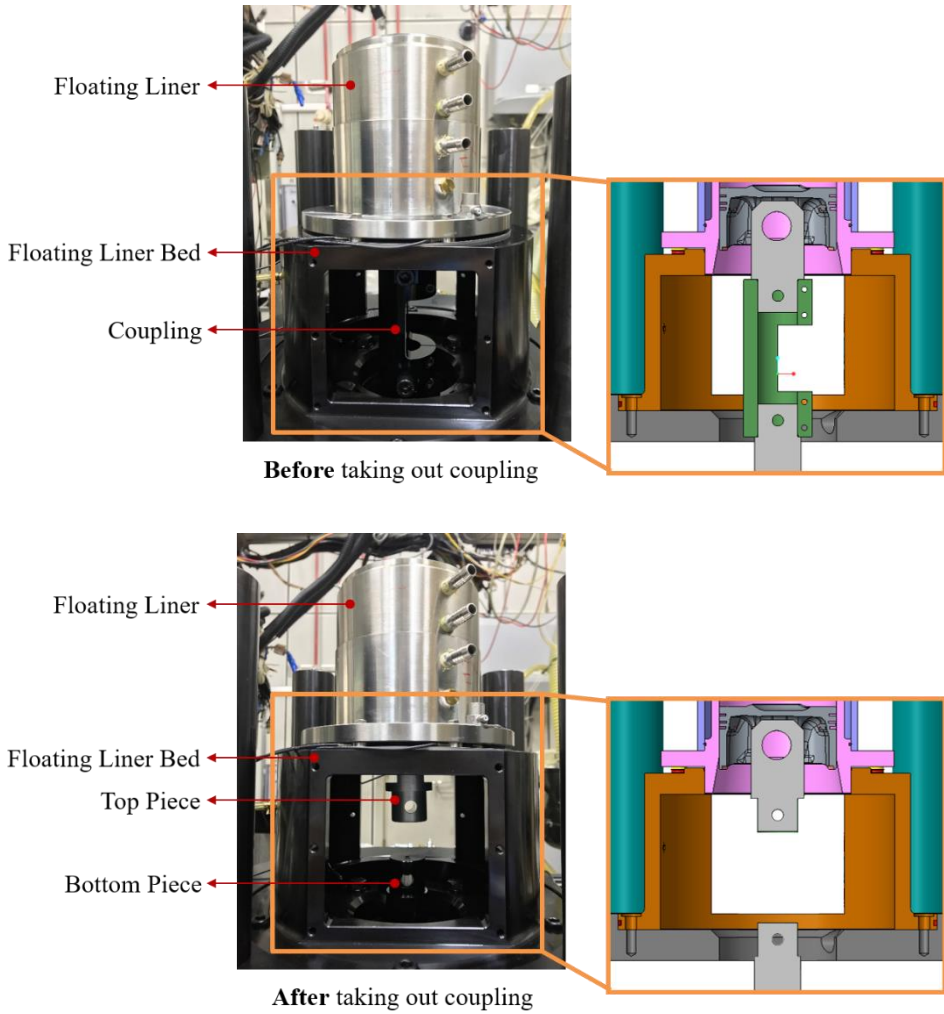


Figure 3-6. Piston disassembly process – 3 pieces extended con-rod

3.2 Extra force elimination

The floating liner can be affected by piston friction force as well as other force factors. The floating liner can move independently from the engine block. As seen in Fig. 3-7 [12], various forces can make an extra movement on the floating liner, and this affects friction measurement. Mainly, 5 different force factors can be considered in the conventional floating liner system.

1) Piston – liner contact force components ; F_N

For the conventional floating liner system, piston has a thrust force when gas force is working on the top of the piston. The contact force between the piston and the liner can distort the friction data with an irregular oscillation. However, the ‘double pistons’ structure is adopted in the new measurement system. This force factor can be negligible.

2) Leaked gas force working on the top of the floating liner ; F_G

When the gas sealing ring loses its function, the gas leaks through the clearance. The leaked gas pressure eventually creates an extra force on the friction measurement. If the clearance is not big enough to release the gas pressure working on the top of the floating liner within a short period of time, it is likely to occur. As seen in Fig. 3-8, film type strain gauges are used to measure leaked gas pressure working on the top of the floating liner. Strain gauges are attached on the top of the floating liner in 4 directions, engine front and rear, intake and exhaust. As plotted in Fig. 3-9, the gas pressure tends to act on exhaust side. However, the effective gas force is negligibly low. And the gas force is not

proportionally increased by cylinder pressure. Even if the effective area is considered, the gas force acting on the floating liner is still negligible.

3) Friction force from gas sealing ring on the floating liner ; $F_s(t)$

In the contrast to the second force factor, when the in-cylinder gas sealing is favorable, sealing ring contacts with the liner wall. This creates an additional friction. For the new system, low friction material is adopted to avoid the extra friction force from the sealing.

4) Crankcase pressure oscillation ; $F_{cc}(t)$

For the conventional engine, the crankcase is in a closed state. Consequently, there is a pressure oscillation in the crankcase as in-cylinder volume changes. The pressure oscillation in the crankcase can interrupt friction measurement. To minimize the crankcase pressure acting on the floating liner, the conventional crankcase needs to be modified.

However, not like conventional floating liner system, the new system has two different volume zones under the measuring piston. Double pistons structure divides crankcase volume in two, which are the one between the upper and the lower pistons and the other under the lower piston. Therefore, as shown in Fig. 3-10, a few breathing holes are applied on the two zones. The floating liner and moving pistons are not affected by the crankcase pressure.

5) Inertia effect of the floating liner ; $F_i(t)$

As shown in Fig. 3-7, the floating liner has the inertia force according to the piston movement. Since the inertia force of the floating

liner dominates in Z-direction which is same as the direction of the piston stroke, the load cells also capture the inertia force. Thus, the inertia force needs to be considered to draw only friction force results out [19]. As previously shown in previous chapters, the friction force results trace parameter change, though the results had a signal distortion from inertia effect. One of the same experiment cases shown in the Fig. 2-25 is plotted in Fig. 3-11 as an example of the signal distortion from the inertia effect. As pointed in Fig. 3-11, the absolute friction force values at the close timeline have a big difference. Even though the two points wasn't measured at exactly same time, the boundary friction is increased approximately 5 times when piston switches its direction in opposite. Moreover, the overall absolute friction force of each stroke decreases from the hydrodynamic lubrication zone to the end of the stroke. It's hard to observe each lubrication regime within each stroke and friction force change in each case with the distorted force signals.

The inertia force of the floating liner can be measured with an accelerometer. Kistler 8202A accelerometer is attached on the floating liner block to measure a vibration of the floating liner in piston stroke direction. With the vibration data, therefore, the inertia force of the floating liner can be estimated as seen in Fig. 3-12. As an example, one of the same case of the Fig. 2-25 is used to see how the friction force data changes. Fig. 3-12 shows the original measured friction force data and corresponding inertia force data. The friction force data follows inertia force tendency. When the inertia force is eliminated in the original friction force data, the modified friction force data shows a clear change of the lubrication regime within each stroke as shown in Fig. 3-13.

The inertia effect can also be considered to eliminate the friction force drop at engine firing conditions. The friction and inertia force are plotted with the cylinder pressure in Fig. 3-14. The IMEP 5 bar case is used for an example of the inertia effect on the friction force at firing condition. As seen in Fig. 3-14, the inertia force shows relatively high fluctuation at expansion stroke compared with the other strokes. At the friction force drop point, the inertia similarly changes drastically.

After the inertia force removed from the friction force, the friction force drop has been modified as shown in Fig. 3-15. With the previous friction force data, the friction force increase according to the pressure increase cannot be observed because of the force drop. As indicated in Fig. 3-15, the crank angle at the peak cylinder pressure is pointed with a dot. Moreover, same timing points for the friction force are also indicated with dots. The friction force before eliminating inertia force effect, the force drop occurs near the pressure peak. However, after the force modification, maximum friction force occurs near the pressure peak point.

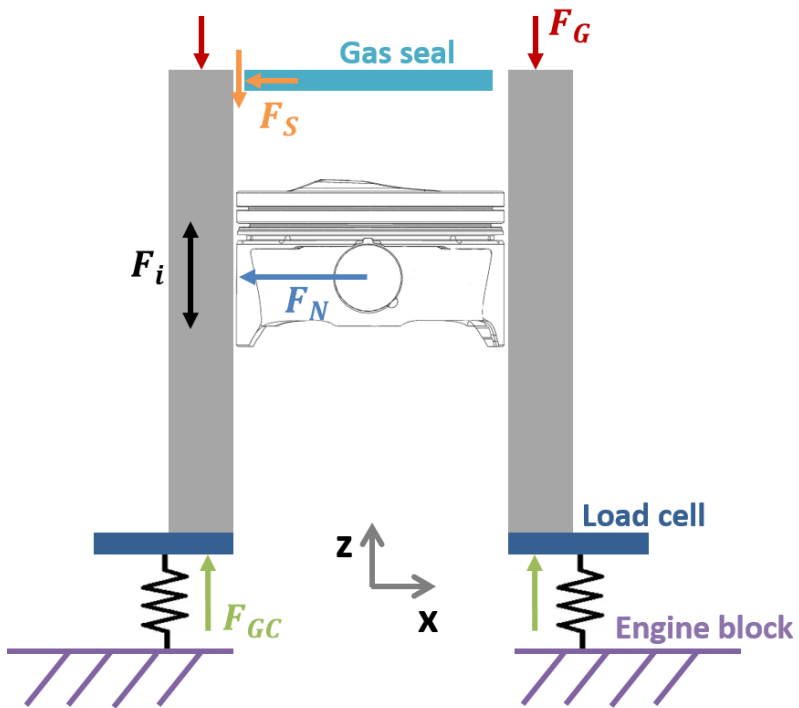


Figure 3-7. Force balance of the floating liner [12]

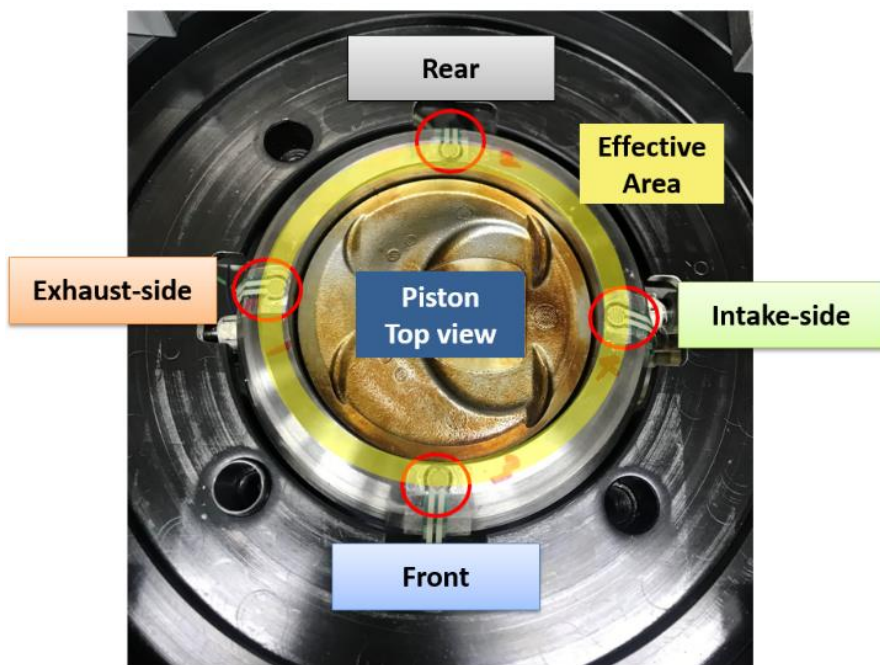


Figure 3-8. Film type strain gauges in 4 engine directions

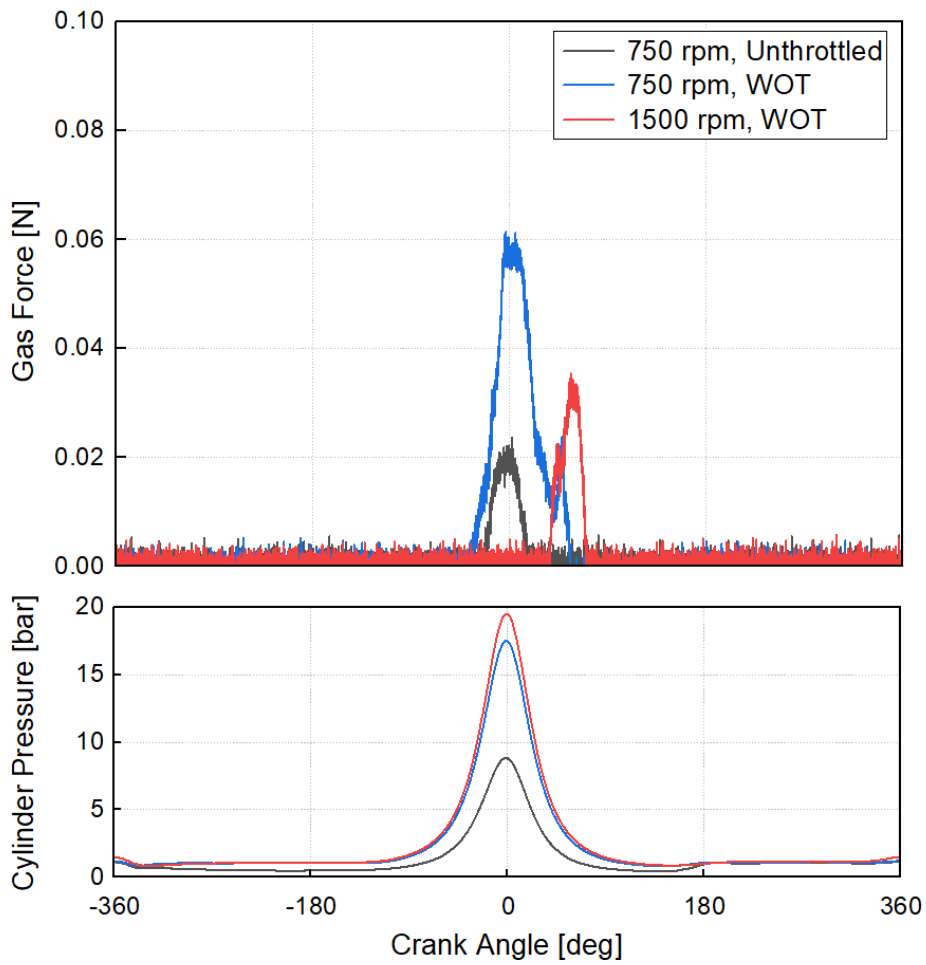
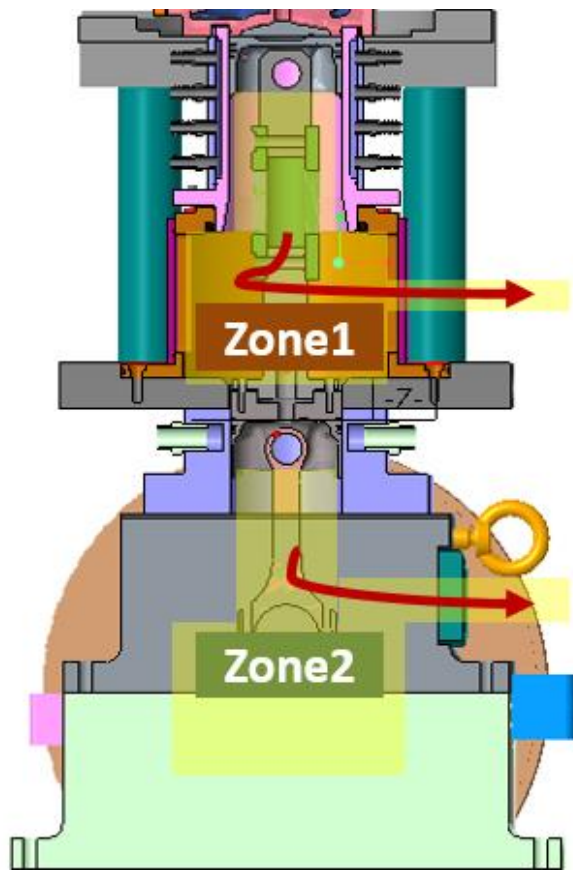
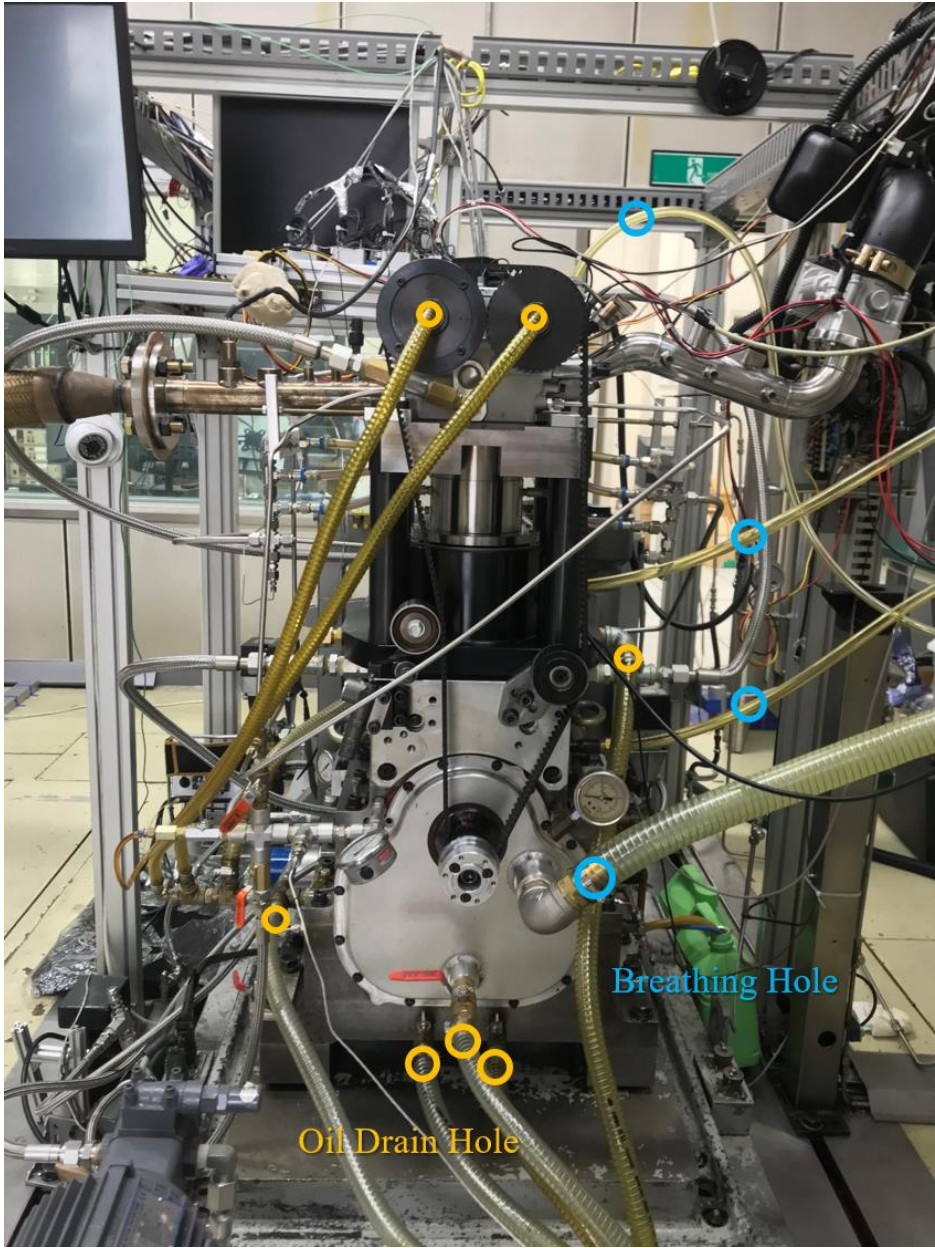


Figure 3-9. Gas force measurement



(a) Two separated crankcase zones by lower piston

the figure (b) continued on the next page.



(b) Breathing holes and oil drains for the final engine
Figure 3-10. Minimization of crankcase pressure oscillation

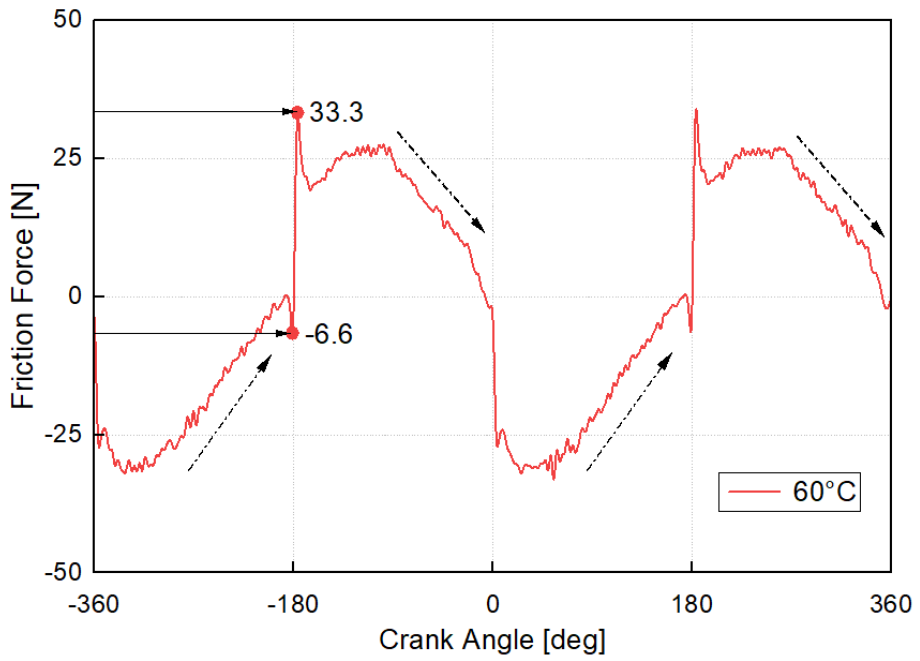


Figure 3-11. Signal distortion from inertia effect

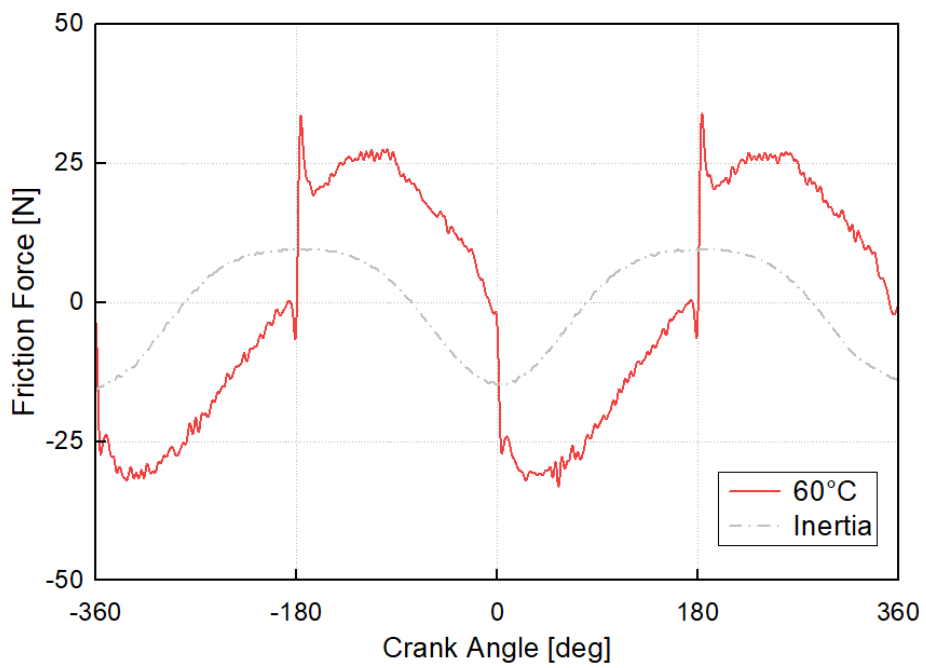


Figure 3-12. Friction force data before inertia force consideration

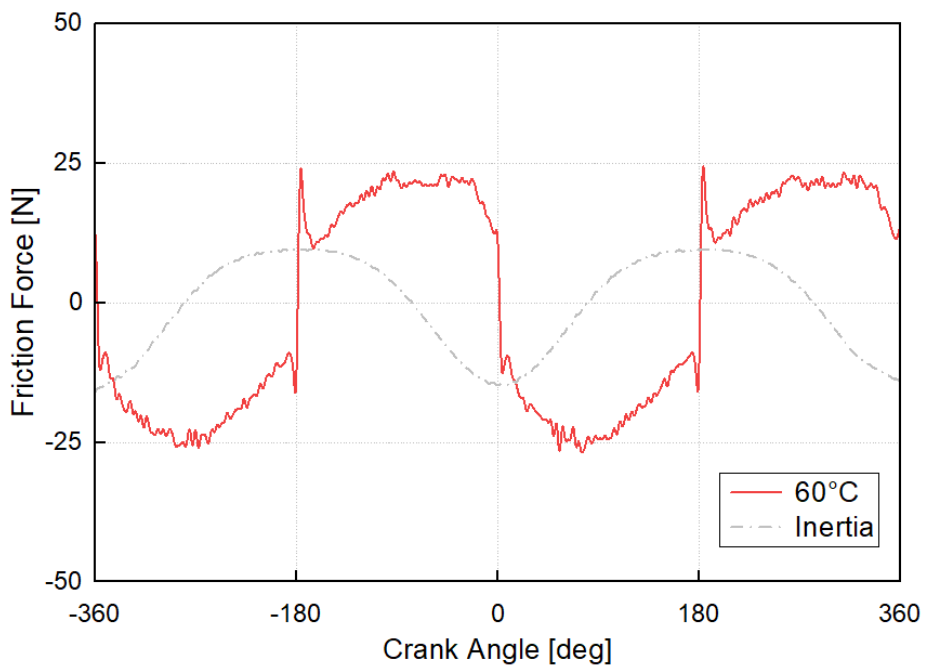


Figure 3-13. Friction force data after inertia force consideration

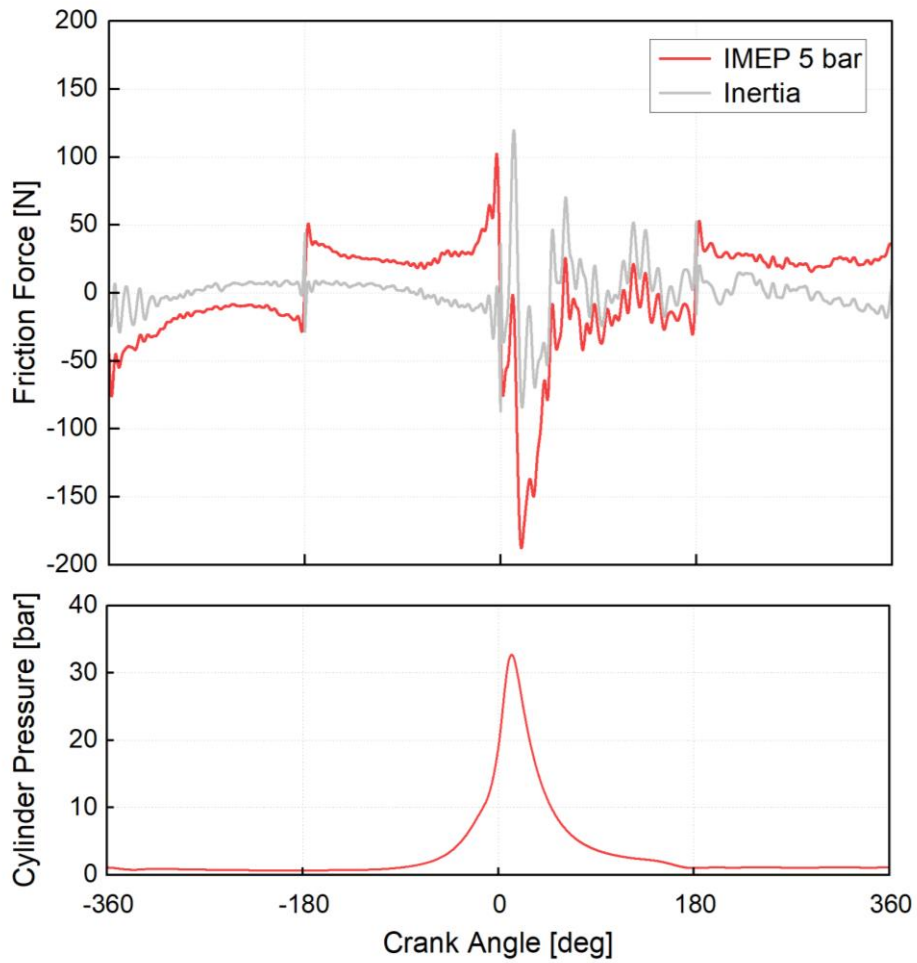


Figure 3-14. Friction force data before inertia force consideration at engine firing condition

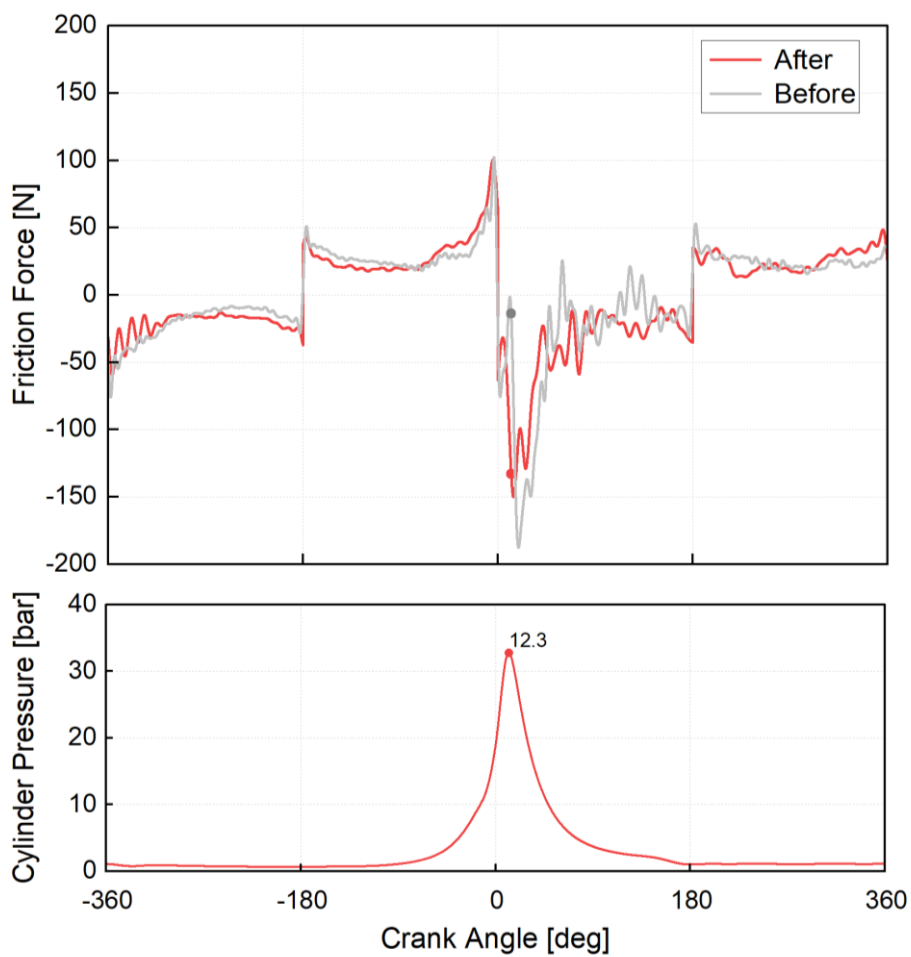


Figure 3-15. Friction force data before and after inertia force consideration at engine firing condition

Chapter 4. System Verification

4.1 Base piston ring friction study

For the final engine, Engine V2, various parameters were tested to verify the system performance and observe friction changes. The three main engine operating parameters were examined, which are oil temperature, engine speed, and engine load. To isolate each parameter, cylinder head was removed for experiments at various oil temperature and engine speed conditions. Because in-cylinder pressure effect can be excluded without cylinder head. And the piston ring strip-down was implemented to investigate each ring and skirt friction. This experiment was also conducted without cylinder head.

For the reference piston ring test, piston ring specifications are listed below in Table 4-1. TCR and SCR have the same shape as of the previous chapter. The OCR is in three pieces which are top and bottom side rails and a spacer. All measured values and drawings in Table 4-1 are provided by the manufacturing company, KPR (Korea Piston Ring INC.).

The roundness of the liner was measured to check the relative clearance with the measured piston. As seen in Fig. 4-1, the diameter of the liner fluctuates along the radial directions. It is shown that the diameter is bigger than the perfect circle around intake-exhaust side (90°-270°). It is smaller around front-rear side (0°-180°). With the measurement results, it is confirmed that the average diameter of the floating liner is within the design tolerance.

As described in Table 4-3, the radial clearance at the smallest point between the floating liner and the test piston with the uncoated skirt is targeted in

the range from 40 μ m to 60 μ m. The radial clearance with the coated skirt is approximately from 12 μ m to 48 μ m.

The roughness of the floating liner was examined before friction measurement. The measured liner roughness is listed in Table 4-2. Engine was operated with the floating liner many times before. Therefore, the roughness at two different points were measured to confirm the roughness variation between piston ring contacted area and non-contacted area. The roughness around 35mm from the top of the liner was measured to see the roughness where the piston ring has scratched. On the other hand, the roughness around 120mm from the top represents nearly the initial honed liner condition. As expected, averaged roughness (R_z) at contacted area is comparably lower than averaged roughness at non-contacted area. All measured values of Fig. 4-1 and Table 4-2 and design values of Table 4-3 are provided by Hyundai Kia Namyang R&D Center.

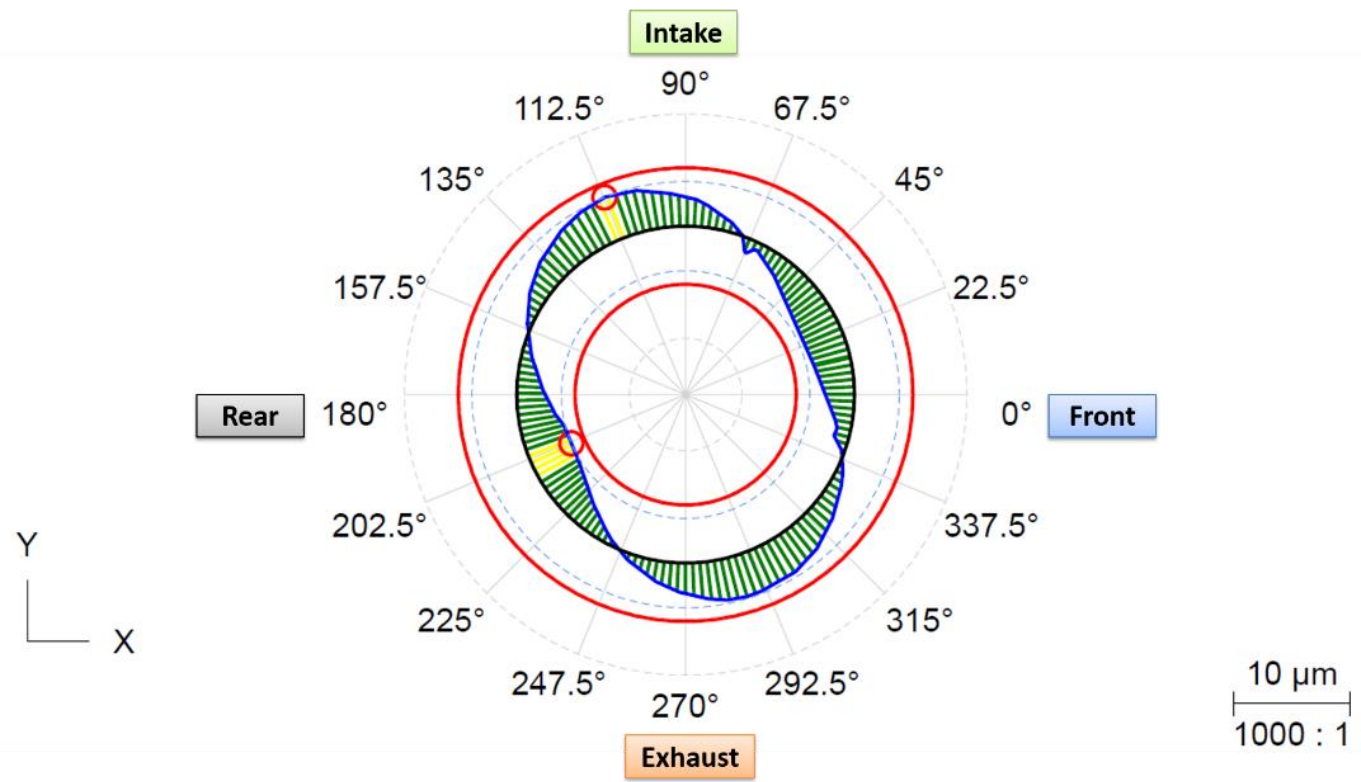


Figure 4-1. Floating liner roundness profile

Table 4-1. Ring specifications

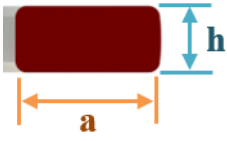
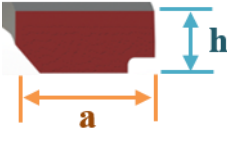
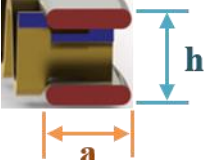
	TCR	SCR	OCR
Tension [N]	7.9	8.0	27.9
End gap [mm]	0.17	0.41	0.22 / 0.23 for each rail
Description	Symmetric Barrel Faced	Taper / Balance Under Cut	Two side rails / Spacer
Cross-sectional view			
Width ; h [mm]	1.18	1.18	1.94
Thickness ; a [mm]	3.13	3.63	2.61

Table 4-2. Floating liner roughness

Distance from liner top	35 mm	120 mm
R_Z	0.74	0.83
R_{pk}	0.02	0.03
R_{vk}	0.26	0.25
R_k	0.12	0.12

*Unit; μm

Table 4-3. Liner-piston clearance (design target values)

	Min.	Max.
Liner bore	+10	+20
Piston skirt profile max.	-40	-30
Clearance without coating	40	60
Clearance with coating	12	48

*Unit; μm

4.1.1 Oil temperature effect

As explained in previous chapters, oil temperature affects lubrication regime change in each stroke. The piston friction force at three different oil temperature, 30°C, 60°C, and 90°C, is plotted in Fig. 4-2. Each case was implemented at 800 rpm, motoring condition, but there is no pressure on the top of the piston. As oil temperature increases, lubrication condition tends to shift towards boundary lubrication. The friction force at the boundary lubrication zone near TDCs and BDCs, where the piston speed has the lowest value, increases as oil temperature increases. In comparison, the friction force at hydrodynamic lubrication zone nearly center of TDCs and BDCs, where the piston speed is the highest, decreases as oil temperature increases. Therefore, boundary lubrication zone expands within a stroke as oil temperature increases. However, the friction force at BDCs, -180° and 180°, is lower than friction force at TDCs, -360°, 0°, and 360°. It is considered that relatively more lubricants would act near BDCs as oil flows downwards to BDCs. The oil starvation gets severe when the oil temperature increases. Therefore, the friction at TDCs tends to increase drastically as the oil temperature increases compared with the friction at BDCs. This tendency can also be confirmed in the previous research [46].

Moreover, the surface roughness of the liner also influences on the different friction behavior at TDCs and BDCs. As shown in Fig. 4-3, the roughness was measured in four engine directions, exhaust-side, intake-side, engine rear, and engine front. Both R_z and R_a surface roughness values at BDCs are higher than the values at TDCs for three different engine directions. For more areal observation, the honing conditions at TDCs and BDCs were captured with a microscope. As shown in Fig. 4-4, the honing lines are more faded out at TDCs

than at BDCs. Since the liner has been used for a few hundred hours over break-in time, the honing line at TDCs is more likely to have been scratched out by top ring with high pressure compared with the honing at BDCs. Thus, the amount of the oil retention could be reduced at TDCs with decreased honing effect. The friction force at TDCs is relatively higher than the friction force at BDCs.

The piston friction power considering piston speed from friction force is shown in Fig. 4-5. As observed in Fig. 4-2, the friction power has a tendency to increase near TDCs with the oil temperature increase. The dotted lines indicate the averaged friction power, and its colors present the cases in the same colors. As plotted in the right of the power graph, it shows kinematic viscosity change of oil type 5w 30 according to the temperature change. As seen in Fig. 4-5, oil viscosity is exponentially decreases as the oil temperature. The same colored dots on the viscosity graph indicates the tested temperature points, which plotted in power graph with the same color. It can be confirmed that the amount of averaged friction power change follows the amount of oil viscosity change as oil temperature changes. With the new measurement system, the oil temperature effect on piston friction can be correctly captured.

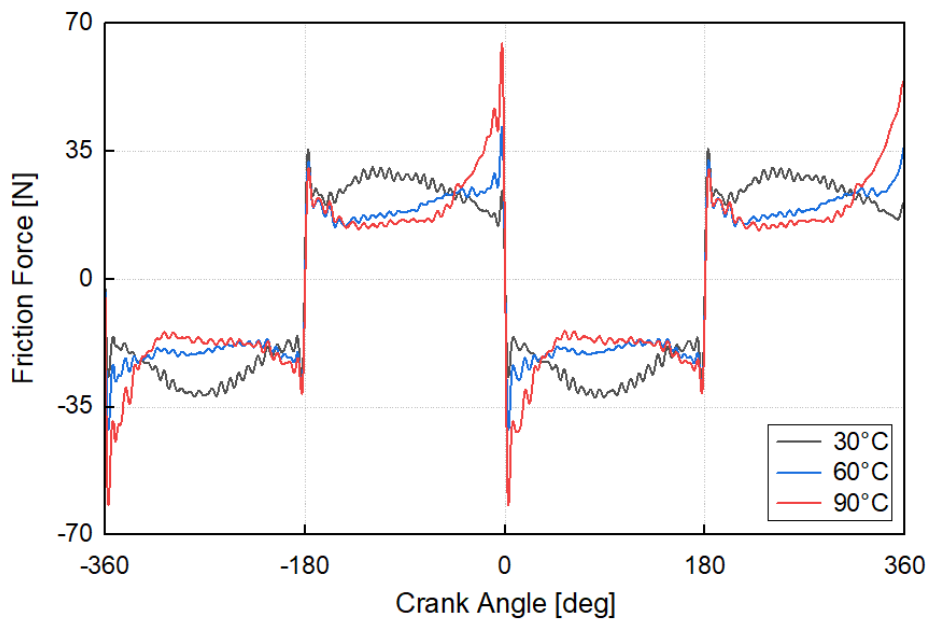


Figure 4-2. Oil temperature effect on piston friction

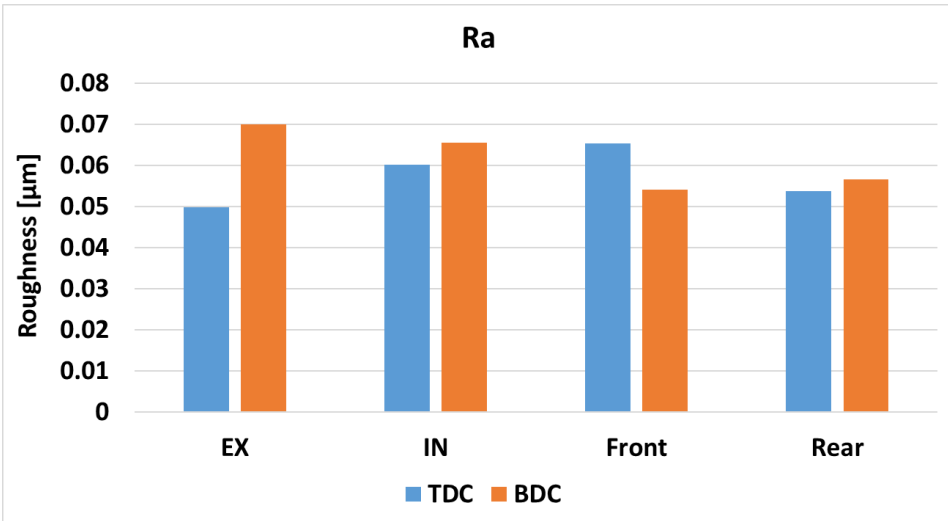
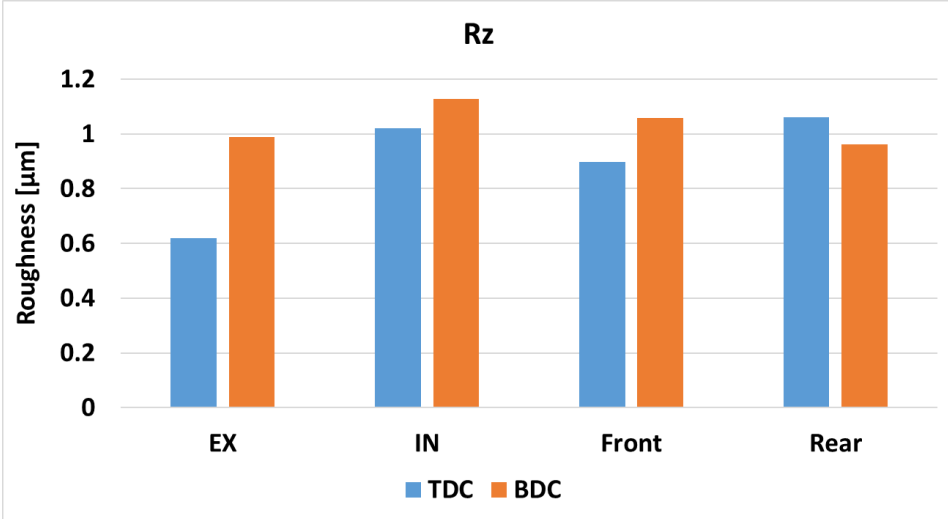
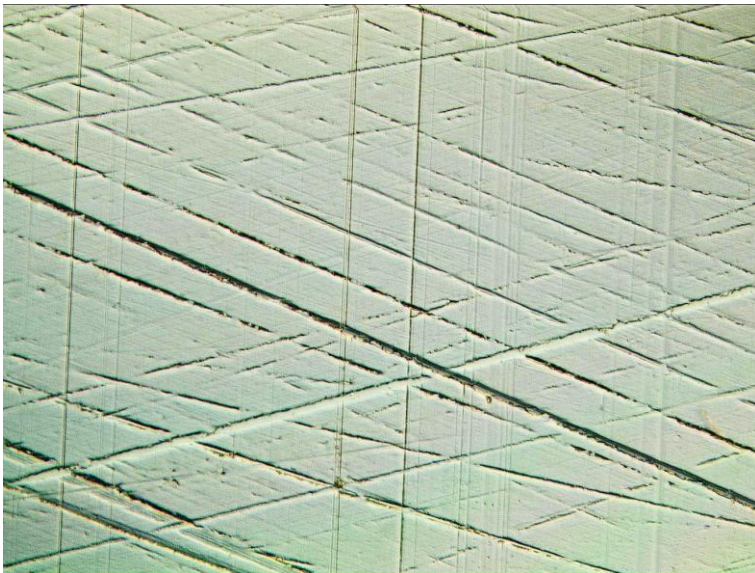


Figure 4-3. Liner roughness measurements (R_z, R_a)



(a) TDC



(b) BDC

Figure 4-4. Horning condition – microscopy

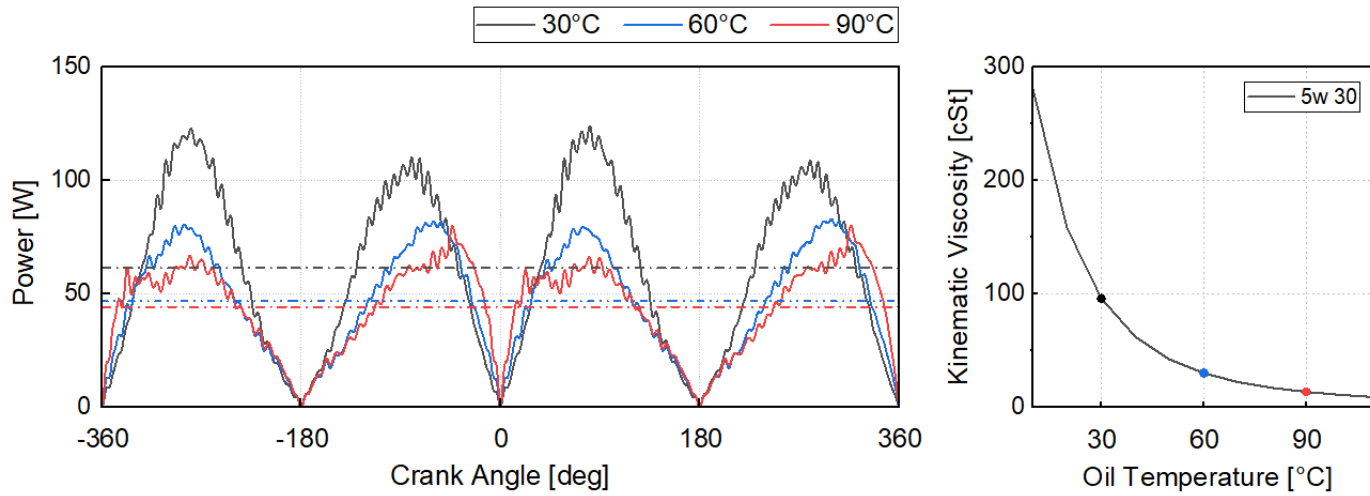


Figure 4-5. Piston friction power at various oil temperature

4.1.2 Engine speed effect

The piston friction is varied as engine speed changes. As shown in Fig. 4-6, the friction force is plotted at 3 different engine speeds, 600 rpm, 800 rpm, and 1000 rpm. The cases in the graph were implemented at 30°C oil temperature with no load on the top of the piston. Piston frictional power and piston speed corresponding cases with the friction force data are also plotted in the graph. Piston friction force at the middle of the TDCs and BDCs where the piston speed shows the highest is in hydrodynamic lubrication. Additionally, the friction force increases as the engine speed increases at this point. On the other hand, piston friction force at TDCs and BDCs where the piston speed goes to zero shows friction force increase. However, since the piston speed has reached zero, there is no significant friction change on boundary lubrication for the higher engine speed cases.

Figures 4-7 and 4-8 show the friction force change at 60°C and 90°C oil temperature each as the engine speed changes. As the oil temperature increases, the lubrication regime shifts towards the boundary lubrication. The friction force difference between each case at different engine speeds decreases as the oil temperature increases. Therefore, the frictional power change isn't significant as much as the lowest oil temperature case, 30°C. However, the piston speed effect remains. The piston frictional power loss increases as engine speed increases. In other words, the piston speed effect becomes dominant at high oil temperature.

Similar with the friction power, FMEP can also be calculated from the result as shown in Fig. 4-9. As oil viscosity increases drastically with oil temperature decrease, the FMEP increases drastically from oil temperature 90°C

to 30°C for all 3 different engine speed cases. The amount of FMEP change increases as engine speed increases. Especially, from oil temperature 60°C to 30°C, where the oil viscosity difference is about 4 times bigger than the viscosity difference between oil temperature 90°C and 60°C, FMEP shows a bigger difference than the one between oil temperature 90°C and 60°C. The drastic change of the FMEP at 30°C represents that the friction increase dominates at hydrodynamic lubrication period as engine speed increases.

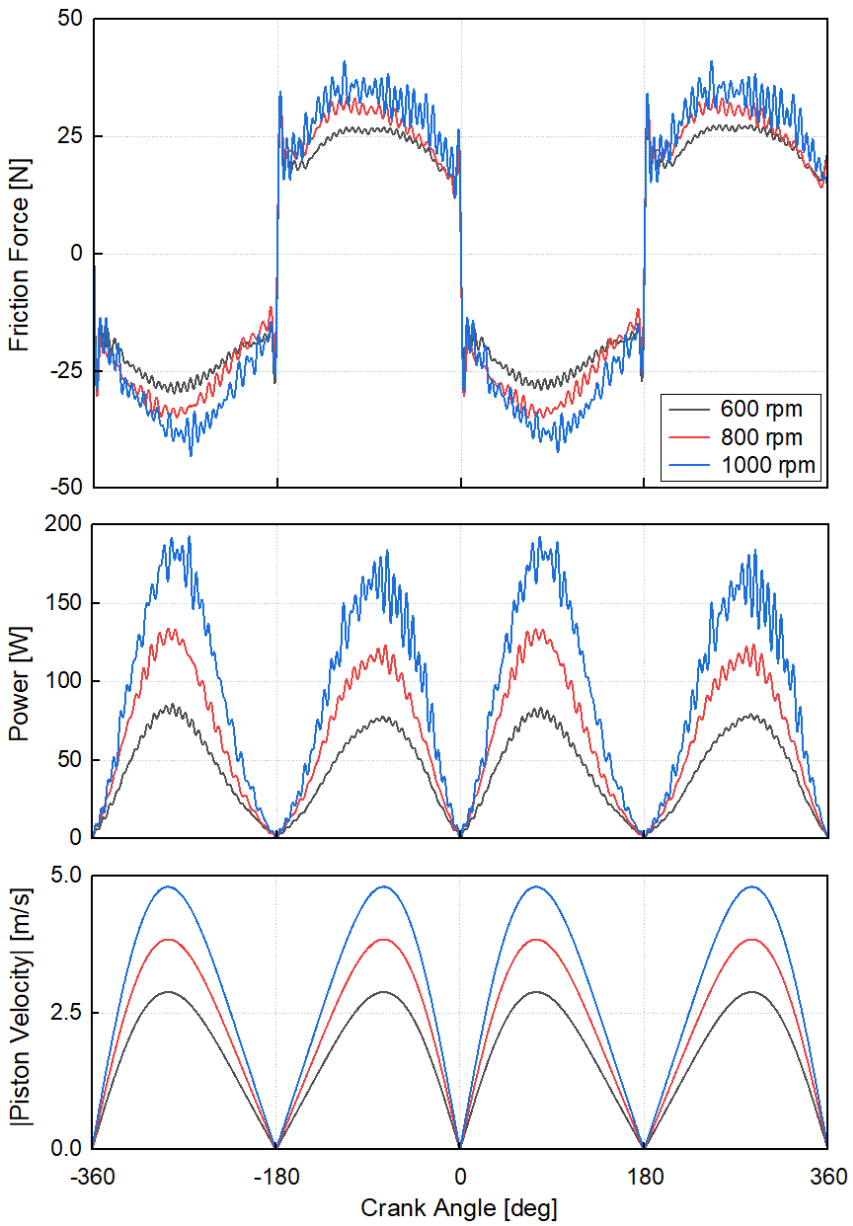


Figure 4-6. Engine/piston speed effect on piston friction at 30°C

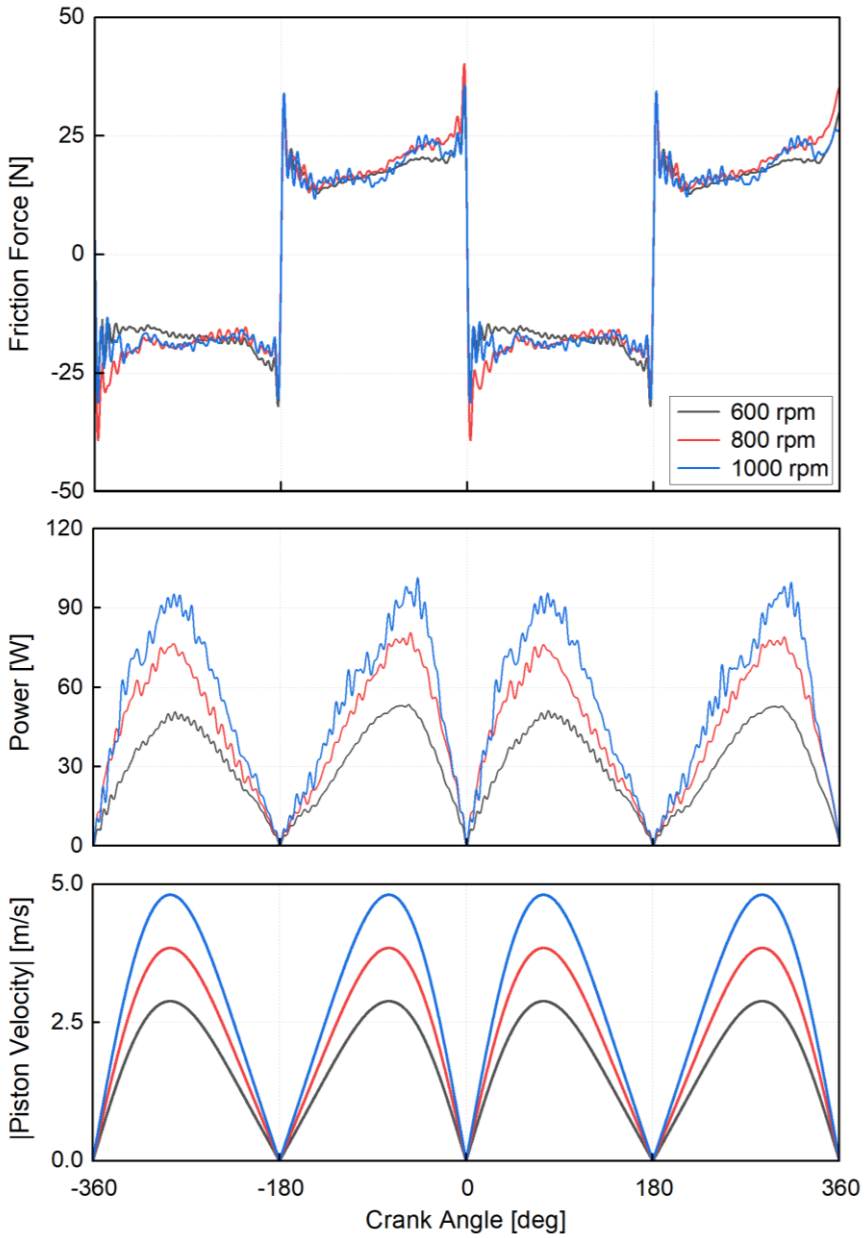


Figure 4-7. Engine/piston speed effect on piston friction at 60°C

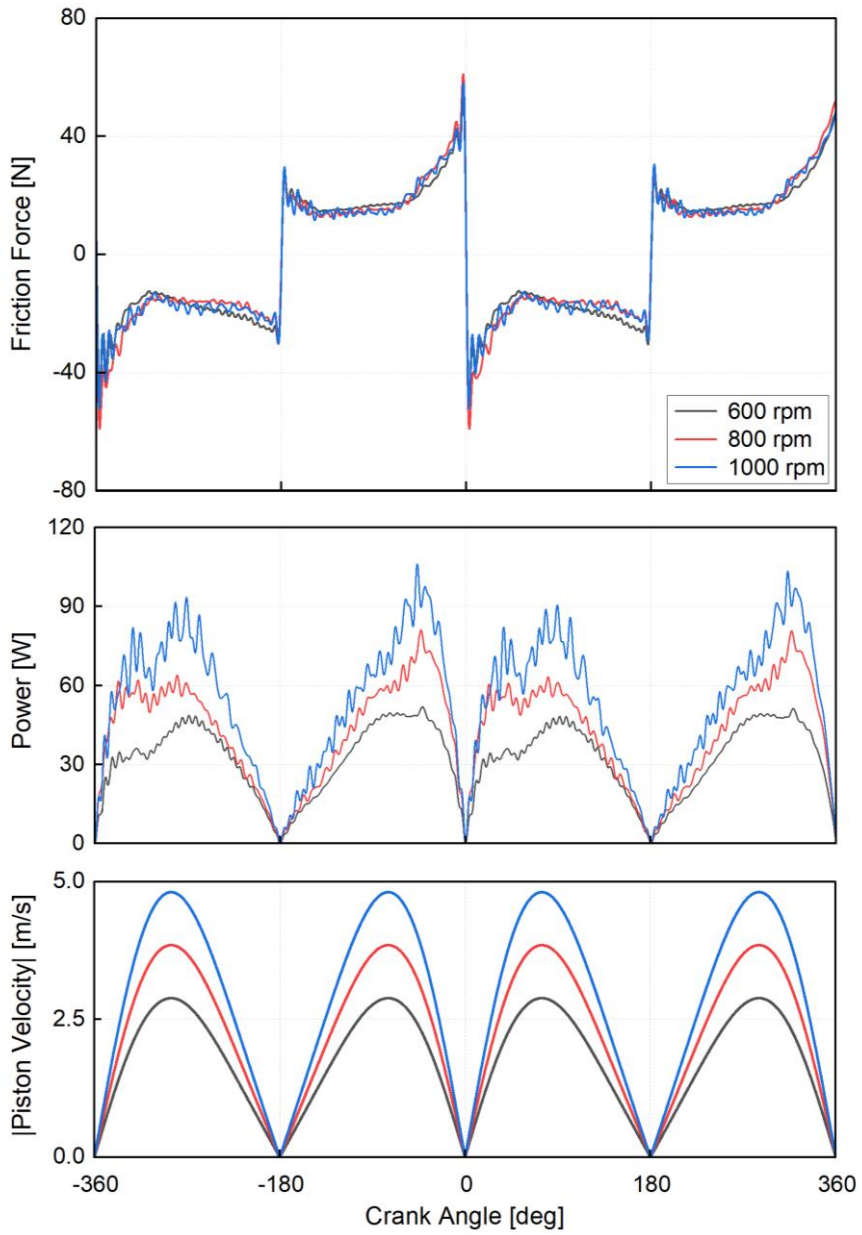


Figure 4-8. Engine/piston speed effect on piston friction at 90°C

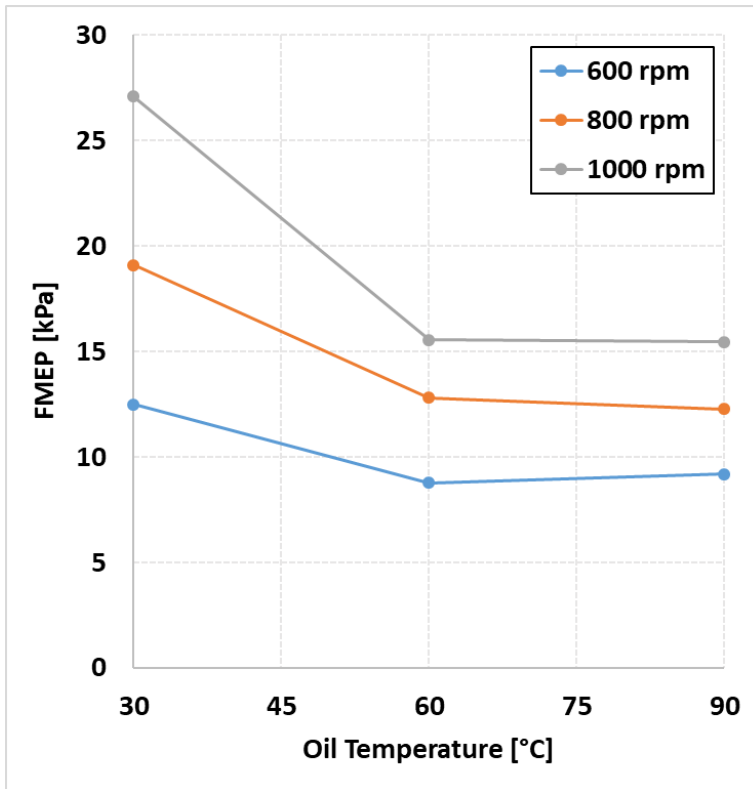


Figure 4-9. FMEP at various engine speed and oil temperature

4.1.3 Data repeatability

Each experiment case was tested at least 3 times, and each time it was not sequential. Every experiment at the same condition was gone through in-between different cases. As shown in Fig. 4-10, the friction force was measured at various engine operating conditions including engine speed and oil temperature. The bar chart shows the average friction power of these cases. And the standard error is marked on each case. The standard error is within 2% average. Therefore, the experimental results show a good repeatability with the new measurement system.

In Fig. 4-10, the averaged frictional power chart shows the overall piston friction change at various engine oil temperature and speed cases. As explained in the previous chapters, the frictional power loss increases as the engine speed increases regardless of oil temperature change. However, as time term is considered on the friction power, averaged friction power is relatively more focused on hydrodynamic lubrication change. Therefore, the averaged power at comparably lower engine speed shows smaller frictional power change between the highest and the lowest engine oil temperature. As the engine speed increases, the oil temperature effect increases. And the averaged power at the lowest oil temperature case increases more drastically the one at the highest oil temperature case. This represents engine speed effect on piston friction which becomes dominant as oil temperature increase.

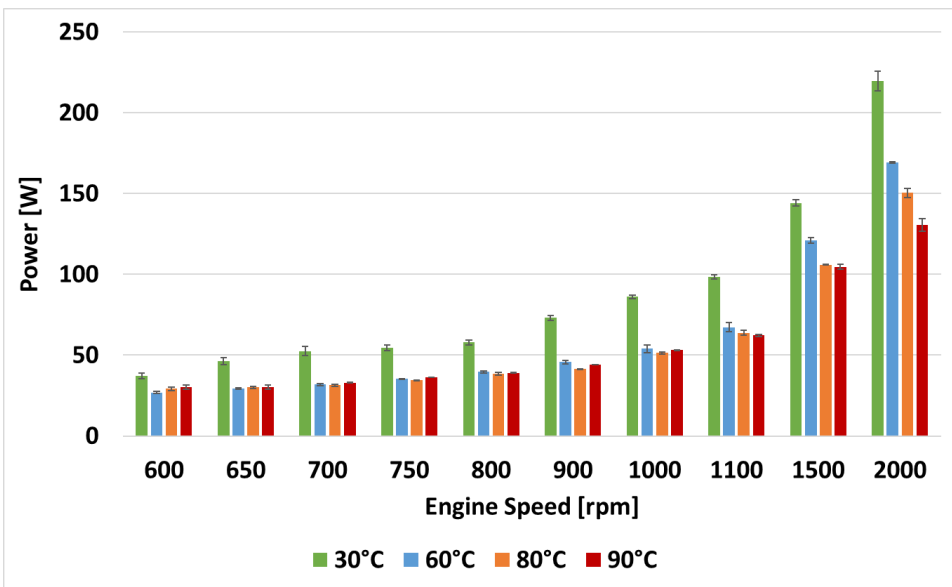


Figure 4-10. Averaged friction power and standard error at various engine operating conditions

4.1.4 Each ring friction

With the new measurement system, each ring friction can be measured to observe the influence on the entire piston friction. Since the measured piston has the same geometry with the conventional piston, the skirt friction is also measured. The test was also implemented at 3 different engine speed, 600 rpm, 800 rpm, and 1000 rpm. And two different oil temperatures, 30°C and 60°C was tested. Due to the ring strip-down process, the experiment could not be implemented at engine load conditions. The experiment for each ring friction was implemented, primarily when there is no load on the top of the piston.

As shown in Fig. 4-11, overall averaged frictional power increases as piston speed increase at 30°C oil temperature as explained in the Chapter 4.1.2. and 4.1.3. Similarly, the averaged power of each ring increases as the engine speed increases. However, the averaged power of the piston skirt shows a bigger change according to the engine speed than piston rings. As the hydrodynamic lubrication is dominant on the piston skirt, the averaged power of the piston skirt becomes more significant at 1000 rpm.

The test procedure was done by measuring piston friction force with one ring missing to maintain the relative piston and liner position the same with the comparing cases as much as possible. The piston skirt friction was calculated by excluding ring pack friction from the total piston friction. Therefore, as the oil temperature increases, oil film between the liner and the piston skirt is hardly maintained. It can be seen in Fig. 4-12, and the friction portion has been decreased at 60°C case compared with 30°C. Additionally, although the power loss of the piston skirt has been decreased as oil temperature increase, the power loss of each

piston ring maintains the same comparing two different oil temperature cases. This indicates that the majority of the piston frictional power loss comes from the hydrodynamic lubrication of the piston skirt.

As shown in Fig. 4-12, overall piston friction power loss increases as the engine speed increases, as observed in Fig. 4-11. Moreover, the power loss of each ring at both oil temperature cases follows the tension property of each ring. The ring tensions are measured with the verified tension measurement system before starting the test. As the ring tension decreases in order OCR, SCR, and TCR, the power loss shows the same tendency.

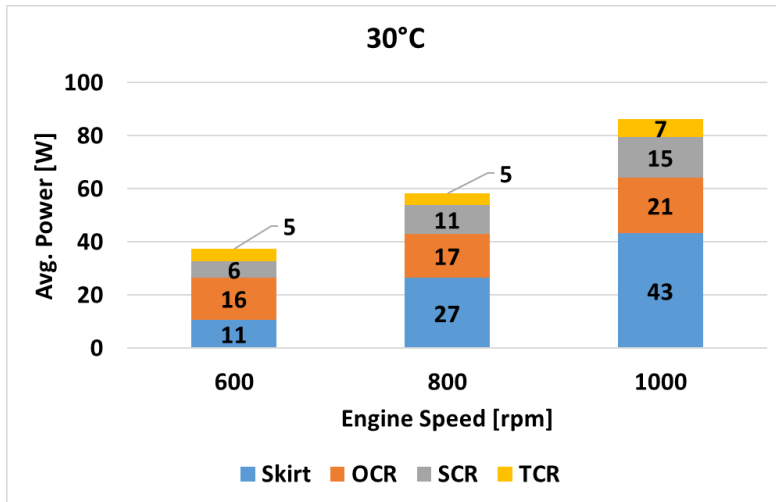


Figure 4-11. Averaged friction power of each piston ring and skirt at 30°C

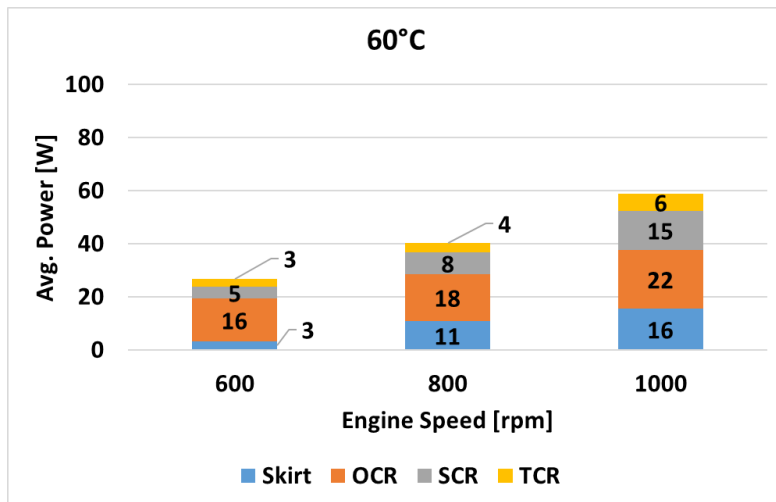


Figure 4-12. Averaged friction power of each piston ring and skirt at 60°C

4.1.5 Engine load effect

Piston friction can be measured at engine firing conditions with maintaining combustion stability and liner in floating state at the same time with the new system. As shown in Fig. 4-13, both engine motoring and firing conditions were tested at 800 rpm, 70°C oil temperature. The friction force changes at motoring and IMEP 5 bar conditions is plotted in Fig. 4-13.

Through the experimental results, it can be confirmed that friction force change follows in-cylinder pressure change. IMEP 5 bar case shows a higher pressure rise compared with motoring case. The friction force increases as the in-cylinder pressure increases. Especially, the pressure peak occurs near TDC where the piston speed becomes zero. Therefore, the lubrication regime shifts towards boundary lubrication. With the new measurement system, the piston thrust force can be highly negligible, therefore, the friction force increases predominantly by the increased amount of the gas pressure acting on piston rings.

The friction force change can also be observed at various engine firing conditions in Fig. 4-14. Similar with the previous comparison in Fig. 4-13, the friction force near firing TDC increases as in-cylinder pressure increases from IMEP 3 bar to IMEP 5 bar. However, excluding the pressure peak region, the friction force does not show a noticeable difference. Since the oil temperature and engine speed were kept the same for all three cases, the piston friction force shows a similar change especially at intake and exhaust stroke.

The engine load effect can also be observed in Fig. 4-15. The friction power and its mean value are plotted according to the engine load. At the compression stroke, before firing TDC, the cylinder pressure at motoring condition

shows the highest. The power loss at motoring condition also shows the highest at the compression stroke. At the expansion stroke, the power loss increases as in-cylinder pressure increases. However, the averaged power value at motoring case, which is plotted in dot lines and same colors with according cases, shows a higher value than the power loss at IMEP 3 and 4 bar cases. It is interpreted that the hydrodynamic lubrication at motoring condition is comparably higher than firing cases. For the firing conditions, the heat transfer from the combustion can affect the piston lubrication conditions.

Furthermore, as plotted on the right side in Fig. 4-15, maximum absolute piston friction force and maximum cylinder pressure are indicated at both engine motoring and firing conditions. Because the piston friction force shows highest at the cylinder pressure peak point. The same tendency for both parameters can be expected when the two maximum values compared. For the firing conditions, from IMEP 3 bar to 5 bar case, maximum friction force increases as maximum pressure increases. However, the maximum friction force at motoring condition shows a higher value than IMEP 3 bar case, although the maximum pressure at the motoring case is lower than the maximum pressure at IMEP 3 bar. This can be explained with the maximum cylinder pressure timing. The timing of the maximum pressure is at the firing TDC for the motoring case, but the maximum pressure at IMEP 3 bar case occurs after firing TDC. As the timing shifts toward the middle of the stroke, the friction force gets more influence of the piston speed. This could be resulted in lower maximum friction force of IMEP 3 bar compared with the motoring case as the peak pressure point of IMEP 3 bar case shifts to the mixed lubrication regime.

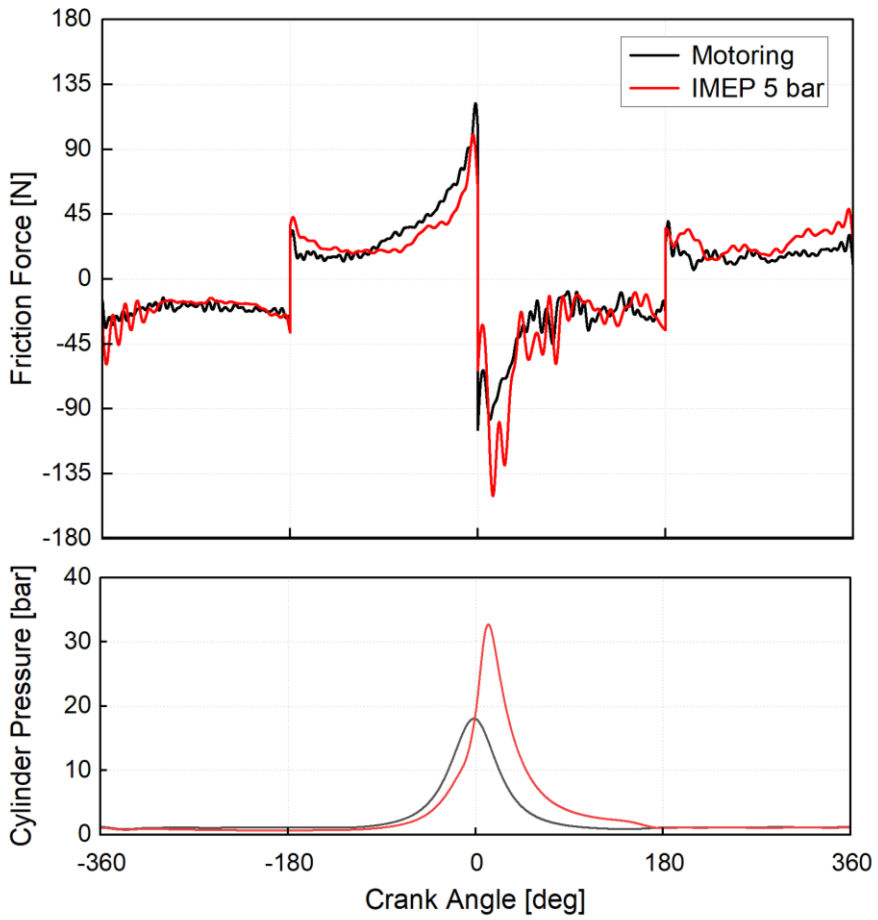


Figure 4-13. Piston friction force at motoring and firing conditions

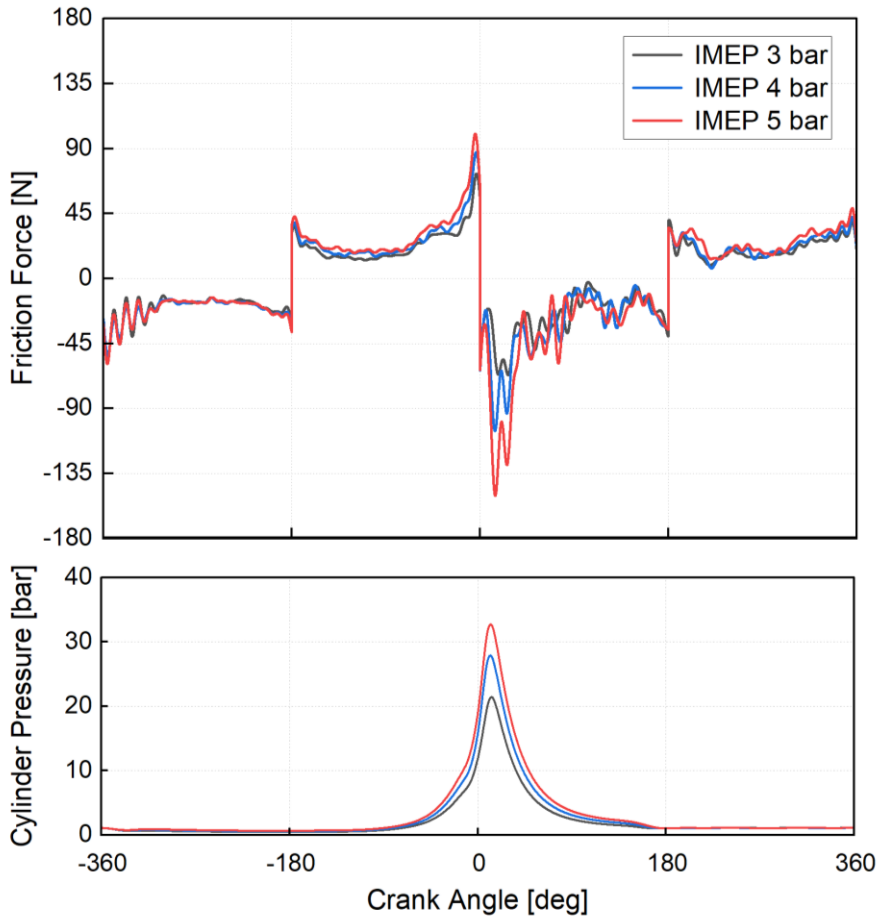


Figure 4-14. Piston friction force at various firing conditions

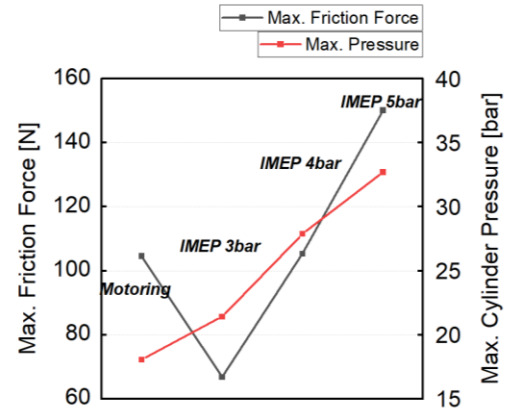
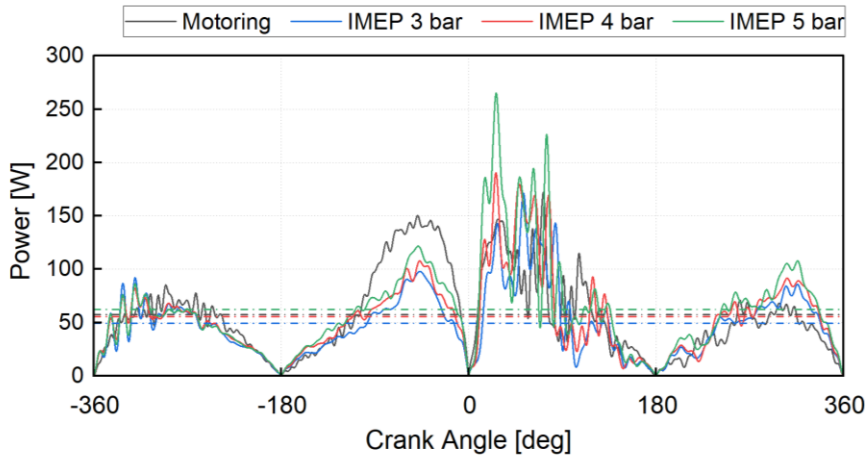


Figure 4-15. Piston friction power at various firing conditions

4.1.6 Piston thrust force effect

In order to exclude the effect on friction from piston secondary motion and accordingly piston ring motion, double pistons were adopted for the new floating liner system. As explained in chapter 2.1, it is proven that the piston thrust force can be reduced 100 times with the double pistons structure by using simulation. The actual piston contact force on the liner can be estimated with engine vibration measurement. Kistler 8766A accelerometer is used to estimate the force acting on the axis of thrust and anti-thrust directions. The measurement was done at engine motoring condition, 800 rpm. The measured acceleration signal can be calculated in force value similar with the inertia force calculation. In Fig. 4-16, the measured inertia force, thrust force, and gas force on the top of the piston are plotted. The positive force value of thrust force indicates force direction towards thrust-side of the liner from anti-thrust-side. The peak value of the inertia force is over 500 times smaller than the gas force on the piston. The measured thrust force shows even lower value compared with the gas force and the inertia force. It can also be compared with the calculated thrust force of the lower piston for the same experimental condition by using RecurDyn simulation model. As shown in Fig. 4-17, the thrust force range of the upper piston is 100 times lower than the one of the lower piston. The measured thrust force from the experiments showed a similar thrust force reduction with the simulation results. Even though the thrust force working on the upper piston cannot be fully excluded, the friction change caused by thrust force is negligible.

In Fig. 4-18, the skirt wear of the upper and lower pistons is shown after over 50 hours of experiments. The skirt wear of the lower piston is prominent than the one of the upper piston for both thrust and anti-thrust sides. The lower piston

has the obvious vertical lines for both sides that imply solid contacts with the liner caused by the strong thrust force. On the other hand, the upper piston only has blacked area around the relatively low piston-liner radial clearance area, known as piston bearing area. The piston skirt color changed in darker color compared with the non-used state, for piston-liner overlap occurs from piston thermal expansion. No solid scratches are found for the upper piston. This is additionally evident to prove low piston thrust force.

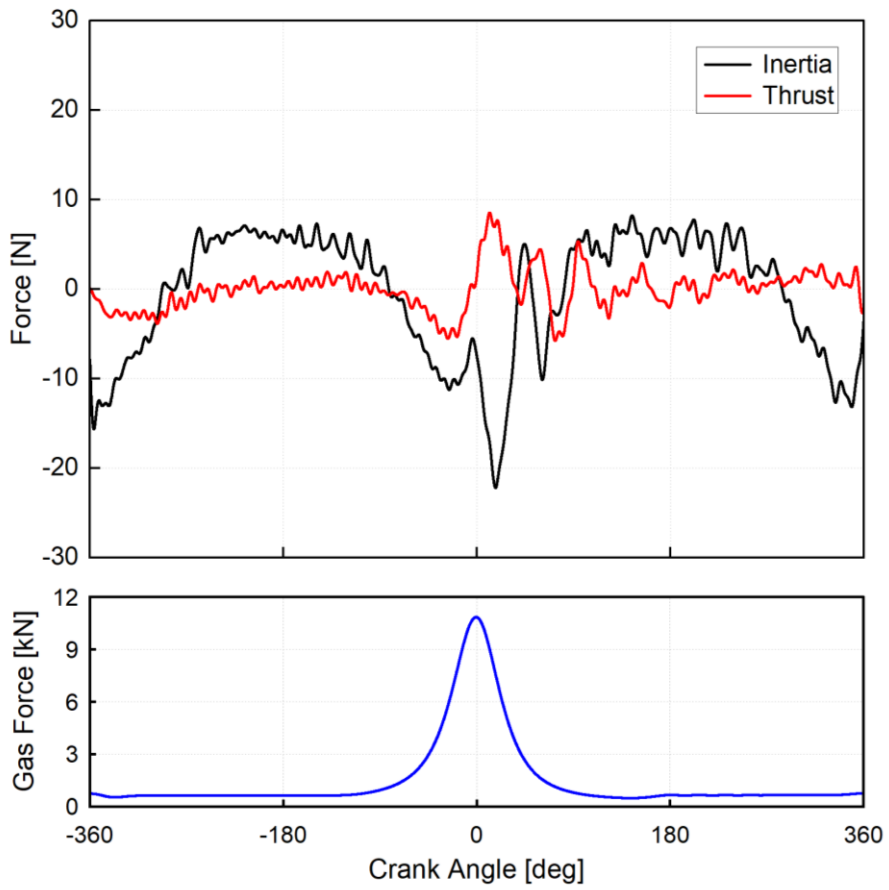


Figure 4-16. Thrust and inertia force comparison at motoring condition (800 rpm)

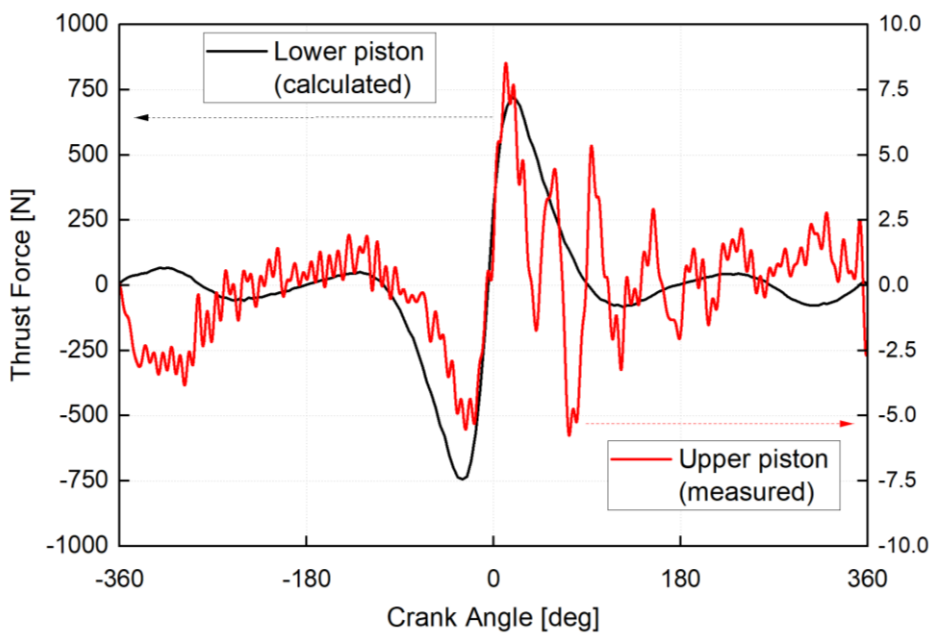


Figure 4-17. Thrust force comparison of upper and lower pistons

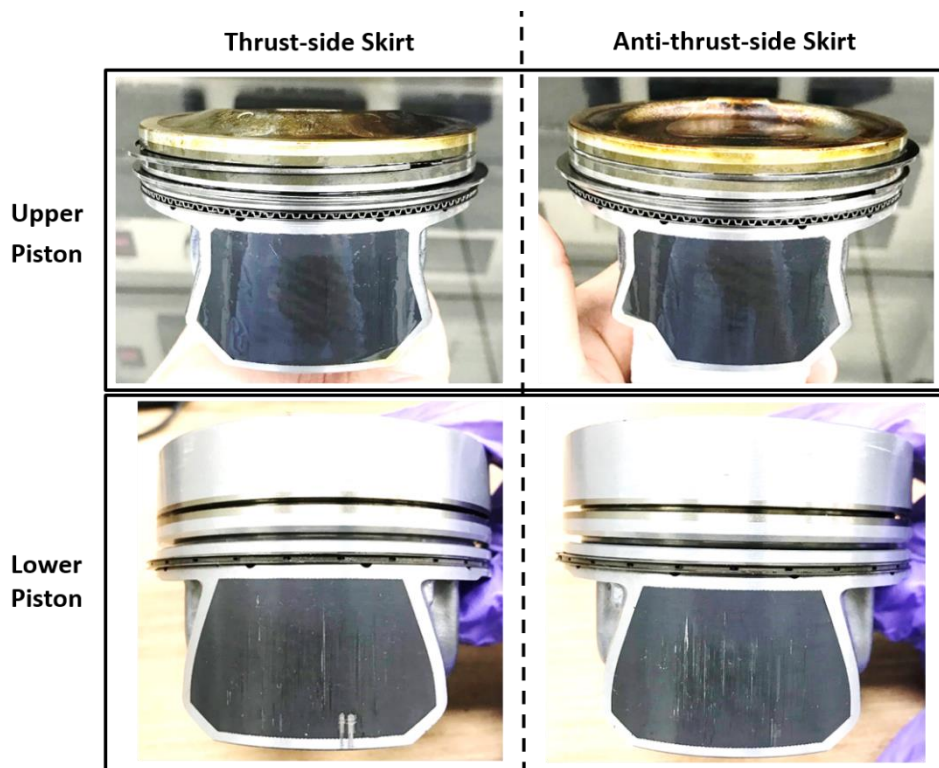


Figure 4-18. Wear comparison of piston skirts for upper and lower pistons

4.2 Piston ring design parameter study

4.2.1 Ring tension effect

The two different types of OCR were tested to investigate the OCR tension effect on friction compared with the reference OCR. The two types of OCR tensions are reduced in 20% and 37% each from the reference specification. The test was implemented at 800 rpm with no load on the piston top. Oil temperature were varied in 30°C, 60°C, and 90°C. As shown in Fig. 4-19, the piston friction force shows decrease at both boundary and hydrodynamic lubrication regimes as OCR tension decreases. The experimental results at the higher oil temperature conditions plotted in Figs. 4-20 and 4-21 also show the same tendency.

In Fig. 4-22, the friction force change according to the OCR tension can be seen in averaged frictional power. Figure 4-22 shows the piston friction power for each OCR type as oil temperature changes. Overall power loss of all three OCR types tends to decrease as the friction at the hydrodynamic lubrication decreases at the higher oil temperature. As oil temperature decreases, the effect of the hydrodynamic lubrication increases on piston skirt. Therefore, the OCR tension effect doesn't show up as much as the OCR tension difference at low oil temperature. However, regardless of the oil temperature change, the piston friction power loss follows OCR tension variation. As expected from the experimental results, an amount of the OCR tension is directly related to the friction change. And OCR tension affects oil consumption for higher engine speeds [49]. As indicated in Fig. 4-23, FMEP of three different OCR increases with engine speed

increase. The FMEP of the 37% decreased ring tension case at 90°C oil temperature shows 21.6% lower value than the FMEP of the reference ring case. The desirable OCR tension can be set by considering friction change.

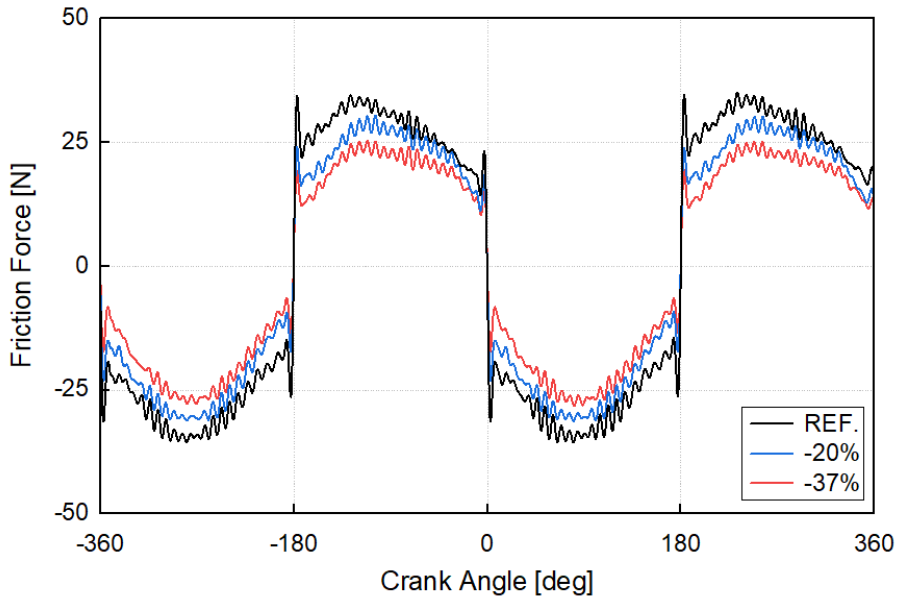


Figure 4-19. Piston friction force as OCR tension change at 30°C



Figure 4-20. Piston friction force as OCR tension change at 60°C

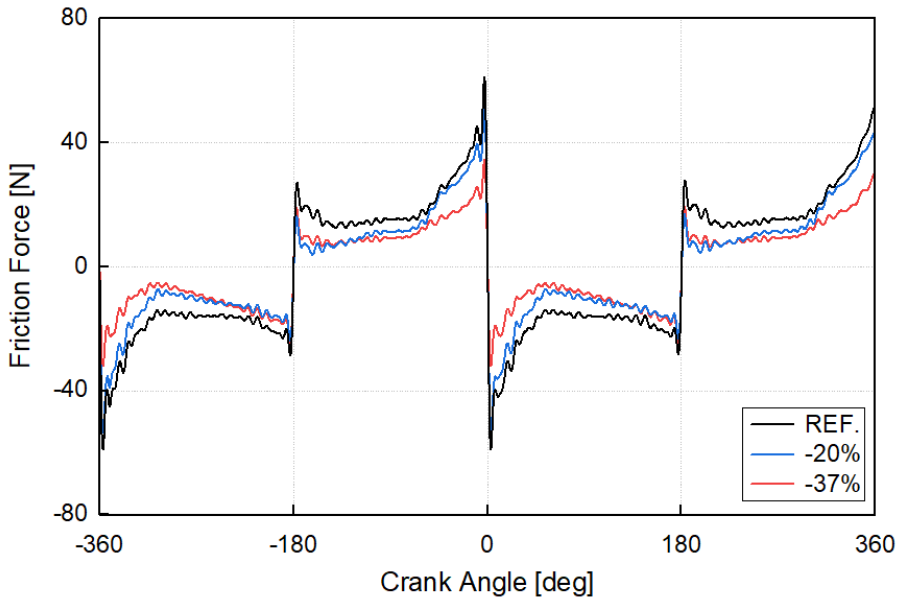


Figure 4-21. Piston friction force as OCR tension change at 90°C

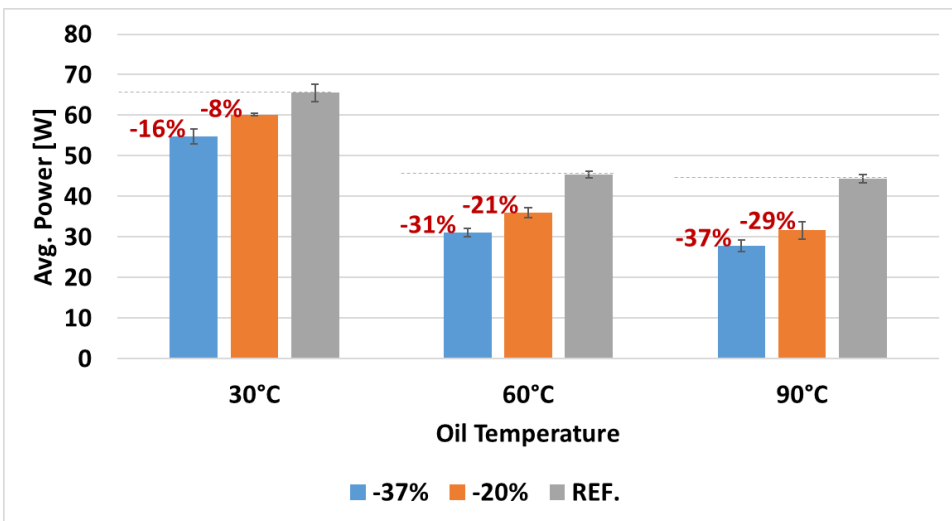


Figure 4-22. Averaged frictional power change according to OCR tension with corresponding error bars

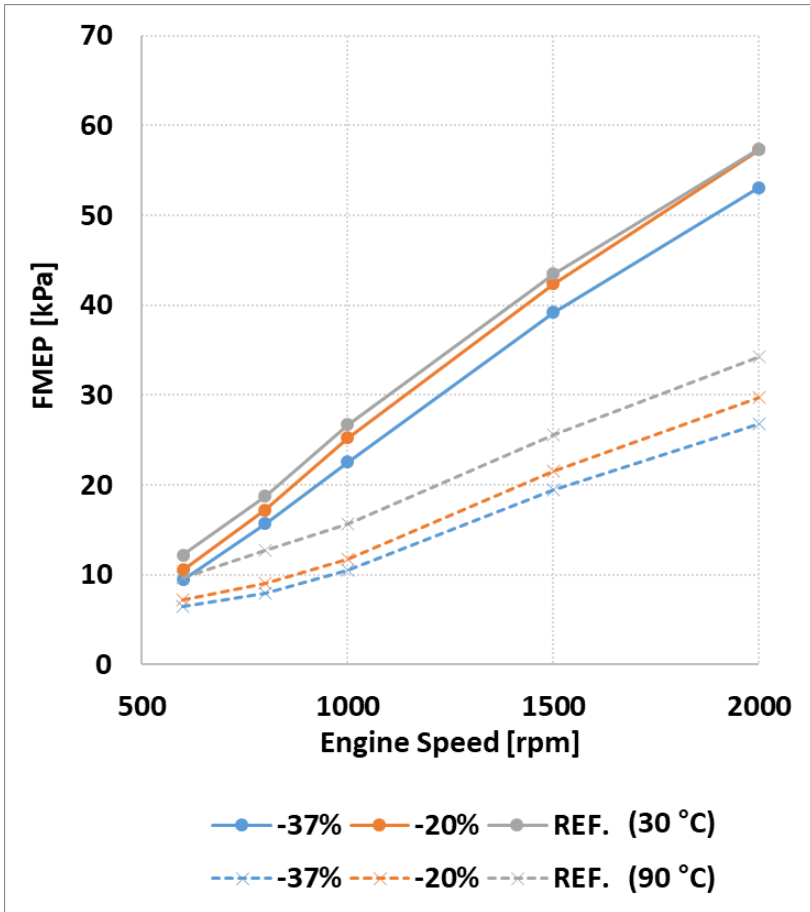


Figure 4-23. FMEP for each OCR tension at various engine speed and oil temperature (30°C and 90°C)

Chapter 5. Conclusion & Future Works

5.1 Conclusion

Floating liner method is a powerful method to investigate piston friction. However, it is yet a challenge to exclude piston thrust force. The piston thrust force interrupts the piston friction force measurement, because the liner is in the floating state. In previous researches, several devices are applied outside of the floating liner to compensate the piston thrust force. Lateral stoppers are a representative for eliminating liner thrust movement. The majority of the floating liner system with a conventional crankshaft-piston structure use these devices. As the piston thrust force changes according to the engine operating conditions, this could result in an additional uncertainty of friction measurement on the system.

Moreover, researches of the piston ring friction have never been performed without friction effect of the piston secondary motion. Despite the versatility of piston ring specification, the affecting parameters on piston ring friction have not been studied in further details. The piston ring parametric study has never done especially at the engine firing condition. Because it is difficult to investigate piston ring friction only from irregular piston dynamics and corresponding piston ring dynamics with high pressure and thermal interactions.

With the newly developed friction measurement system, the double piston structure is adopted, which is different from conventional engine structure for floating liner method. The floating liner is installed for the friction measurement of upper piston. The measuring piston, upper piston, has a longer connecting rod effect and a longer piston effect at the same time. The piston thrust force and the

piston angular motion for the upper piston can be reduced nearly zero compared to the conventional piston according to the simulation results of the Recurdyn Multi-body Dynamics (MBD). Therefore, the piston skirt-liner interaction and piston ring groove gas interaction from piston tilting can be highly excluded for the piston ring friction research.

Several trials have been made to overcome the structural problem of making liner in floating state with maintaining in-cylinder pressure for the stable combustion. To compromise these two opposite aspects, a thermo-resistive, low friction, and low wear material gas seal is applied between the cylinder head and the floating liner. The gas seal expands when the in-cylinder gas is pressurized. And the sealing function is proven by comparing the gas pressure with the conventional piston-fixed liner set up. The gas pressure difference between two set-ups is below 0.1 bar.

To implement more reliable piston ring investigation, the new piston and ring replacement method is considered by utilizing an advantage of the ‘double pistons’ structure. The former extended connecting rod for Engine V1 is divided in three pieces. The piston and ring pack set can be disassembled simply by taking out the coupling. The only piston and ring pack assembly can be detached from the entire system. Therefore, the experimental boundary condition such as clearances between floating liner components and the initial load cell set-up can be kept the same for piston ring parameter study. The experimental results show significant data repeatability within 2% error for the same cases.

It is important to isolate the friction force from other interrupting force factors on the measurement, for the liner is in floating state. Five possible extra force factors are considered for the new system. The piston thrust force and the leaked gas force working on the liner and the inertia force of the liner are measured,

and the raw friction force data is after-treated according to the dominance of each force factor. The friction force from the gas seal and the crankcase pressure oscillation are inferred from the load cell data. Through several updates of the engine geometries, the effects of the extra force factors are minimized.

The experiments were implemented considering various engine operating conditions, such as oil temperature, engine speed, and engine load. The experimental results show the lubrication regime changes from boundary to hydrodynamic lubrication according to the engine operating condition change. Furthermore, the ring tension values of the Oil Control Ring (OCR) were varied in three types to observe its effect on friction force. With the 37% decreased tensioned ring, the friction can be improved to 21.6% in FMEP from the reference ring at 90°C oil temperature.

Through the parametric study, the experimental result proves the performance of the newly developed system as a reliable piston ring friction measurement system. It is expected that the new measurement system allows piston ring parametric study without interaction from piston secondary dynamics possible. Thus, the new system can fully provide a valuable reference to further fundamental piston ring friction researches.

5.2 Future works

Piston friction force is typically over a hundred times smaller than in-cylinder gas force. It is very small yet a measureable amount with the floating liner method. However, the method itself has some issues on acceptable measurement range because of its operating mechanism. The load cell captures the movement of the floating liner. The floating liner can be highly affected by the engine vibration and the inertia force of the floating liner. The engine vibration could fluctuate by engine operating conditions such as combustion pressure, by every engine moving parts, and even by dynamometer. The range of causing factors on the engine vibration is wide. Although it is difficult to fully exclude from the measured friction force data, the interruption from the engine vibration could be minimized. To extract the friction force from the original data, the inertia force of the floating liner was also measured at the same time with load cells for every cases. And the inertia force was excluded from the measured data, as mentioned in the earlier chapter 3.2.

However, for relatively smaller piston friction force cases such as no load motoring conditions, inertia force exceeds piston friction force. It would be challenging to exclude the inertia effect from the original signal. For example, the original measured friction force data could be achieved with the inertia force as shown in Fig. 5-1 and Fig. 5-2. However, the friction force shows similar force range with the inertia force for higher engine speeds like 1500 rpm and 2000 rpm. Therefore, when the inertia force effect is excluded from the original force data, the modified friction force data could be over-fitted as shown in Fig. 5-3. To draw the reliable friction force results over 1500 rpm and no load operating conditions, the affecting factors on floating liner inertia force such as liner mass need to be

reconsidered.

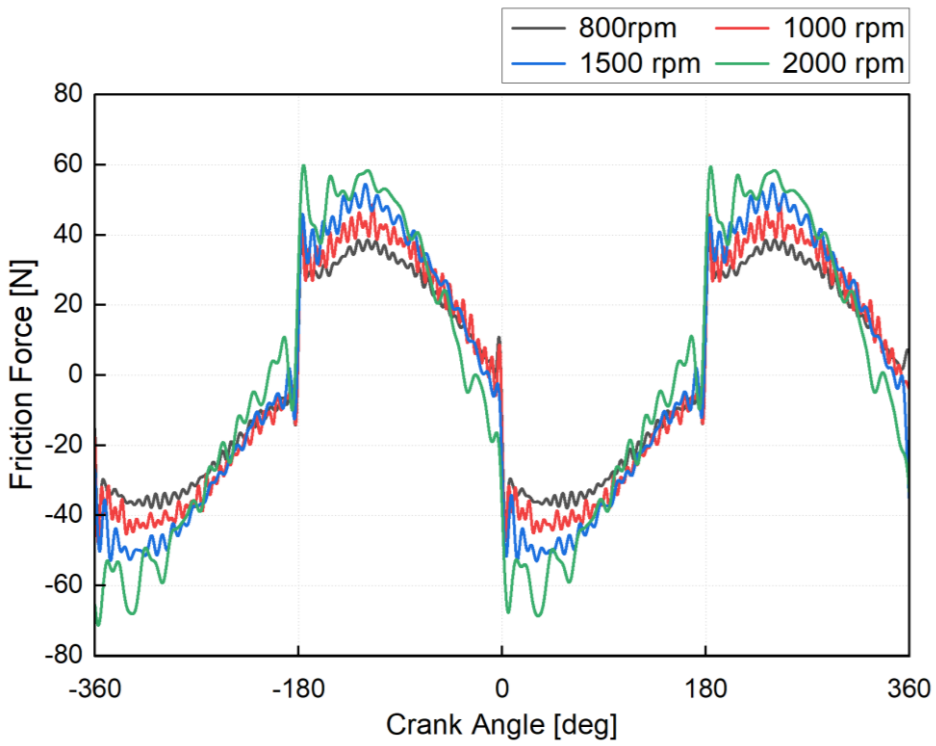


Figure 5-1. Friction force at various engine speeds

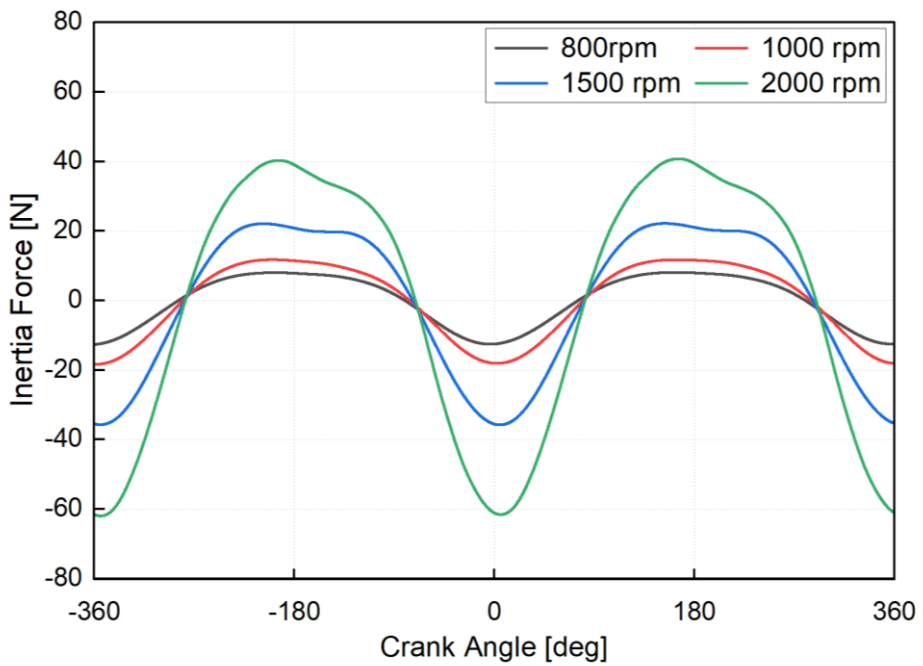


Figure 5-2. Floating liner inertia force at various engine speeds

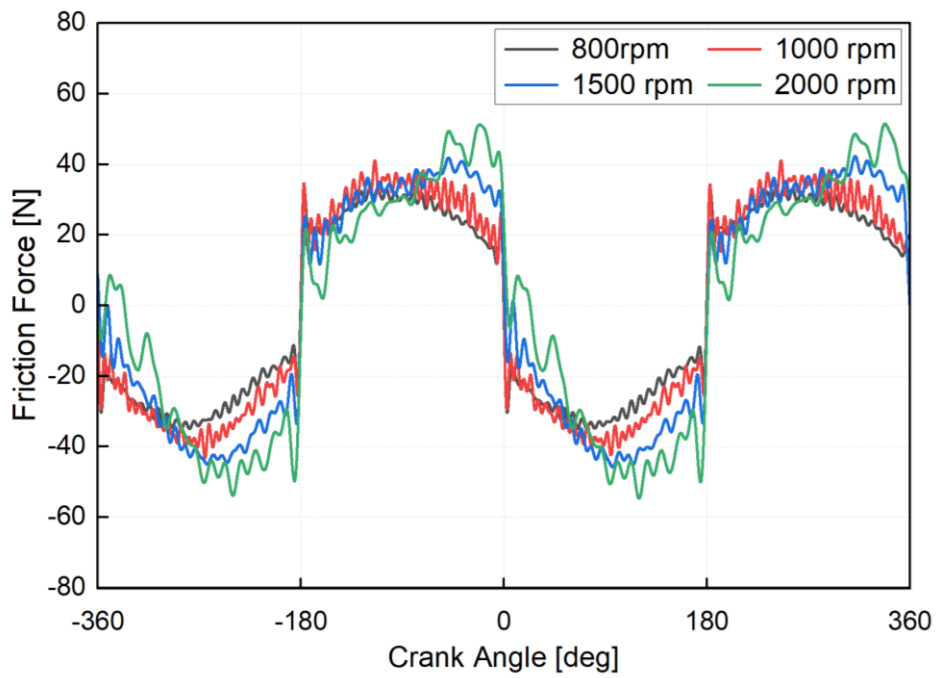


Figure 5-3. Modified friction force at various engine speeds

References

1. Holmberg, K. and Erdemir, A., *The impact of tribology on energy use and CO₂ emission globally and in combustion engine and electric cars. Tribology International* 2019; 135: 389-396
2. *COP26 declaration on accelerating the transition to 100% zero emission cars and vans. 2021*

<https://www.gov.uk/government/publications/cop26-declaration-zero-emission-cars-and-vans/cop26-declaration-on-accelerating-the-transition-to-100-zero-emission-cars-and-vans>
3. Wong, V. W. and Tung, S. C., *Overview of automotive engine friction and reduction trends– Effects of surface, material, and lubricant-additive technologies. Friction* 2016; 4(1): 1–28
4. Nakada, M., *Trends in engine technology and tribology. Tribology International* 1994; 27(1): 3-8
5. Smedley, G., *Piston Ring Design for Reduced Friction in Modern Internal Combustion Engines. Massachusetts Institute of Technology. 2004.*
6. Holmberg, K and Erdemir, A., *Influence of tribology on global energy consumption, costs and emissions. Friction* 2017; 5: 263–84
7. *IEA Energy Technology Perspectives 2010. Scenarios & Strategies to 2050 IEA International Energy Agency, Paris, France 2010.*

8. Plettenberg, M., Schäffer, J., Edtmayer, J., et al., *A holistic Development Method Based on AVL FRISC as Enabler for CO2 Reduction with Focus on Low Viscosity Oils*. SAE Technical Paper 2020-01-1060, 2020
9. Senatore, A. and Aleksendric, D., *Advances in Piston Rings Modelling and Design*. *Recent Patents on Engineering* 2013; 7: 51-67
10. Mock P. *CO2 emission standards for passenger cars and light commercial vehicles in the european union*. *The International Council on Clean Transportation* 2019.
11. 환경부교통환경과 and 국립환경과학원교통환경연구소. 2050 탄소중립을 향한 2030 년 자동차 온실가스 기준 확정. 2021.2. 환경부.
12. Winklhofer, E., Loesch, S., Satschen, S., *High precision piston to liner friction measurement*. *JSAE* 2016
13. Heywood, J.B., *Internal Combustion Engine Fundamentals Second Edition*, 2018; 772-774
14. Furuhashi, S. and Sasaki, S., *New Device for the Measurement of Piston Frictional Forces in Small Engines*, SAE Technical Paper 831284, 1983
15. Plettenberg, M., Henaux, D., Hammermüller, B., *Measurement Studies on the Tribological System Piston – Piston Ring – Cylinder*, SAE International 2015-01-1776, 2015
16. Nakayama, K., Seki, T., Takiguchi, M., et al., *The Effect of Oil Ring Geometry on Oil Film Thickness in the Circumferential Direction of the Cylinder*, SAE Technical Paper 982578, 1998

17. Fang, C., Meng, X., Xie, Y., et al., *An Improved Technique for Measuring Piston-assembly Friction and Comparative Analysis with Numerical Simulations: Under Motored Condition, Mechanical Systems and Signal Processing* 2019; 115: 657-676
18. Furuhashi, S. and Takiguchi, M., *Measurement of Piston Frictional Force in Actual Operating Diesel Engine, SAE International* 790855, 1979
19. Gore, M., Theaker, M., Howell-Smith, S., et al., *Direct measurement of piston friction of internal-combustion engines using the floating-liner principle, Proc IMechE Part D: J Automobile Engineering* 2014; 228(3): 344–354
20. Cho, S. W., Choi, S. M., and Bae, C. S., *Frictional modes of barrel shaped piston rings under flooded lubrication, Tribology International* 2000; 33: 545–551
21. Söderfjäll, M., Herbst, M. H., Larsson, R., et al., *Influence on friction from piston ring design, cylinder liner roughness and lubricant properties, Tribology International* 2017; 116: 272-284
22. Sherrington, I., II. *Measurement techniques for piston-ring tribology, Tribology and Dynamics of Engine and Powertrain, Fundamentals, Applications and Future Trends* 2010; 387-425
23. Winklhofer, E., Loesch, S., Satschen, S., et al., *Reduction of Friction Losses by Means of Cylinder Liner Offset in a Floating Liner Single Cylinder Engine, JSAE* 2018

24. *Westerfield, Z., Tian, T., Liu, Y., et al., A Study of the Friction of Oil Control Rings Using the Floating Liner Engine, SAE International 2016-01-1048, 2016*
25. *하경표, 김중수, 조명래, et al., 피스톤계 마찰 측정 장치 개발, 대한기계학회논문집 A 권 2002; 26(8): 1608-1614*
26. *Kaneko, N., Tabata, H., Mihara, Y., et al., Friction Reduction Effect Between Piston and Cylinder Surface Treatment Using Floating Liner Engine, COMODIA 2017; C313*
27. *Law, T., MacMillan, D., Shayler, P. J., et al., A New Floating-Liner Test Rig Design to Investigate Factors Influencing Piston-Liner Friction, SAE International 2012-01-1328, 2012*
28. *Liao, K., Factors Affecting Piston Ring Friction, Doctor of Philosophy, Massachusetts Institute of Technology 2013*
29. *Wakuri, Y., Hamatake, T., Soejima, M., et al., Piston ring friction in internal combustion engines, Tribology International 1992; 25(5): 299-308*
30. *Ting, L.L. and Mayer, J.E., Piston ring lubrication and cylinder bore analysis part 1-theory, Trans. ASME Series F 1974; 96(3): 305-314*
31. *Patir, N. and Cheng, H.S., Application of average flow model to lubrication between rough sliding surfaces, ASME Journal of Lubrication Technology 1979; 101: 220-230*

32. *D'Agostino, V. and Senatore, A., 10. Fundamentals of lubrication and friction of piston ring contact, Tribology and Dynamics of Engine and Powertrain – Fundamentals, Applications and Future Trends, 2010*
33. *Greenwood, J.A. and Williamson, J.B.P., Contact of nominally flat surfaces, Philosophical Transactions of the Royal Society London, Series A 1966; 19: 295–300*
34. *Gelinck, E.R.M., Schipper, D.J., Calculation of Stribeck curves for line contacts, Tribology International 2000; 33: 175–181*
35. *Hidekazu, S., Analysis of the lubrication characteristics of the piston system research on friction reduction, Doctoral thesis, Gunma University, 2008*
36. *Furuhama, S., and Tada, T., Gas flow through the piston ring (1st report, leaked gas flow, quantitative coefficient, and temperature), Proceedings of the Japan Society of Mechanical Engineers, 1961; 27(174): 240-247*
37. *Piston Ring Function, B-2 Basic Ring Function, RIKEN Corp.
<https://www.riken.co.jp/english/pistonring/piston/basic.html>*
38. *Piston Ring Function, B-1 Piston & Piston Ring Assembly, RIKEN Corp.
<https://www.riken.co.jp/english/pistonring/piston/combined.html>*
39. *Baelden, C., A Multi-Scale Model for Piston Ring Dynamics, Lubrication and Oil Transport in Internal Combustion Engines, Doctor of Philosophy in Mechanical Engineering, Massachusetts Institute of Technology, 2014*
40. *Ejakov, M.A., Schock, H.J., and Brombolich, L.J., Modeling of Ring Twist For an IC Engine, SAE Technical Paper 982693, 1998*

41. Takiguchi, M., Machida, K., and Furuhashi, S., *Piston Friction Force of a Small High Speed Gasoline Engine*, *ASME J. Tribol.*, 1988; 110(1): 112-118
42. Kim, D., Ito, A., Ishikawa, Y., et al., *Friction Characteristics of Steel Pistons for Diesel Engines*, *Journal of Materials Research and Technology*, 2012; 1(2): 96–102
43. Tian, T., Noordzij, L.B., Wong, V.W., et al., *Modeling Piston-Ring Dynamics, Blowby, and Ring-Twist Effects*, *J. Eng. Gas Turbines Power*, 1998; 120(4): 843-854
44. Furuhashi, S., Hiruma, M., and Tsuzita, M., *Piston Ring Motion and Its Influence on Engine Tribology*, *SAE Technical Paper 790860*, 1979
45. *Technologies that Assure Ring Function, C-7 Serving a Broad Range of Applications*, *RIKEN Corp.*
<https://www.riken.co.jp/english/pistonring/technology/application.html>
46. Werner, M.K., *Entwicklung eines Motorprüfstands zur Untersuchung der Kolbengruppenreibung und deren Haupteinflussgrößen*, *Doctoral thesis*, *Technische Universität München*, 2014
47. Tian, T., *Modeling The Performance of The Piston Ring-Pack in Internal Combustion Engines*, *Doctoral thesis*, *Massachusetts Institute of Technology*, 1997
48. Shin, K., Tateishi, Y., and Furuhashi, S., *Measurement of Oil-Film-Thickness Between Piston Ring and Cylinder*, *SAE International*, 1983; 92(1): 187-201

49. *Basaki, M., Saito, K., Nakashima, T., et al., Analysis of Oil Consumption at High Engine Speed by Visualization of the Piston Ring Behaviors, Journal of Fuels and Lubricants, 2000; 109(4): 2656-2664*
50. *Furuhama, S., Takiguchi, M., and Tomizawa, K., Effect of Piston and Piston Ring Designs on the Piston Friction Forces in Diesel Engines, SAE International, 810977, 1981*
51. *Ohsawa K., Kiyama S., Nakamura Y., et al., Visualization Study on Lubricant Oil Film Behavior around Piston Skirt, SAE International 2011-01-2119, 2011*

국 문 초 록

최근 지구 온난화에서 기인하는 기후, 생태계 변화가 가속화되면서 본 위기를 극복하기 위한 다양한 노력이 범국가적 차원에서 논의되고 있다. 지구 온난화의 주범으로 꼽히는 자동차 내연기관에서의 이산화탄소 배출로 인해 내연기관 자동차의 생산을 중단하고 판매를 금지하는 법을 오는 2035년부터 독일을 제외한 유럽 국가에서 시행하게 된다. 그러나 여전히 실 도로의 많은 교통수단이 내연기관을 사용하고 있고, 하이브리드 및 전기차로의 인프라 변경 과정에서 내연기관의 활용은 필연적이다. 내연기관에서의 연비를 향상시키고 이산화탄소를 줄이는 방법에는 다양한 효율 저감 인자를 개선시키는 방법이 있는데, 본 연구에서는 내연기관 기계적 마찰 손실에 기여하는 바가 큰 피스톤 링 마찰력에 대한 실험적 연구를 수행하였다.

피스톤 링 마찰력을 줄이고 개선하기 위해서는 우선 실제 내연기관에서의 피스톤 링 마찰력을 정량적으로 측정하는 것이 중요하다. 피스톤 링 마찰력을 측정하기 위해 다양한 측정방법이 고안, 개발되었으나, 여전히 해당 장비의 신뢰성이 엔진 고온 고압의 연소상황에서 현저히 떨어지며, 피스톤 링에 집중된 기초적인 측정 장비가 엔진 전체 구동 상황을 반영하기 어려운 실정이다. 따라서 본 연구에서는 엔진 모터링, 연소 조건에서 모두 구동 가능한 피스톤 링 마찰력 측정 장치를 개발하고 그 성능을 다양한 조건에서의 실험 결과를 기반으로 마찰 기초 이론과 비교, 검증하였다.

본 연구에서 새로 연구 개발한 피스톤 링 마찰력 측정 시스템은 기존의 부동라이너 기법을 활용하고 있으며, 실험 조건을 연구의 목적에 따라 다양하게 변경할 수 있는 단기통 엔진으로 제작, 완성되었다. 선행연구에서의 부동 라이너 기법은 엔진 연소시에 오직 피스톤 및 링 팩의 마찰력을 측정할 수 있는 장점을 가지나, 기존 피스톤-크랭크 시스템을 사용하여 피스톤 이차 거동까지 반영되므로, 순수 피스톤 링에서 기인하는 마찰력을 측정하기 어렵고, 피스톤 이차 거동에 의한 큰 피스톤 축력의 작용으로 부동 라이너에 추가 진동이 작용하여 마찰력 측정에 어려움이 있다. 그러나 본 장치는 이중 피스톤 구조를 고안하여, 기존 피스톤-크랭크 장치에 연장 콘로드를 활용하여 하나의 피스톤을 더 없는 방식으로, 피스톤 축력을 0에 가까운 수준으로 크게 줄였다. 따라서 새롭게 개발된 장치는 구조적 특징으로 피스톤 축력에 의한 부동라이너의 추가 진동을 줄여 마찰력 데이터의 신뢰성을 높일 수 있다. 또한 피스톤의 각 운동, 즉 피스톤 경사각(Piston Tilting Angle)의 영향을 기존 피스톤-크랭크 시스템 대비 1/17 수준으로 줄일 수 있어, 피스톤 경사각으로 인해 발생하는 피스톤 링의 무작위적 각 운동이 마찰력에 끼치는 영향을 배제할 수 있다. 따라서 본 장치로 피스톤 이차 거동에 의한 피스톤 스커트 마찰력뿐만 아니라, 피스톤 경사각 발생에 의해 무분별하게 생성되는, 피스톤 링 Twist, Fluttering 현상에서 기인한 마찰력 변화 또한 배제한 순수 피스톤 링 제원에 따른 마찰력 측정을 가능케 하였다.

개발된 장비가 기존의 선행연구에서의 현상, 기초 마찰 이론에

근거한 마찰력 변화를 잘 따라가는지 확인하기 위해 다양한 엔진 구동 조건에서의 실험을 수행하였다. 피스톤 상면에 압력이 걸리지 않는 상황에서 엔진 속도, 오일 온도에 따른 피스톤 링 마찰력 변화를 확인하는 기초적인 실험을 수행하였고, 피스톤 상면에 압력이 걸리는 모터 링, 연소 조건에서의 마찰력 또한 측정하였다. 측정된 마찰력 데이터는 마찰 기초 이론인 Stribeck curve를 잘 따라가며, 윤활 조건의 변화에 따라서 마찰력 값의 변화를 확인할 수 있었다. 또한 세가지 피스톤 링에서 오일 컨트롤 링(OCR)의 장력 변화에 따른 마찰력 변화를 오일 온도, 엔진 속도에 따라 관찰하여, 오일 컨트롤 링 장력의 변화량이 마찰력에 기인하는 정도를 본 개발된 장비를 통해 확인할 수 있음을 입증하였다. 따라서 새롭게 고안된 본 장비를 활용하여 피스톤 링 개발 단계에서, 개발 방향에 대한 마찰력 측면에서의 정량적인 지표를 높은 신뢰도로 제공할 수 있다. 더욱이 본 장비에서 측정된 데이터는 추후 보다 신뢰성 높은 피스톤 링 마찰 시뮬레이션 모델 구축에 중요한 검증 자료로 활용될 수 있을 것이다.

**주요어 : 피스톤 링 마찰, 이중 피스톤, 부동 라이너,
피스톤 측력, 피스톤 이차 동역학, 피스톤 경사각,
연장 콘로드**

학 번 : 2014-21875